Universidad del País Vasco
Euskal Herriko Unibertsitatea

BIOENGINEERING BIOMIMETIC MEMBRANES: COMBINING S-LAYER TECHNOLOGY, POLYELECTROLYTE MULTILAYERS AND LIPIDS

Dissertation presented to the
Departamento de Ingeniería Química y del Medio Ambiente,
Universidad del País Vasco

for the degree of Doctor

presented by

MIHAELA DELCEA

Thesis advisor: Prof. Dr. José Luis Toca-Herrera

Bilbao, 2009

This PhD thesis has been carried out at:

Biosurfaces Unit
CICbiomaGUNE Institute
San Sebastian, Spain

Center for Nanobiotechnology
University of Natural Resources and
Applied Life Sciences (BOKU)
Vienna, Austria

Paul Scherrer Institute
Villigen PSI, Switzerland

Acknowledgements

It is my pleasure to express my sincere gratitude to those people, both past and present, who encouraged me to start, conduct and complete this thesis:

Firstly, I would like to thank my supervisor, Professor José Luis Toca-Herrera, for giving me the opportunity to join S-layer project and for the maximum freedom in taking decisions, organizing experiments, analyzing and presenting results.

I am particularly thankful to Professor Jose Ramón Sarasua from ETS de Ingeniería de Bilbao for the great help with the beaurocracy of the thesis.

Many thanks to all PhD committee members and to Dr. Seta Küpcü, Dr. Rumen Krastev and Dr. Mădălin Enache, who enthusiastically accepted to be external evaluators of the thesis.

The financial support from CICbiomaGUNE Institute is greatly appreciated.

Paul Scherrer Institute from Villigen, Switzerland is acknowledged for NR research stay.

I wish to thank Professor Uwe B. Sleytr and Professor Dietmar Pum for giving me the opportunity to work in their lab in BOKU University from Vienna, and Jacqueline Friedmann for helping me with the AFM and also for friendship and nice atmosphere.

Dr. Susana Moreno-Flores for help with Langmuir trough and for valuable discussion about LB technique, Marco Muller for TEM measurements and Dr. Daniel Padró for NMR measurements and help with NMR data interpretation.

My thanks go to my friends from Tarragona where I started as a PhD student: Rasa Monkaityte, one of my best friends, always on the same wavelength with me, Iuliana Cota for great parties and for making me realize that I should live my life, Georgiana Stoica, Oana Nae Moldovan and Silvana Tomici for changing my mood any time I needed, and Susana Rodriguez Couto for support and for friendship.

I would like to thank to all present and former colleagues from CICbiomaGUNE Institute for nice atmosphere, especially to the second floor, for the nice coffee breaks and for the time spent outside.
Verónica Saravia for being a very good friend, always helping me to calm down when the things didn't go well and for nice coffees, talks (scientific too) and walks.
Aitziber Eleta with her smile, for creating a nice atmosphere in the lab and also for initiating me in euskera and Basque culture. Eskerrik asko eta gero arte!
Edurne Teiletxea for being my best friend in San Sebastian, for the nice time spent together, for cheering me up so many times. Nire maitea, eskerrik asko eta asko faltan botako zaitut.
I cannot forget the nice time spent in the "gogoşi" dinners with Olga Martínez, Isabel García and Elena Martines. Special thanks to Olga for movies, biking, friendship and for being my best Spanish teacher ever.

Muchas gracias Josune Martin por ser mi “gran hermana” y ayudarme mejorar mis días.
Joseba Irigoyen for AFM tricks and for encouraging me whole the time.
Naiara Vazquez for correcting my Spanish and teaching me “nunca hacer por hacer”.

I could have not reached this stage of my life without meeting great people during my studies. I am particularly thankful to my Diploma supervisor, Professor Grigore Mihăescu, for all support and Professor Anca Dinischiotu for giving me the chance to complete my Master studies at University of Bonn as Erasmus student. Thanks all my colleagues from the Institute of Biology Bucharest and specially Dr. Lucia Dumitru and Dr. Ioan Ardelean for initiating me in S-layers world and also Gabriela Teodosiu-Popescu for being a good colleague and friend.

Impossible to forget Beatriz Perez, answering always with amability to my questions and solving the burocratical problems.

Many thanks to “madame” Oana Creangă-Negruță for taking care that I finally answer to her offline messages and for making me feel better so many times, and to my very good friends, Mihaela and Cristian Gurgui, for listening and encouraging me so much during these years. Thanks Cristina Molan for encouraging me to be strong like a rock.

Thanks to all my friends, especially to those I did not mention here.

I wish to thank my cousin, Mariana, the person who most supported me during the thesis with advices and money when I needed, and nice words when I was down. Many thanks to my nephews, especially Ştefan, who took care that I have nice holidays in Romania.

Last but not least, I wish to thank my parents and my brothers for their care and support and for loving me enough to let me follow my own way, even when it brought me thousands of kilometers far away from them. Vă mulțumesc!

CONTENTS

Summary

A promising approach to generate biomimetic systems includes the combination of bacterial surface layer (S-layer) technology with polyelectrolyte multilayer (PEM) or lipids. In the last decade, protein adsorption on PEM and lipidic systems has shown to have many applications in biotechnology (biosensor building, biomimetic membranes, and artificial cells). As protein model, we use S-layers, which are one of the most common cell envelope components of prokaryotic organisms and archaea, composed of a single (glyco)protein, representing the simplest biological membrane developed during evolution. We have used the ability of S-layer subunits to self-assemble into 2-D crystalline arrays to generate biomimetic membranes. The affinity of S-layers to polyelectrolytes has been investigated through the building of sandwich-like supramolecular structure (PEM/S-layer/PEM/S-layer). The influence of the pH on the surface nanostructure, viscoelasticity and wetting properties of recrystallized S-layers has been also studied. The mechanical and thermal stability of the 2-D protein crystal on PEM have been determined. The amount of adsorbed S-protein and water content in the hybrid system has been estimated for the first time. The interaction of S-layer proteins with lipids varying charge and headgroup size has been also investigated.

Keywords: biomimetics; S-layers; polyelectrolyte multilayers; lipids; monolayer and bilayer lipid films; mechanical stability; thermal stability; water content; wetting properties; pH treatment; atomic force microscopy; quartz crystal microbalance with dissipation monitoring; neutron reflectometry; contact angle; Langmuir-Blodgett technique; transmission electron microscopy.

Resumen

En este trabajo presentamos una propuesta con futuro para la generación de sistemas biomiméticos combinando tecnología de proteínas bacterianas (Capas-S) con multicapas de polilectrolitos (MPE) y/o lípidos. En la última decada, la absorción de proteinas sobre MPE y sistemas lipídicos ha proporcionado aplicaciones en biotecnología (biosensores, membranas biomiméticas y celulas artificiales). Como proteína modelo para nuestro estudio hemos utilizado proteínas bacterianas (proteínas-S) que forman parte de la pared celular de bacterias y arcaea, representando la membrana biológica evolutiva mas simple. Las proteínas S tienen la capacidad de auto-ensamblarse en estructuras cristalinas bidimensionales generando superficies (membranes) biomiméticas. Hemos investigado la afinidad entre polielectrolitos y proteínas S generando superficies supramoleculares (MPE/Capa-S/MPE/Capa-S); así como la influencia del pH sobre la nanoestructura, la viscoleasticidad y las propiedades de mojado de la capa cristalina de proteínas. En otro estudio a pH constante hemos investigado la estabilidad térmica y las propiedades mecánicas del cristal de proteínas sobre MPE. Previamente se determinaron la cantidad de proteínas adsorbidas y el contenido de agua de la estructura supramolecular por vez primera. Por último, se presentan resultados sobre la interacción de proteínas S con lípidos en los que se ha variado su carga y el tamaño de la cabeza.

Palabras clave: biomimética, capas S, multicapas de polielectrolitos, lípidos, monocapa y bicapa lipídicas, estabilidad mecánica, estabilidad térmica, contenido de agua, propiedades de mojado, tratamiento de pH, microscopía de fuerza atómica, microbalanza de cuarzo con disipación, reflectometría de neutrones, ángulo de contacto, técnica Langmuir-Blodgett, microscopía de transmisión.

Chapter 1

General Introduction

Nanoscale science and engineering has provided in the last decades new possibilities to create and manipulate materials that mimic biological systems, achieving molecular scale control via self-assembly and directed assembly techniques. Nature holds the largest knowledge about hierarchical supramolecular structures, making it a source of inspiration for new design strategies. Using DNA, RNA and a huge variety of proteins, living cells build complex molecules and nanoscale organelles, and create nonliving materials with nanoscale structures.

Researchers are trying to discover and mimic the procedures that govern self-assembly in nature, in order to develop new materials with biotechnological activity [1]. The understanding of the building mechanism of materials with biotechnological activity offers new ways to improve our knowledge of how Nature builds biomaterials and further on, helps to develop nanoscale devices, such as drug delivery devices, that combine diagnostic and therapeutic actions for instantaneous administration of therapy. Biomimetics is the extraction of good design from nature. Collaborations between biologists, physicists, engineers, chemists and materials scientists have ventured beyond experiments that merely mimic what happens in nature, leading to a thriving new area of research involving biomimetics [2].

The building of biomimetic surfaces of defined nanostructure with well-oriented functional molecules (antibodies, receptors) by combining different macromolecules (lipids, proteins, carbohydrates, etc) helps to understand and develop the hierarchical

nature of self-assembly process, as well as to investigate the dynamical nature of non-covalent but specific biological interactions such as ligand-receptor, protein-lipid and carbohydrate-protein interactions.

Early conceptual ideas [3] envisioned the formation of two-dimensional molecular structures that could self-organize on self-assembling monolayer (SAM) surfaces. It is desirable in many biotechnological applications to link biomolecules irreversibly through a highly specific protein-ligand interaction. The high-affinity interaction between streptavidin and its small-molecule ligand biotin [4], which can readily be linked covalently to a variety of other biomolecules, has been widely used for biotechnological applications.

Biomimetic approaches are also useful in surface science; biology has, for example, guided researchers to a new strategy for the creation of self-cleaning surfaces [5-8]. Nonwettable plant leafs, such as those of the lotus plant, have a built-in cleaning mechanism where contaminants (dust, spores etc) are removed by rain, fog or dew [9, 10]. The surface of the Lotus leaf is ultrahydrophobic, with a contact angle of 162°, caused by a combination of surface roughness and hydrophobic properties of the surface material. The contaminating particles are picked-up by water droplets and then removed with the droplets as they roll off the leaves; this is called “Lotus-effect”.

Biomimetic design where surface roughness influences the wettability, is also utilized when trying to solve the problems of biofouling [11].

In biomimetics, an important role is played by the interaction between the biomolecules and materials. Surface functionalization is used to favor the interaction between biomolecules [12]. When considering such an interface, three criteria need to be considered: i) nonspecific binding of biomolecules to nanomaterials; ii) inhibition of nonspecific biomolecules interaction to nanomaterials; iii) control of specific selective

binding of biomolecules to nanomaterials. There are several ways by which biomolecules can be immobilized to nanomaterials: i) passive adsorption is perhaps the simplest way of immobilization; ii) cross-linking, one of the best-known methods of immobilizing enzymes; iii) covalent binding which involves direct covalent attachment of the biomolecule to the surface of the nanomaterial; iv) physical entrapment in which the biomolecules are confined in a gel or a polymer.

In the context of developing new materials with biotechnological activity, the polyelectrolyte multilayers (PEM) have been introduced as highly versatile surface coatings by Decher and coworkers using the Layer-by-Layer technique which will be explained in detail later [13]. The thickness of such multilayers can be controlled down to molecular dimensions and varied by the number of adsorption cycles. Polyelectrolyte deposition can be used to form freestanding membranes [14] and microcapsules [15], and to encapsulate yeast [16] and microcrystals [17].

Polyelectrolytes (PEs) have many applications, mostly related to modifying flow and stability properties of aqueous solutions and gels as well as to stabilize colloidal suspensions [18]. PEs can also be used to induce a surface charge to neutral particles, enabling them to be dispersed in aqueous solution. Because PEs are water-soluble, they are also investigated for biochemical and medical applications. There is currently much research in using biocompatible polyelectrolytes for implant coatings, for controlled drug release [19], and other applications [20].

The main benefits of PEM coatings are the ability to conformably coat objects, the environmental benefits of using water-based processes, reasonable costs, and the utilization of the particular chemical properties of the film for further modification, such as the synthesis of metal or semiconductor nanoparticles, or porosity phase transitions to create anti-reflective coatings, optical shutters and superhydrophobic coatings. PEM are

permeable to different ions and can also mimic until certain extent the structure of the secondary cell wall polymer of bacteria which is difficult to synthesize and purify in the laboratory or, on the contrary, can serve as antibacterial surfaces [21, 22].

PEM films are built using Layer-by-Layer deposition technique. The layer-by-layer (LbL) coating of charged surfaces with oppositely charged materials is a powerful and versatile approach for the fabrication of functional molecular assemblies and interfaces. An advantage of this technique over other existing methodologies for the preparation of thin films, such as self-assembled monolayers (SAM), is its unparalleled flexibility in combination with its simplicity and inexpensiveness. With simple instrumentation and easy preparation steps, it is possible to assemble highly complex and stable architectures with nanoscale control over their composition and structure. The origin of the LbL technique can be found in the work of Iler, who in 1966 reported on the sequential deposition of colloidal particles on solid substrates [23]. In 1991, Decher and Hong [24, 25] demonstrated that polyelectrolytes could also be electrostatically assembled onto solid supports in a sequential fashion, establishing the basis for a rapid development of the technique. In the original approach, a charged surface is exposed in alternating order to solutions of polycations or polyanions. After each deposition step the surface charge is reversed, allowing for the adsorption of a new layer of oppositely charged species, and in this way a polyelectrolyte multilayer film is assembled as is shown in Figure 1.1.

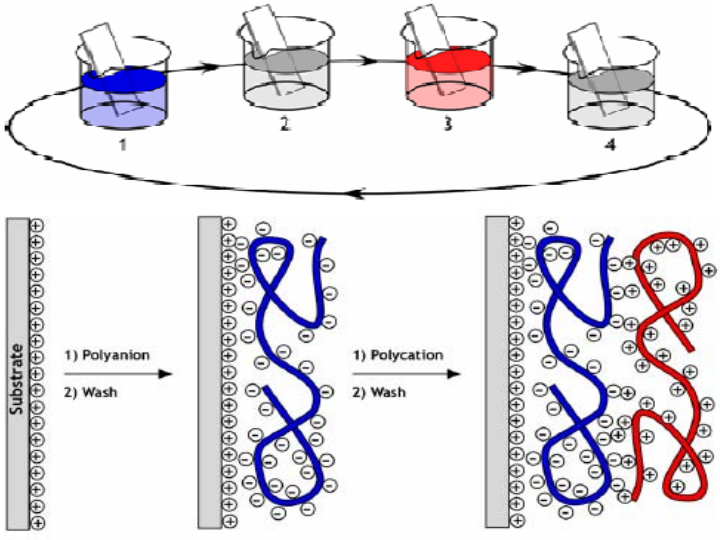

Figure 1.1. Schematic representation of a polyelectrolyte multilayer film building by Layer-by-Layer technique. Steps 1 and 3 represent the adsorption of a polyanion and polycation, respectively, and steps 2 and 4 are washing steps [13].

By simply varying the number of adsorbed layers, different film thicknesses can be easily specified. The thickness of a polyelectrolyte bilayer is typically close to 1 nm, and therefore nanometer scale control can be achieved. Moreover, the thickness and physicochemical properties of the films are influenced by parameters like pH [26, 27], ionic strength [28], temperature [29] or solvent polarity [30], and can be varied in a controlled way by adjusting the experimental conditions. Thus, finely tuned structures can be assembled with nanometric resolution. Initially, the most commonly employed polyelectrolytes were synthetic polyanions like poly(styrenesulfonate) (PSS), poly(vinylsulfonate) (PVS), poly(acrylic acid) (PAA) and polycations like poly(allylamine hydrochloride) (PAH), poly(diallyldimethylammonium chloride) (PDADMAC) and poly(ethyleneimine) (PEI).

Figure 1.2 presents the chemical structures of some of the most common polyelectrolytes:

Poly(ethylenimine) (PEI), Poly(sodium 4-styrenesulfonate) (PSS) and Poly(allylamine hydrochloride) (PAH).

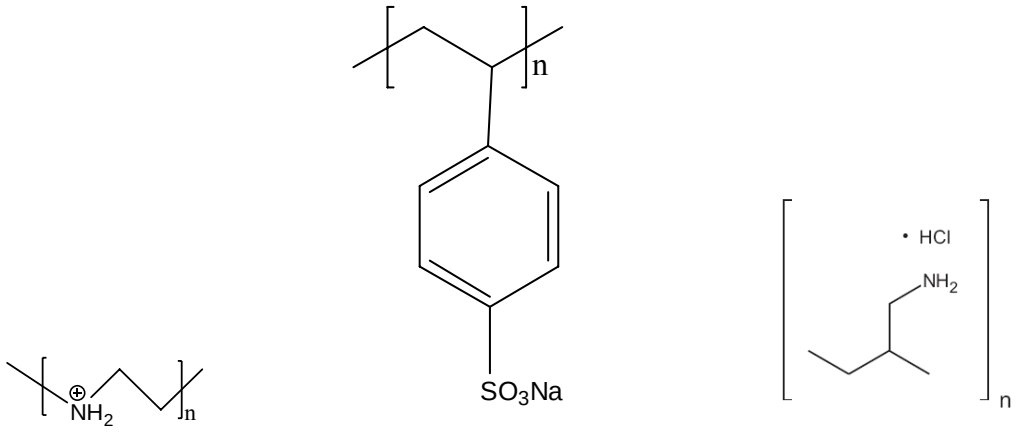

PEI **PSS** **PAH**

Figure 1.2. Chemical structures of some of the most common polyelectrolytes.

The LbL technique was found to be applicable to many other inorganic and organic materials. The assembly of multilayer films incorporating nanoparticles, crystals, dyes, proteins, nucleic acids, polysaccharides and a wide variety of other functional materials as layer constituents have been largely described [31]. In the last years it has been shown that the LbL method is not restricted to charged species. Other driving forces apart from electrostatics can be employed for the construction of this kind of controlled multilayers, such as hydrogen bonding, covalent bonding or affinity interactions [31]. This has opened the way to a broader range of materials that can be used for the sequential assembly of ultrathin films with tailor-made functional properties.

The LbL approach is particularly suitable for the integration of biomolecules into functional multilayers, since layer build-up is carried out under mild conditions, and many relevant biomaterials (proteins, DNA, lipids) are charged molecules, which further facilitates the process. Several studies have demonstrated that biomolecules and other biologically important species can be incorporated into multilayer films while retaining or improving their biological functions. Some examples include the Layer-by-Layer immobilization of nucleic acids, lipid vesicles, polypeptides and different

bioactive proteins into functional LbL-based devices for sensing and biomedical applications [31, 32].

An analogous technique, which also uses a Layer-by-Layer approach, is the Langmuir-Blodgett (LB) technique [33, 34]. The LB technique has been used successfully to adsorb many different types of molecules, such as lipids, peptides and to recrystallize proteins [33, 35].

Several biomolecules have been found to have a biomimetic behavior. One of them is chitin [36-38], a polysaccharide which can be found in algae, the cell walls of fungi, the exoskeletons of arthropods, etc. Its deacetylated form, chitosan, have several interesting properties such as non-toxic, nonallergenic, anti-microbial, and biodegradable, have fiber- and film-forming properties and adsorb metal ions. In the medical field, chitin and its derivatives have been used for drug delivery, contact lenses, wound dressing materials, suture materials, and tissue engineering, but they are also used in fields like cosmetics, textiles, nutritional supplements, water purification, foods and agriculture.

A major biomimetic approach uses natural or newly designed proteins to create nanostructures. Natural proteins can form repetitive, crystalline structures to serve as biological substrates for assembly and organization of functional nanocomponents. Most of the bacteria and archaea have crystalline protein layers as a cell wall component, the so-called S-layers, which represent the simplest biological membranes developed during evolution [39-41].

These crystalline bacterial surface layers are composed of identical protein or glycoprotein subunits, which turned out to be ideal for the development of biomimetic membranes and new approaches in molecular nanotechnology. S-layer lattices exhibit oblique (p1, p2), square (p4) or hexagonal (p3, p6) lattice symmetries consisting of one, two, three, four and six monomers (see Figure 1.3).

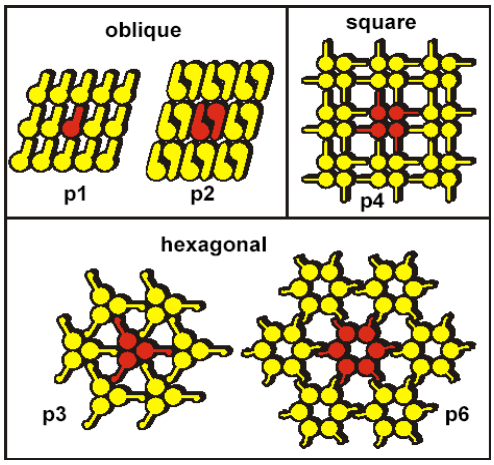

Figure 1.3. Schematic illustration of S-layer lattice types. The two-dimensional space group symmetry may be p1, p2, p3, p4 or p6. One morphological unit consists of one, two, three, four or six identical subunits, respectively [42].

The morphological units have a center-to-center spacing in the range 3-30 nm [43]; the monomolecular lattices present a thickness ranging from 5 to 25 nm, and pore dimensions from 2 to 8 nm diameter. Structural, genetic and chemical analyses have shown that S-layer glyco(protein) species have molecular masses ranging from 40 to 200 kDa. Most S-layer proteins are weakly acidic with isoelectric points (pI) in the range 4-6. S-layers are highly anisotropic structures with regard to their inner and outer surfaces. Generally the outer surface is more hydrophobic than the inner one. The inner surface reveals a net negative charge due to an excess of carboxylic acid groups whereas the outer surface is charged neutral due to an equimolar amount of carboxylic acid and amino groups.

S-layer proteins isolated from bacteria have shown the ability to reassemble into (mono)molecular arrays at the air water-interface [44], on lipid films [45], liposomes [46], solid supports [44, 47] (see Figure 1.4).

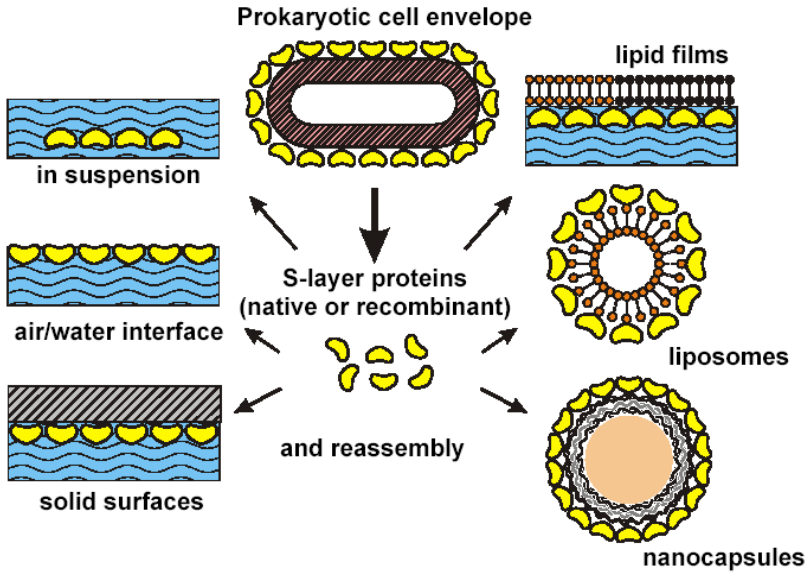

Figure 1.4. Schematic illustration of the recrystallization of isolated S-layer subunits into crystalline arrays. The self-assembly process can occur in suspension, at the air–liquid interface, at the solid–liquid interface, on lipid films, on liposomes, or on nanocapsules [48].

S-layers are ideal patterning structures for supramolecular engineering due to their high molecular order, defined mass distribution and isoporosity, high binding capacity and the stability to recrystallize over a large number of substrates. S-layers have proved to be particularly suited as building blocks and patterning elements in a biomolecular construction kit involving all major classes of biological molecules (proteins, lipids, glycans, nucleic acids and combinations of them) enabling innovative approaches for the controlled 'bottom-up' assembly of functional supramolecular structures and devices. The wealth of information accumulated on the general principles of S-layers led to a broad spectrum of applications in many areas of both life and material sciences.

These isoporous protein lattices are an ideal patterning structure for supramolecular engineering, genetic approaching being currently used for the construction of functional S-layer fusion proteins. S-layers can be used for the production of isoporous ultrafiltration membranes with very precisely defined molecular sieving properties [39]. The high density, defined position and well-orientation of surface-located functional

groups on S-layer lattices have been exploited as matrices for the immobilization of different functional molecules such as, protein A, streptavidin, biotinylated human IgG, invertase, glucose oxidase, naringinase, β-glucosidase [49, 50] and had led to the development of amperometric and optical biosensors such as a glucose sensor for monitoring the glucose concentration in blood [51-53]. During the past three decades, a considerable knowledge has been accumulated on the application potential and use of native, recombinant and genetically or chemically modified S-layer (glyco)proteins as carrier/adjuvants for vaccination and immunotherapy functioning as specific immune enhancers [54, 55].

The use of S-layers as patterning structure in the formation of tantalum-tungsten perfectly ordered nanoparticle arrays was firstly reported by Douglas and co-workers [56]. Optical lithography with deep ultraviolet radiation, a standard technique in the microelectronic industry, was shown to be suitable to pattern S-layer protein monolayers on silicon wafers, which is very important for the fabrication of well-defined nanoelectronic devices [47].

Even though S-layers represent a promising future as biological substrates for assembly and organization of functional nanocomponents, little work has been done focused on the making of arrays of biomimetic surfaces using fusion proteins based on S-layer technology. The recrystallization of S-layer fusion proteins on flat polymeric surfaces and hollow polyelectrolyte capsules has been shown recently [57]. Due to the crystalline structure of the S-layer, artificial cell membranes with defined functionalities well oriented spatially can be built using new fusion proteins [58, 59].

One of the novelties presented in this work is the experimental approach of using polyelectrolytes in combination with bacterial cell surface layers. PEMs offer many ways to change the physico-chemical properties of the surface hosting the protein layers

with the functional molecules. The biomimetic systems built by this combination can serve as model systems to address current biological and technological issues that are of medical interest since only recrystallization control can lead to large and organized nanofunctional surfaces. The characteristic of S-layers (repetitive physico-chemical properties, pores identical in size and morphology, high molecular order, defined mass distribution and isoporosity and high binding capacity) together with the versatility of the polyelectrolytes (length, molecular weight, degree of charge) are an important issue for making artificial membranes that could mimic the cell membrane function, stability, the ability to interact with other molecules. The use of proteins for the building of biomimetic structures involves also the study of the protein-surfaces interactions.

The surface protein used in this work is SbpA protein from *Lysinibacillus sphaericus* CCM 2177 (former *Bacillus sphaericus*). The nomenclature for the SbpA is based on an internal referencing system combining the name of the selected bacterial strain and genetic information: S-layer protein from previously named *Bacillus sphaericus* CCM2177 gene A. The characteristic features of the S-layer from *Lysinibacillus sphaericus* CCM 2177 can be summarized as follows: i) identical nonglycosylated protein subunits (molecular mass of 120 kDa) composition, ii) the isoelectric point of this protein in solution is 4.69, iii) square lattice symmetry with 13.1 nm lattice spacing, iv) a thickness of 9 nm, v) pores of identical size (3.5 to 6.5 nm) and morphology, and vi) anisotropic surface properties with respect to topography and physicochemical properties (the inner surface is highly negatively charged, while the outer face is charged-neutral non-hydrophobic).

S-layer-supported lipid membranes can be considered supramolecular structures that mimic archaeal cell envelopes. These composite architectures may ascend toward

exciting new key devices, particularly in fields of membrane protein-based biosensors or lab-on-a-chip technology [60].

Lipidic systems, such as liposomes, supported phospholipid monolayers or supported phospholipid bilayers (Figure 1.5) have a wide range of biological and biotechnological applications: carrier systems in genetic engineering and drug delivery, cell adhesion and cell-cell interactions, protein-lipid interactions, protein crystallization studies, biosensors and biomaterial areas, etc.

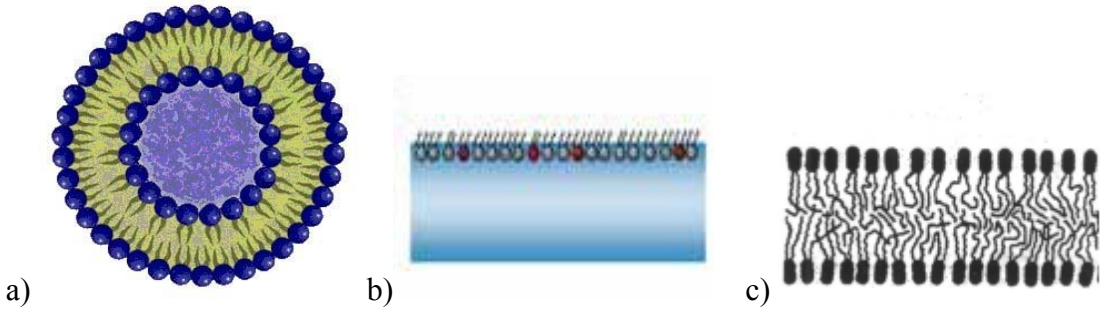

Figure 1.5. Models of biological membranes: (a) liposomes; (b) lipid monolayers at the air-water interface; (c) lipid bilayer.

Two important examples of biomembrane model systems are unilamellar phospholipid vesicles [61, 62] and supported phospholipid bilayers (SPBs) [63, 64]. In the former, a bilayer of amphiphilic phospholipid molecules forms a spherical shell, separating an "intracellular" liquid volume from the "extracellular" space, while SPBs are planar, two-dimensional, extended bilayers of the same composition as vesicles, adsorbed on a suitable solid surface.

Typically, lipid vesicles adsorb on the surface and subsequently rupture or fuse with each other before rupturing. In either case single bilayer disks are formed, which will then grow and coalesce to form a continuous SPB. The mechanisms of vesicle rupture are presented in Figure 1.6.

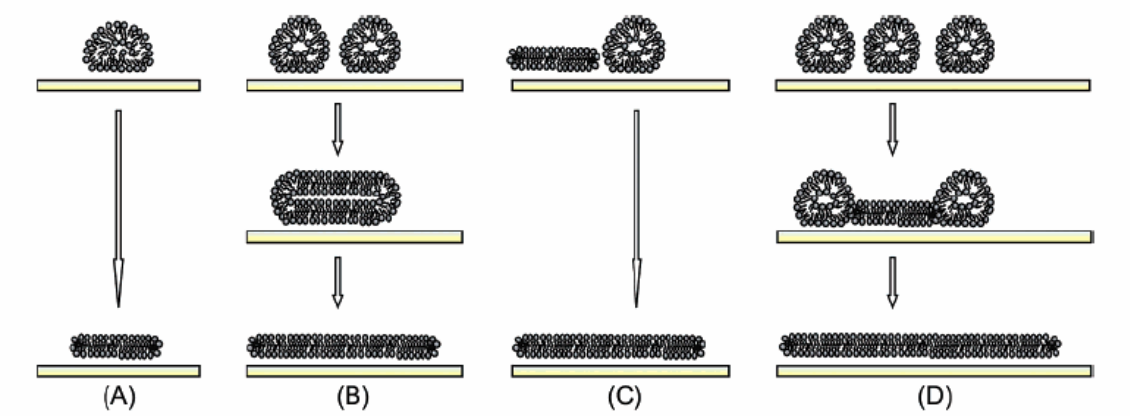

Figure 1.6. Mechanisms of vesicle rupture: (A) an isolated adsorbed vesicle ruptures spontaneously, driven by its support-induced deformation; (B) neighboring adsorbed vesicles fuse and eventually rupture; (C) the active edge of a supported bilayer patch induces the rupture of a neighboring vesicle; (D) the cooperative action of several neighboring vesicles leads to the rupture of a first vesicle (at the critical vesicular coverage). The active edge thereby exposed triggers the rupture of adjacent vesicles [65].

The immobilization of intact liposomes onto solid substrates such as, SiO_2, Si_3N_4, TiO_2, oxidized Pt and oxidized Au, mica, glass, etc, has been extensively investigated [66-73]. Supported phospholipid bilayers (SPBs) have become useful tools for studying processes such as cell adhesion and cell-cell interactions [74, 75], protein lipid interactions and protein crystallization [76, 77], as well as membrane properties in general [78, 79]. The SPB formation from vesicle solutions has been studied in the last decades using quartz crystal microbalance [80, 81], surface plasmon resonance [82], neutron reflectivity [83], atomic force microscopy [84], confocal fluorescence correlation spectroscopy and null ellipsometry [85].

Phospholipid monolayers are on one hand, a good model system to study interactions in two-dimensional arrangements of amphiphilic molecules; on the other hand, they can serve as models for biomembranes. As a model system of biological membrane, Langmuir-Blodgett films have been investigated by many researchers for many years [86, 87].

Langmuir monolayers offer the unique advantage that density and composition of lipids at the interface can be varied in a defined way, and the energetics can be studied via surface pressure-area measurements. The characteristic properties of molecules at the air/water interface are generally characterized by π-A isotherms [88-93] which give information at molecular level. For example, Gibbs elasticity of a monolayer can be determined from the slope of the π-A isotherms. It is also known that the shape of the π-A isotherms depends on many parameters including temperature [94], impurities [95] and speed of compression.

S-layer supported lipid membranes are biomimetic structures mimicking the supramolecular building principles of archaeal cell envelope which have been optimized for billions of years of evolution in most extreme habitats. In this work, we extend the knowledge of previous studies carried out on the interaction between S-layer proteins and Langmuir lipid monolayers [35, 44, 96], planar lipid membranes [97, 98] and liposomes [46, 99].

Objectives and aim of the thesis

In this PhD work, several goals were achieved:

i) the *in situ* monitoring of SbpA protein recrystallization on different supports;

ii) the mapping of the bacterial surface affinity to polyelectrolytes;

iii) the study of the thermal stability, mechanical properties and water content of bacterial recrystallized S-layers on polyelectrolyte multilayers and also the structural stability under different pH conditions;

iv) biomembrane formation through the recrystallization of SbpA protein on lipidic systems.

References

[1] T.M. Cooper (2000). *Handbook of Nanostructured materials and nanotechnology*. H. S. Naiwa. London, Academic Press.

[2] A.R. Parker and H.E.Townley (2007). *Nature Nanotechnology* 2: 347-353.

[3] S.L. Sligar and F.R. Salemme (1992). *Current Opinion in Structural Biology* 2: 587-592.

[4] P.C. Weber, D.H. Ohlendorf, J.J. Wendoloski and F.R. Salemme (1989). *Science* 243: 85-88.

[5] C. Sanchez, H. Arribart and M.M.G. Guille (2005). *Nature Materials* 4: 277-288.

[6] R. Blossey (2003). *Nature Materials* 2: 301-306.

[7] U. Mock, R. Förster, W. Menz and J. Rühe (2005). *Journal of Physics: Condensed Matter* 17: S639-S648.

[8] S. Herminghaus (2000). *Europhysics Letters* 52: 165-170.

[9] W. Barthlott and C. Neinhuis (1997). *Planta* 202: 1-8.

[10] C. Neinhuis and W. Barthlott (1997). *Annals of Botany* 79: 667-677.

[11] A. Marmur (2006). *Biofouling* 22: 107-115.

[12] V. Renugopalakrishnan, R. Garduño-Juarez, G. Narashimhan, C.S. Verma, X. Wei and L. Pingzuo (2005). *Journal of Nanoscience and Nanotechnology* 5: 1759-1767.

[13] G. Decher (1997). *Science* 277: 1232-1237.

[14] S.T. Dubas, T.R. Farhat and J.B. Schlenoff (2001). *Journal of the American Chemical Society* 123: 5368-5369.

[15] E. Donath, G.B. Sukhorukov, F. Caruso, S.A. Davis and H. Möhwald (1998). *Angewandte Chemie International Edition* 37: 2202-2205.

[16] A. Diaspro, D. Silvano, S. Krol, O. Cavalleri and A. Gliozzi (2002). *Langmuir* 18: 5047-5050.

[17] A. Yu and F. Caruso (2003). *Analitical Chemistry* 75: 3031-3037.

[18] D.J. Shaw (1999). Colloid and Surface Chemistry. Butterworth-Heinemann. Oxford.

[19] G.B. Sukhorukov, M. Brumen, E. Donath and H. Möhwald (1999). *Journal of Physical Chemistry B* 103: 6434-6440.

[20] V. Smuleac, D.A. Butterfield and D. Bhattacharyya (2006). *Langmuir* 22: 10118-10124.

[21] P.-H. Chua, K.-G. Neoha, E.-T. Kanga and W. Wangb (2008). *Biomaterials* 29: 1412-1421.

[22] J. Fu, J. Ji, W. Yuan and J. Shen (2005). *Biomaterials* 26: 6684-6692.

[23] R.K. Iler (1966). *Journal of Colloid and Interface Science* 21: 569–594.

[24] G. Decher and J.D. Hong (1991). *Berichte der Bunsen-Gesellschaft für Physikalische Chemie* 95: 1430–1434.

[25] G. Decher and J.D. Hong (1991). *Makromolekulare Chemie, Macromolecular Symposia* 46: 321–327.

[26] D. Yoo, S.S. Shiratori and M.F. Rubner (1998). *Macromolecules* 31: 4309–4318.

[27] S.S. Shiratori and M.F. Rubner (2000). *Macromolecules* 33: 4213–4219.

[28] S.T. Dubas and J.B. Schlenoff (1999). *Macromolecules* 32: 8153–8160.

[29] H.L. Tan, J. McMurdo, G. Pan and P.G.V. Patten (2003). *Langmuir* 19: 9311–9314.

[30] E. Poptoshev, B. Schoeler and F. Caruso (2004). *Langmuir* 20: 829–834.

[31] K. Ariga, J.P. Hill and Q. Ji (2007). *Physical Chemistry Chemical Physics* 9: 2319–2340.

[32] Z. Tang, Y. Wang, P. Podsiadlo and A. Kotov (2006). *Advanced Materials* 18: 3203–3224.

[33] H. Möhwald (1990). *Annual Review of Physical Chemistry* 41: 441-476.

[34] G. Brezesinski and H. Möhwald (2003). *Advances in Colloid and Interface Science* 100-102: 563-584.

[35] B. Schuster, P.C. Gufler, D. Pum and U.B. Sleytr (2003). *Langmuir* 19: 3393-3397.

[36] K. Kurita (2006). *Marine Biotechnology* 0: 1-24.

[37] B. Bensaude-Vincent, H. Arribart, Y. Bouligand and C. Sanchez (2002). *New Journal of Chemistry* 26: 1-5.

[38] Y. Kato, H. Onishi and Y. Machida (2003). *Current Pharmaceutical Biotechnology* 4: 303-309.

[39] U.B. Sleytr, P. Messner, D. Pum and M. Sára (1999). *Angewandte Chemie International Edition* 38: 1034-1054.

[40] U.B. Sleytr, E.M. Egelseer, N. Ilk, D. Pum and B. Schuster (2007). *FEBS Journal* 274: 323–334.

[41] U.B. Sleytr, C. Huber, N. Ilk, D. Pum, B. Schuster and E.M. Egelseer (2007). *FEMS Microbiology Letters* 267: 131-144.

[42] U.B. Sleytr, M. Sara, D. Pum, B. Schuster, P. Messner and C. Schaffer (2003). *Biopolymers*. A.Steinbuchel and S.Fahnenstock. New York, Wiley/VCH. 7**:** 285-338.

[43] P. Messner and U.B. Sleytr (1992). *Advances in Microbial Physiology* 33: 213-275.

[44] D. Pum, M. Weinhandl, C. Hödl and U.B. Sleytr (1993). *Journal of Bacteriology* 175: 2762-2766.

[45] B. Schuster and U.B. Sleytr (2000). *Reviews in Molecular Biotechnology* 74: 233-254.

[46] C. Mader, S. Küpcü, U.B. Sleytr and M. Sara (2000). *Biochimica et Biophysica Acta* 1463: 142-150.

[47] E.S. Györvary, A. O'Riordan, A.J. Quinn, G. Redmond, D. Pum and U.B. Sleytr (2003). *Nano Letters* 3: 315–319.

[48] U.B. Sleytr, M. Sára, D. Pum and B. Schuster (2001). *Progress in Surface Science* 68: 231–278.

[49] U.B. Sleytr and M. Sara (1996). *Trends Biotechnology* 15: 20-26.

[50] U.B. Sleytr, D. Pum and M. Sara (1997). *Advances in Biophysics* 34: 71-79.

[51] A. Neubauer, D. Pum and U.B. Sleytr (1993). *Analytical Letters* 26: 1347-1360.

[52] A. Neubauer, C. Hödl, D. Pum and U.B. Sleytr (1994). *Analytical Letters* 27: 849-865.

[53] A. Neubauer, S. Pentzien, S. Reetz, W. Kautek, D. Pum and U.B. Sleytr (1997). *Sensors and Actuators B* 40: 231-236.

[54] U.B. Sleytr (1997). *FEMS Microbiology Review* 20: 5-12.

[55] A.J. Malcolm, P. Messner, U.B. Sleytr, R.H. Smith and F.M. Unger (1993a). *Immobilised macromolecules: application potentials*. U. B. Sleytr, P. Messner, D. Pum and M. Sára. London, Springer**:** 195–207.

[56] K. Douglas, N.A. Clark and K.J. Rothschild (1986). *Applied Physics Letters* 48: 676-678.

[57] J.L. Toca-Herrera, R. Krastev, V. Bosio, S. Küpcü, D. Pum, A. Fery, M. Sàra and U.B. Sleytr (2005). *Small* 1: 339-348.

[58] D. Moll, C. Huber, B. Schlegel, D. Pum, U.B. Sleytr and M. Sára (2002). *Proceedings of the National Academy of Sciences* 99: 14646-14651.

[59] C. Völlenkle, S. Weigert, N. Ilk, E.M. Egelseer, V. Weber, F. Loth, D. Falkenhagen, U.B. Sleytr and M. Sára (2004). *Applied and Environmental Microbiology* 70: 1514-1521.

[60] B. Schuster, P.C. Gufler, D. Pum and U.B. Sleytr (2004). *IEEE Transactions on Nanobioscience* 3: 16-21.

[61] M.M. Parmar, K. Edwards and T.D. Madden (1999). *Biochimica et Biophysica Acta* 1421: 77-90.

[62] A.R. Curran, R.H. Templer and P.J. Booth (1999). *Biochemistry* 38: 9328-9336.

[63] P. Nollert, H. Kiefer and F. Jähnig (1995). *Biophysical Journal* 69: 1447-1455.

[64] E. Sackmann (1996). *Science* 271: 43-48.

[65] R.P. Richter, R. Bérat and A.R. Brisson (2006). *Langmuir* 22: 3497-3505.

[66] Q. Yang, X.-Y. Liu, S.-I. Ajiki, M. Hara, P. Lundahl and J. Miyake (1998). *Journal of Chromatography B* 707: 131-141.

[67] H. Rongen, T.v. Nierop, H.v.d. Horst, R. Rombouts, P.v.d. Meide, A. Bult and W.v. Bennekom (1995). *Analytica Chimica Acta* 306: 333-341.

[68] K. Yun, E. Kobatake, T. Haruyama, M.-L. Laukkanen, K. Keinanen and M. Aizawa (1998). *Analytical Chemistry* 70: 260-264.

[69] M. Liebau, G. Bendas, U. Rothe and R. Neubert (1998). *Journal Sensors and Actuators B* 47: 239-245.

[70] B. Pignataro, C. Steinem, H. Galla, H. Fuchs and A. Janshoff (2000). *Biophysical Journal* 78: 487-498.

[71] T. Redelmeier, J.-G. Guillet and M. Bally (1995). *Drug Delivery* 2: 98-109.

[72] A. Albersdorfer, T. Feder and E. Sackmann (1997). *Biophysical Journal* 73: 245- 257.

[73] L. Jung, J. Shumaker-Parry, C. Campbell, S. Yee and M. Gelb (2000). *Journal of the American Chemical Society* 122: 4177-4184.

[74] H.M. McConnell, T.H. Watts, R.M. Weiss and A.A. Brian (1986). *Biochimica et Biophysica Acta* 864: 95-106.

[75] J.T. Groves and M.L. Dustin (2003). *Journal of Immunological Methods* 278: 19-32.

[76] K.H. Pearce, R.G. Hiskey and N.L. Thompson (1992). *Biochemistry* 31: 5983-5995.

[77] S. Terrettaz, T. Stora, C. Duschl and H. Vogel (1993). *Langmuir* 9: 1361-1369.

[78] Y.F. Dufrene and G.U. Lee (2000). *Biochimica et Biophysica Acta* 1509: 14-41.

[79] P.E. Milhiet, V. Vie, M.C. Giocondi and C.L. Grimellee (2001). *Single Molecules* 2: 109-112.

[80] C.A. Keller and B. Kasemo (1998). *Biophysical Journal* 75: 1397-1402.

[81] L.M. Williams, S.D. Evans, T.M. Flynn, A. Marsh, P.F. Knowles, R.J. Bushby and N. Boden (1997). *Langmuir* 13: 751-757.

[82] C.A. Keller, K. Glasmastar, V.P. Zhdanov and B. Kasemo (2000). *Physical Review Letters* 84: 5443-5446.

[83] B.W. Koenig, K. Gawrisch, S. Krueger, W. Orts, C.F. Majkrzak, N. Berk and J.V. Silverton (1996). *Biophysical Journal* 70: Wp229-Wp229.

[84] H. Egawa and K. Furusawa (1999). *Langmuir* 15: 1660-1666

[85] M. Benes, D. Billy, W.T. Hermens and M. Hof (2002). *Biological Chemistry* 383: 337-341.

[86] G. Weidemann, U. Gehlert and D. Vollhardt (1995a). *Langmuir* 11: 864-871

[87] R.C. Haddon and A.A. Lamola (1985). *Proceedings of the National Academy of Sciences* 82: 1874-1878.

[88] M.C. Phillips and D. Chapman (1968). *Biochimica et Biophysica Acta* 163: 301-313.

[89] G. Colacicco (1968). *Journal of Colloid Interface Science* 29: 345-664.

[90] G. Colacicco (1972). *Annals of the New York Academy of Sciences* 195: 224-261.

[91] G. Colacicco, A.J. Buckelew and E.W. Scarpello (1974). *Journal of Colloid and Interface Science* 46: 147-151.

[92] M. Lösche, C. Helm, H.D. Mattes and H. Möhwald (1985). *Thin Solid Films* 133: 51-64.

[93] E. Okamura, J. Umemura and T. Takenaka (1985). *Biochimica et Biophysica Acta* 812: 139-146.

[94] P. Tchoreloff, A. Gulik, B. Denizot, J.E. Proust and F. Puisieux (1991). *Chemistry and Physics of Lipids* 59: 151-165.

[95] Y.F. Hifeda and G.W. Rayfield (1992). *Langmuir* 82: 197-200.

[96] B. Wetzer, A. Pfandler, E. Györvary, D. Pum, M. Lösche and U.B. Sleytr (1998). *Langmuir* 14: 6899-6906.

[97] B. Schuster, D. Pum, O. Braha, H. Bayley and U.B. Sleytr (1998). *Biochimica et Biophysica Acta* 1370: 280-288.

[98] B. Schuster, D. Pum and U.B. Sleytr (1998). *Biochimica et Biophysica Acta* 1369: 51-60.

[99] S. Küpcü, M. Sara and U.B.Sleytr (1995). *Biochimica et Biophysica Acta* 1235: 263-269.

Chapter 2

Experimental techniques

In this PhD thesis, we have used different experimental methods and techniques such as: quartz crystal microbalance with dissipation monitoring, atomic force microscopy, contact angle, neutron reflectometry, dynamic light scattering, ζ-potential, transmission electron microscopy, Langmuir-Blodgett technique, nuclear magnetic resonance. The basic principles of the techniques are described here.

2.1. Quartz Crystal Microbalance with Dissipation Monitoring (QCM-D)

The quartz crystal microbalance (QCM) is a technique based on monitoring the resonance behavior of an oscillating quartz crystal loaded with an overlayer of interest. In the last decades, this technique has been extensively used in order to detect thin film deposition on the surface of the crystal with a resolution down to ng/cm^2. QCM can be operated in vacuum, in gaseous environment or in liquid and has been used to study thin films of polymers, proteins [1,2] and cells [3]. In the 90's, Rodahl and coworkers developed the QCM with dissipation (QCM-D) which quantifies the deposited mass and also characterizes the viscoelastic properties of the films [4]. The basic set-up is shown in Figure 2.1 and consists of a single crystal of quartz sandwiched between a pair of electrodes.

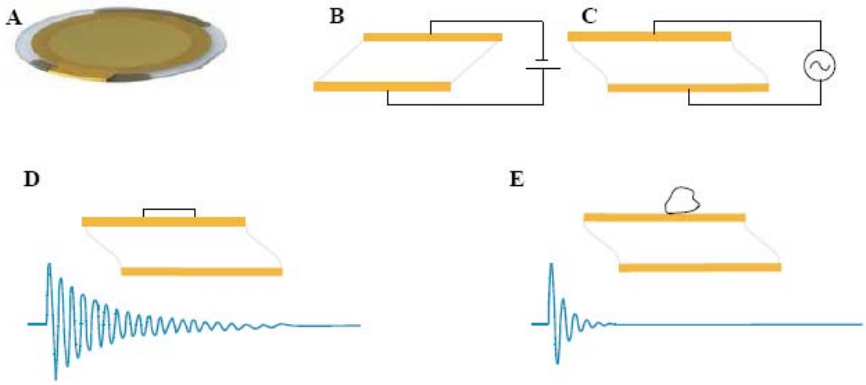

Figure 2.1. The principle of operation of the Quartz Crystal Microbalance with Dissipation monitoring. (A) 5MHz AT-cut quartz crystal, (B) the application of an electric field across the piezoelectric quartz results in shear motion of the crystal, (C) resonance in the shear motion can be excited applying an alternating current of appropriate frequency. (D, E) After cutting the driving circuit, the decaying oscillation of the crystal is monitored. Attachment of a rigid mass (D) or soft mass (E) leads to different responses (taken from Q-Sense, www.q-sense.com).

Due to the fact that the quartz is a piezoelectric material which deforms when an electric field is applied, the crystal can be driven to oscillate at its resonant frequency (f_0) by applying an alternating current. The resonance frequency is determined by the thickness of the crystal (d) and the speed of shear waves in quartz (v_Q). As a function of loading a crystal, the resonance frequency is changed. The change in resonance frequency of the crystal before and after loading (Δf) is directly proportional to the mass of the overlayer (Δm) according to Sauerbrey's equation [5]:

$$\Delta f = -\frac{1}{nC}\Delta m$$

where, Δf is the change in the resonance frequency, or frequency shift, 1/C = mass sensitivity of quartz, with C = 17.7 ng/(cm^2 Hz), for a 5 MHz crystal, and n = the overtone number. The change in resonance frequency is not the only type of information that QCM-D gives.

The contact of the crystal with the surrounding medium generates losses of frictional energies which can be used to obtain additional information about the material deposited on the crystal. QCM-D measures both changes in frequency (f) and energy losses (dissipation, D). When a rigid material is attached to the crystal, a decrease in frequency takes place, while when a more viscoelastic mass is attached, an increase in dissipation is also recorded. Sauerbrey's equation is valid under several conditions: i) the frequency decrease due to loading must be smaller than 2% of the resonance frequency of the bare crystal, ii) the adsorbed mass must be distributed homogeneously on the sensor surface, iii) there must be no slip between the crystal and the coupled overlayer, and iv) the overlayer must be rigid (that is, no viscoelastic deformation can occur).

2.2. Atomic Force Microscopy (AFM)

The atomic force microscopy (AFM) belongs to a series of scanning probe microscopes invented in the 1980s. This series started with the scanning tunnelling microscope (STM), which was invented by Binning et al. [6]. Few years later, Binning, Quate and Gerber developed the atomic force microscope (AFM) [7]. The AFM allowed the imaging of the surfaces topography, in some cases with atomic resolution. Moreover, it can be used to study samples in air as well as in liquid. For these reasons, AFM has become a useful tool in different fields of research such as surface science, material engineering and biology. Basically, in the AFM the sample is scanned by a tip mounted to a cantilever spring. While scanning, the force between the tip and the sample is measured by monitoring the deflection of the cantilever using in most cases an optical lever (see Figure 2.2).

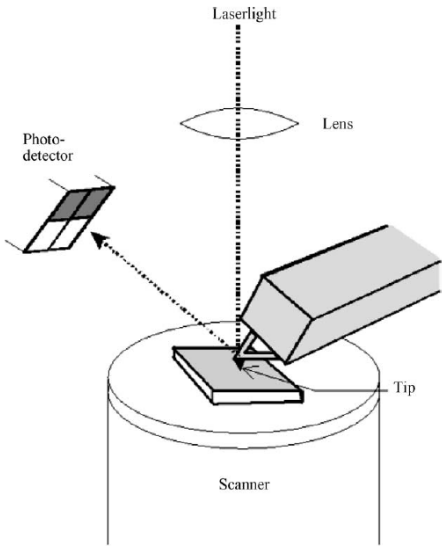

Figure 2.2. Principle of operation of the AFM [8].

The optical lever operates by reflecting a laser beam on the cantilever, which strikes a position-sensitive photo-detector. When acquiring an image, a feedback loop maintains a constant force between tip and sample. The image contrast arises because the force between the tip and sample is a function of both tip-sample separation and the material properties of the tip and sample. By plotting the deflection of the cantilever versus its position on the sample a topographic image of the sample is obtained.

Two operating modes are routinely used to image samples: the “contact mode” in which the tip is in the contact with the sample’s surface during imaging, and the “tapping mode”, in which the tip is in an intermittent contact with the sample.

AFM is not only a tool to image the surface topography at nanoscale resolution; it can also be used to measure force-versus-distance curves. Such curves provide valuable information on local material properties such elasticity, hardness, Hamaker constant, adhesion and surface charge densities.

Interactions between tip and sample can be used to investigate properties of the sample,

the tip, or the medium in between [8]. In an AFM force measurement, the tip attached to a cantilever spring is moved towards the sample in normal direction. Vertical position of the tip and deflection of the cantilever are registered and converted to force-versus-distance curve, briefly called "force curves". If one is interested in acquiring a force-versus-distance curve, at a certain point of the sample the deflection of the cantilever is recorded while approaching and retracting the tip from the surface (see Figure 2.3).

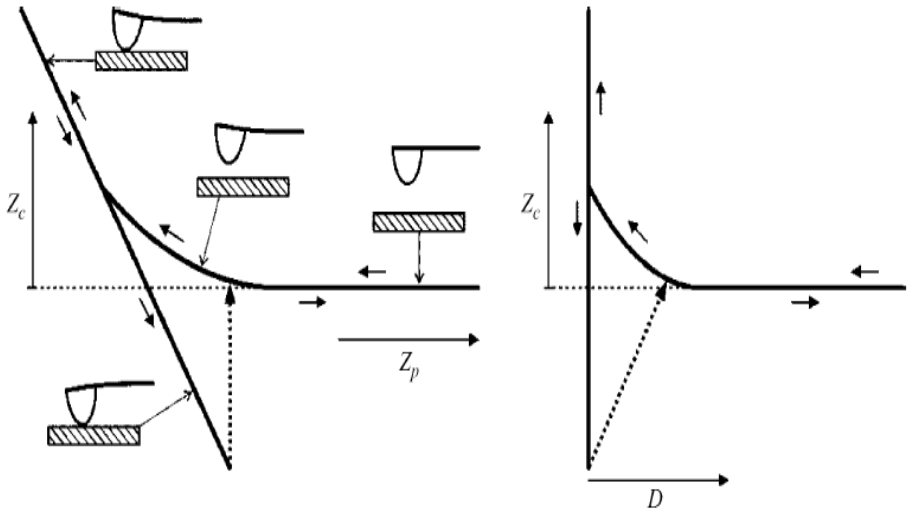

Figure 2.3. Schematic of a typical cantilever deflection-vs.-piezo height (Z_c-vs.-Z_p) curve (left) and corresponding Z_c-vs.-D plot, with $D = Z_c + Z_p$. [8].

The result of a force measurement is a measure of the cantilever deflection, Z_c, versus position of the piezo, Z_p, normal to the surface. To obtain a force-versus-distance curve, Z_c and Z_p have to be converted into force and distance. The force, F, is obtained by multiplying the deflection of the cantilever with its spring constant

$$k_c F = k_c Z_c.$$

The tip-sample separation, D, is called "distance" and is calculated by adding the deflection to the position:

$$D = Z_p + Z_c.$$

However, the direct result of a force measurement is a measure of the photodiode current I_{PSD} versus height position of the piezoelectric translator Z_p. Figure 2.4 presents different types of force curves registered for samples and tips with different properties [9].

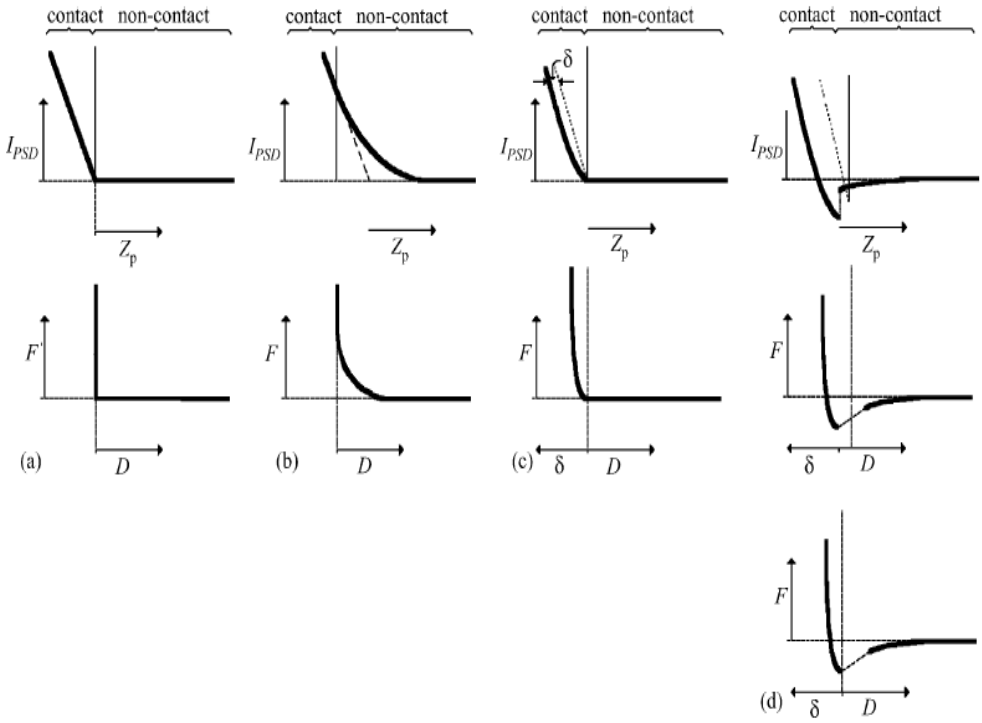

Figure 2.4 indicates how the I_{PSD}-vs.-Z_p curves are converted to force-vs.-distance (F-vs.-D) curves, where D is given by the sum of the cantilever deflection Z_c and the piezo position Z_p. (a) Infinitely hard tip and sample without surface forces. (b) Infinitely hard materials but with a long-range repulsion. (c) Deformable materials without surface forces. (d) Deformable materials with attraction and adhesion force. The additional bottom figure shows the usual misinterpretation, in which zero distance is placed to the end of the jump-in. For (a) and (b) approaching and retracting parts of force curves are identical. For (c) approaching and retracting parts are identical if the deformation is elastic. For (d) the retraction shows an adhesion force. [8].

2.3. Contact Angle

Contact angle measurements are of fundamental importance in industrial and daily phenomena such as flotation, painting, lubrication and water-proofing [10-13]. Contact angle analysis is normally used to investigate the wetting properties of a given surface.

The contact angle (θc) can be defined as the angle at which three phases (gas, liquid and solid) coexist in mechanical equilibrium (see Figure 2.5).

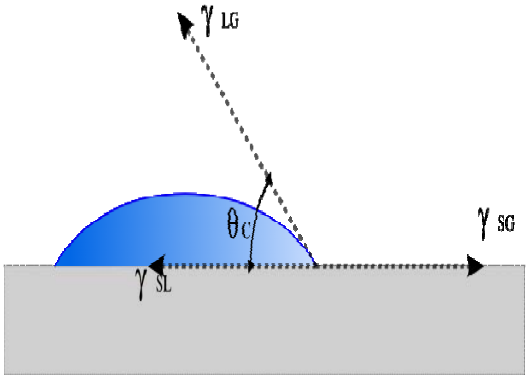

Figure 2.5. Aqueous drop on a substrate. γ_{SL} is the interfacial tension between solid and liquid; γ_{LG} is the interfacial tension between liquid and gas. γ_{SG} is the interfacial tension between solid and gas and θc is the contact angle between a drop of liquid and a chemically homogeneous, non-adsorbing, smooth, and horizontal solid surface.

The contact angle gives a qualitative description of the force balance between the molecules within the droplet versus the attraction or repulsion those droplet molecules experience towards the surface molecules [14]. The contact angle is specific for any given system and is determined by the interactions across the three interfaces. The contact angle is not limited to a liquid/vapour interface; it is equally applicable to the interface of two liquids or two vapours.

For good and reproducible contact angle measurements few requirements should be followed: i) the size and the volume of the drops should be kept constant since it is known that variations in the volume of the drops can lead to inconsistent contact angle measurements, ii) at least three different drops should be measured for every sample all over the sample. However, contact angle is a macroscopic method and it should be combined with other methods in order to obtain accurate information about the molecular properties of surfaces.

2.4. Neutron reflectometry (NR)

Neutrons can penetrate matter far better than charged particles. Neutrons interact with atoms via *nuclear* rather than electrical forces and can travel large distances through most materials without being scattered or adsorbed [15]. Early applications of neutron reflection included the determination of scattering lengths, the production of neutron guides and neutron spin polarizers. Later on, interest has been focused on the application of the reflection of neutrons to the study of surface and interfacial phenomena, since neutron experiments give information about the neutron refractive index profile normal to the interface.

Recently, neutron reflectometry (NR) has emerged as powerful tool for the investigation of the surface behavior of polymers [16, 17]. NR provides excellent spatial resolution, down ~ 1.0 nm with penetration depths over hundreds of nanometers, detecting the variation in thickness, roughness and scattering length density. It is a non-destructive technique and, consequently, repetitive measurements on the specimen can be performed. Due to these advantages, the interest and use of the reflectivity technique has surged. According to the general laws of reflection, a beam impinging a surface at a certain angle θ_i is split into a scattered or reflected and a transmitted or refracted portion [16, 18] (see Figure 2.6).

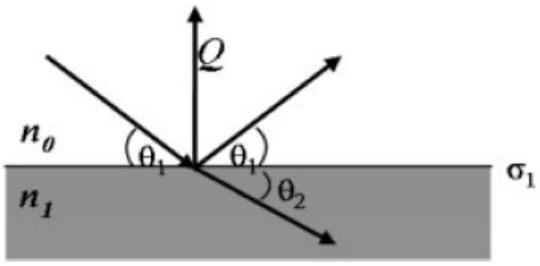

Figure 2.6. Scattering geometry of a neutron beam impinging on a surface.

The momentum transfer of the incident and the scattered wave vector is:

$$q = (4\pi / \lambda) \sin \theta_i.$$

The ratio between the refractive index of the media above and below the surface, n_1 and n_2, determines the refraction angle $\theta_{i,t}$, $n_0 / n_1 = \cos \theta_{i,t} / \cos \theta_i$ or, in the case of $n_0 = 1$ for air or vacuum, $n_1 = \cos \theta_i / \cos \theta_{i,t}$. In case of neutrons, the refractive index is given by the neutron scattering length density ρ of the media. When the refraction angle $\theta_{i,t}$ becomes 0, $n_1 = \cos \theta_i = \cos \theta_c$, the so-called critical angle. For $\theta_i < \theta_c$ total external reflection occurs. The critical angle θ_c is a characteristic value for each material and proportional to the incident wavelength λ. At low incident angles the reflected intensity at an interface is given by the Fresnel reflectivity R_F where q_c is the momentum transfer at the critical angle θ_c. The reflectivity varies monotonous as:

$$R = R_F(q) = \left| \frac{1-[1-(q_c/q)^2]^{1/2}}{1+[1-(q_c/q)^2]^{1/2}} \right|^2$$

In a layered system the incident beam is reflected and refracted at each interface leading to a superposition of individual reflectivities, which shows up in characteristic oscillations of the recorded reflectivity curve along q. The separation distance Δq between adjacent minima in the reflectivity curve gives the individual layer thickness d in the system, $d = 2\pi / \Delta q$. The amplitude of the oscillations depends on the contrast in the refractive indexes at the individual interfaces.

The greater the contrast, the more pronounced oscillation will occur. Furthermore, at the boundary between adjacent layers a smoothing or roughness σ of the interface must be taken into account, which is introduced either as an error function refractive index profile or a Gaussian height distribution of the mean interface location in the calculation of the reflectivity profile [19].

Using a recursion formula developed by Parratt for the reflectivity of an arbitrary number of layers, the reflectivity profile can be calculated describing each individual layer by a set of three parameters, neutron scattering length density ρ_s, layer thickness d and roughness σ. [20].

In a typical neutron reflectivity experiment the reflectivity is measured as a function of the scattered beam angle $\theta_i = \theta_f$ (see Figure 2.6). At constant wavelength λ the sample and the detector are scanned in the Bragg-Brentano mode (θ-2θ), if sample and detector are fixed θ-2θ positions the wavelength is varied to change the wave vector q. Due to the large penetration depth of neutrons into solid materials, neutron reflectivity can be used for measurements with complex sample environments such as sample cells for solid-liquid interfaces. In order to gain detailed insight into properties and structure of different and complex systems, neutron reflectometry is a versatile complementary technique to investigations carried out using in-situ AFM, quartz crystal microbalance, ellipsometry or surface plasmon resonance miscroscopy.

2.5. Dynamic light scattering (DLS)

Dynamic light scattering (DLS), also known as photon correlation spectroscopy is an experimental technique, which is widely used to determine the size of particles in solution [21]. If a laser is used (monochromatic and coherent light), time dependent fluctuations in the scattering intensity can be observed due to the particles Brownian motion [22]. The frequency and the amplitude of the Brownian motion depend on particle size and solvent viscosity. The motion of the particles is described by the diffusion coefficient, D.

Once D is known, the hydrodynamic diameter of the particles can be obtained via the Stokes-Einstein equation:

$$D = \frac{k_B T}{6\pi\eta R_H}$$

where, k_B is Boltzmann's constant, T is the temperature, η is the viscosity of the medium and R_H is the hydrodynamic radius of the given particle. DLS data is usually analyzed by numerical fitting the measured correlation functions with calculations based on assumed distributions. There are several analyses methods: i) cumulant method which assumes nothing about the form and size distribution: it is simply a polynomial fit of the natural logarithm of the normalized correlation function, and ii) regularization method which assumes that the size distribution is an arbitrary, but smooth function, and seeks a non-negative distribution producing the best fit to the experimental data.

2.6. ζ-potential

A charged particle in contact with a solution containing ions (electrolytes solution), generates at the particle-solution interface a charge distribution inducing the formation of a so-called electrical double layer (Figure 2.7).

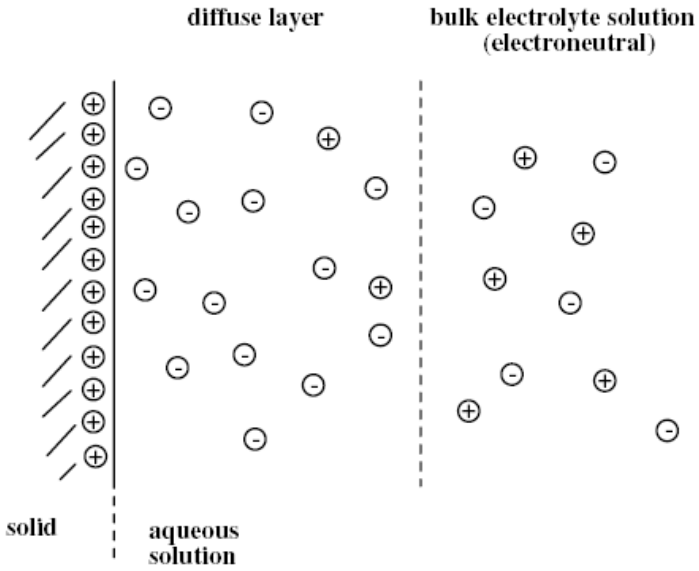

Figure 2.7. The diffuse electrical double-layer in aqueous solution next to a flat surface.

The electrical double consists of two regions, the inner region which may include adsorbed ions (Stern layer), and the diffuse region where the ions are distributed according to electrical forces and thermal motions.

When the particle moves in the medium due to the Brownian motion or the hydrodynamic flow, the structure of the double layer is stable. At this level, the molecules of the solvent are mobile and the zeta potential is measured. The zeta potential is the charge density at the surface. Very important parameter in the evaluation of the ζ-potential is the pH of the suspension and its distance from the isoelectric point (pI), which is the pH at which the ζ-potential is equal to zero. The closer the pH to its pI, the smaller the magnitude of the ζ-potential. Other important parameters in the evaluation of ζ-potential are the concentrations of non-specifically bound and specifically bound ions. A way to calculate the ζ-potential of colloidal particles is to measure their electrophoretic mobility; when an electric field is applied across an electrolyte, the charged particles suspended in electrolyte are attracted towards the electrode of opposite charge. Viscous forces acting on the particles tend to oppose this movement. When the equilibrium between these two opposing forces is reached, the particles move with a constant velocity. The velocity of a particle in a unit electric field is referred to as its electrophoretic mobility (U_e). The zeta potential is related to the electrophoretic mobility by the Henry's equation:

$$U_e = \frac{\varepsilon \xi}{6\pi\eta} f(ka)$$

where: ε is the dielectric constant of the medium, η is the viscosity, ξ is the ζ-potential, and f (ka) is Henry's factor. The factor f (ka) accounts for the ratio between the particle

radius (a) and the thickness of the double layer (1/k). When the particle is much smaller than the double layer, f (k_a) = 1 (Hückel limit), while when the particle is much larger than the double layer, f (k_a) = 1.5 (Smoluchowsky limit) [23].

2.7. Transmission Electron Microscopy (TEM)

Transmission Electron Microscopy (TEM) is a powerful tool for biophysical applications. TEM utilizes the wave properties of moving electrons to generate highly resolved images of specimens. In 1986, Ernst Ruska was Nobel Prize awarded for his fundamental work in electron optics and for design of the first electron microscope. Electrons from the electron gun pass through condenser lenses that focus the electrons onto the sample. The electron beam shines through the specimen. Objective lenses and projector lenses magnify the transmitted beam and project it onto the fluorescent viewing screen. Impact of electrons excites the screen and produces a visible magnified image of the sample. This image is recorded with a CCD camera. A common preparation method to visualize very small biological structures, such as single protein molecules, is negative staining [24], in our case we used uranyl acetate to distinguish under the electron microscope the protein from their surroundings (carbon grid, other molecules). The resolution power of TEM was demonstrated for large protein complexes [25-27].

2.8. Langmuir-Blodgett (LB) technique

Langmuir-Blodgett (LB) films are a special kind of organic thin films at the air/water interface, prepared for the first time in 1919 by Irving Langmuir and Katherine Blodgett [28]. LB films consist of highly organized organic amphiphiles transferred from an insoluble monolayer on an aqueous phase to a support by means of a dipping procedure that can build multilayers when is repeated (in a sense this method is analogous to the

LbL method previously described). These films involve many practical applications of potential importance in microlithography, microelectronics, integrated optics and the developing field of molecular electronics [29]. The formed monolayer at the water/interface is called Langmuir monolayer and is an excellent model system to study ordering in two dimensions. The thermodynamic behaviour of such monolayer can be studied by means of a film balance consisting of a Teflon trough with a movable barrier for surface area control and a Wilhelmy balance for surface pressure determination.

Figure 2.8 shows a typical surface pressure-molecular area curve for a glycerophospho-lipid obtained when the barriers are pressed towards each other. π-A curve presents different phases. At the beginning, with the barriers most apart, the monolayer is in the gaseous phase with the acyl groups most apart in the air as indicated. Further compression (from right to left) forces the monolayer molecules into the liquid phase that causes a slight elevation of the surface pressure, starting with the so-called "lift-off" point. Further compression squeezes the lipid molecules into a solid lipid (they cannot be forced further together), which gives a steep rise in the surface pressure; by even more compression the layer collapses into a many-layered structure.

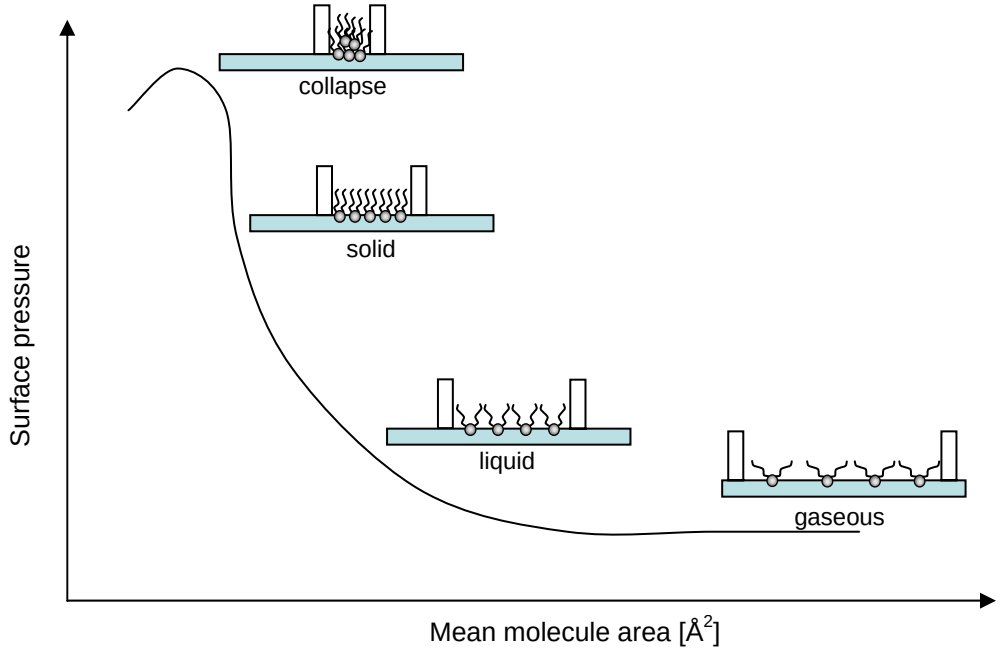

Figure 2.8. Typical film pressure isotherm for a surfactant monolayer.

The various regions of the isotherm are determined by the lateral interaction between the surfactant molecules within the surface phase. In the dilute, 'gaseous' state, the molecules can be considered to be negligible in size and non-interacting. Under these conditions the isotherms obey an ideal, two-dimensional gas equation of the form:

$$\pi A = kT$$

The surface pressure π is measured as a difference between the surface tension of the pure subphase σ_0 and the surface tension σ of the monolayer covered surface according to Wilhelmy's method [30].

$$\pi = \sigma_0 - \sigma$$

As the pressure is increased, a point is reached where the attractive van der Waals forces between the hydrocarbon tails cause a condensation process, analogous to liquid condensation from the vapour phase. However, at the end of this process the surface layer is not completely condensed because of the strong, relatively long-range electrostatic repulsion between the ionic head groups. This head-group repulsion keeps the surface layer fluid, whilst the attractive van der Waals forces between the hydrocarbon chains keep the film coherent. In this state of modified ('real') gas equation can be used to describe the isotherm of the form:

$$(\pi - \pi_0)(A - A_0) = kT$$

where, π_0 and A_0 are correction terms related to the attractive and repulsive forces between the molecules. At still higher pressures, the film becomes completely packed and the limiting area corresponds to the cross-sectional packing area of the surfactant molecule. This region is also interesting because it demonstrates that compressed surface films will respond to even small increases in surface area, such as by stretching a surface through mechanical vibrations, with a large increase in surface energy of the entire film. In the deposition process, a monolayer can be transferred intact onto the flat

surface of a solid support, called substrate, which is lowered through the monolayer, then into the aqueous subphase, and is then withdrawn. During dipping, the surface pressure of the monolayer on the aqueous subphase should be kept constant.

Since the total number of molecules of surfactant spread at the air/water interface is known, the relation between the film pressure and the area per molecule can be calculated (and measured). The mean molecular area A is given by the relation:

$$A = A_T / CVN_A$$

where, A_T is the available area of the trough, C is the concentration, V is the volume of the spreading solution and N_A is Avogadro's number.

2.9. Nuclear Magnetic Resonance (NMR)

Nuclear Magnetic Resonance (NMR) spectroscopy is the most general and direct tool to identify the structure of almost any organic or biological molecule, as well as that of many inorganic molecules.

NMR is a non-invasive and non-destructive technique which can be used to deduce the molecular structure from the magnetic properties of the atomic nuclei and surrounding electrons; to determine the purity of molecules and to quantify the ratio of mixed compounds. The NMR experiment exploits the magnetic properties of nuclei to provide information on molecular structure [31].

For NMR's purposes, the key aspect of the hydrogen nucleus is its angular momentum properties, which resemble those of a classical spinning particle. Because the spinning hydrogen nucleus is positively charged, it generates a magnetic field and possesses a magnetic moment μ, just as a charge moving in a circle creates a magnetic field.

When both the atomic number (the number of protons) and the atomic mass (the sum of the protons and neutrons) are even, the nucleus has no magnetic properties. Common nonmagnetic nuclei are Carbon (^{12}C) and Oxygen (^{16}O), which therefore are invisible to

the NMR experiment. When either the atomic number or the atomic mass is odd, or both are odd, the nucleus has magnetic properties and is said to be spinning. Those nuclei with a spherical shape have a spin of ½, and those with nonspherical, or quadrupolar, shape have a spin of 1 or more. Common nuclei with a spin of ½ include ^{1}H, ^{13}C, ^{15}N, ^{19}F, ^{29}Si, and ^{31}P. The class of nuclei with I = ½ is the most easily examined by the NMR experiment. Quadrupolar nuclei (I > ½) include ^{2}H, ^{11}B, ^{14}N, ^{17}O, ^{33}S, and ^{35}Cl.

To study nuclear magnetic properties, nuclei are exposed to a strong external magnetic field B_O. When this magnetic field is turned on along a direction designated as the z axis, the energies of the nuclei are affected. There is a slight tendency for magnetic moments to align in the general direction of B_O ($+z$) over the opposite direction ($-z$).

For the spin-half nucleus (such as 1H, 13C or 15N), the splitting is done into two energy levels, corresponding to a nucleus taking up two possible orientations with respect to the static field, either parallel (the α-states) or antiparallel (the β states), the former being lower in energy.

The nuclei in the lower energy level will absorb energy and jump to the higher energy level (classically the magnetic moment will orient antiparallel to the external magnetic field). The relaxation of the excited nuclei back to lower energy level is accompanied by release of electromagnetic radiation. The latter is what we measure in a regular NMR experiment.

References

[1] F. Höök, J. Vörös, M. Rodahl, R. Kurrat, P. Böni, J.J. Ramsden, M. Textor, N.D. Spencer, P. Tengvall, J. Gold and B. Kasemo (2002). *Colloids and Surfaces B: Biointerfaces* 24: 155-170.

[2] J. Malmström, H. Agheli, P. Kingshott and D.S. Sutherland (2007). *Langmuir* 23: 9760–9768.

[3] J. Redepenning, T.K. Schlesinger, E.J. Mechalke, D.A. Puleo and R. Bizios. (1993). *Analytical Chemistry* 65: 3378-3381.

[4] F.H. M. Rodahl, A. Krozer, P. Brzezinski, B. Kasemo (1995). *Review of Scientific Instruments* 66: 3924-3930.

[5] G. Sauerbrey (1959). *Zeitschrift für Physik* 155: 206-222.

[6] G. Binnig, H. Rohrer, C. Gerber and E. Weibel (1982). *Physical Review Letters* 49: 57-61.

[7] G. Binnig, C.F. Quate and C. Gerber (1986). *Physical Review Letters* 56: 930-933.

[8] H.-J. Butt, B. Cappella and M. Kappl (2005). *Surface Science Reports* 59: 1-152.

[9] T.J. Senden (2001). *Current Opinion in Colloid and Interface Science* 6: 95-101.

[10] A.W. Adamson (1990). *Physical Chemistry of Surfaces*. New York, John Wiley & Sons.

[11] P.C. Hiemenz and R. Rajagopalan (1997). *Principles of Colloid and Surface Chemistry*.

[12] A. Marmur (1996). *Colloids and Surfaces A* 116: 55-61

[13] P.C. Hiemenz and R. Rajagopalan (1997). *Principles of Colloid and Surface Chemistry*. New York, Marcel Dekker.

[14] J. Pipper, T.-M. Hsieh and P. Neuzil (2007). Agency for Science, Technology and Research. Patent WO/2007/094739.

[15] R. Pynn (1990). *Los Alamos Science*: Summer.

[16] T.P. Russell (1990). *Materials science reports* 5: 171-271.

[17] M.L. Fernandez, J.S. Higgins, J. Penfold, R.C. Ward, C. Shackleton and D. Walsh (1988). *Polymer* 29: 1923-1928.

[18] M. Tolan and W. Press (1998). *Zeitschrift für Kristallographie* 213: 319–320.

[19] L. Nevot and P. Croce (1980). *Revue de Physique Appliquée* 15: 761-779.

[20] L.G. Parratt (1954). *Physical Review* 95: 359–369.

[21] T. Allen (1975). Particle size measurement. Chapman and Hall. London.

[22] A. Einstein (1905). PhD thesis, University of Zurich.

[23] R.J. Hunter (1981). *Zeta potential in colloid science. Principles and applications*. London, Academic Press.

[24] J.R. Harris (1999). Methods in Molecular Biology 117. N. Hajibahen. New York, Humana Press INC.

[25] M.G. Rossmann, M.C. Morais, P.G. Leiman and W. Zhang (2005). *Structure* 13: 355-362.

[26] H.E. White, S. Chen, A.M. Roseman, O. Yifrach, A. Horovitz and H.R. Saibil (1997). *Nature Structural & Molecular Biology* 4: 690-694.

[27] H.S. Rye, A.M. Roseman, S. Chen, K. Furtak, W.A. Fenton, H.R. Saible and A.L. Horwich (1999). *Cell* 97: 325-338.

[28] K.B. Blodgett (1935). *Journal of the American Chemical Society* 57: 1007–1022.

[29] R.M. Pashley and M.E. Karaman (2004). *Applied Colloid and Surface Chemistry*, John Wiley & Sons**:** 159-169.

[30] L. Wilhelmy (1863). *Annalen der Physik* 119: 177-217.

[31] J.B. Lambert and E.P. Mazzola (2004). *Nuclear Magnetic Resonance Spectroscopy: An Introduction to Principles, Applications, and Experimental Methods*. J. B. Lambert and E. P. Mazzola. New Jersey, Pearson Prentice Hall.

Chapter 3

Mapping bacterial surface layers affinity to polyelectrolytes through the building of hybrid macromolecular structures

3.1 Introduction

Protein adsorption on polyelectrolyte multilayer films has many applications in biotechnology (e.g. biosensor building, enzyme immobilization, protein separations, preparation of stimuli-responsive systems, micropatterning, nanobioreactors, artificial cells and drug delivery systems) [1-3]. It has been found that natural and synthetic polyelectrolytes form strong complexes with a variety of proteins, even when the protein and the polyelectrolyte carry the same charge, a phenomenon explained by charge regulation [4]. Investigations carried out on polyelectrolyte/protein systems such as the interaction of concanavalin A with fucoidan, RNA, heparin and bacterial lipopolysacharides [5] showed that concanavalin A presents common binding sites to neutral polysaccharides and polyelectrolytes that do not contain hexoses or other neutral sugars. The influence of electrolyte concentration on protein/polyelectrolyte complex formation has also been studied for BSA/poly(dimethyldiallylammonium chloride) [6], lysozyme/hyaluronic acid [7], and lysozyme/chondroitin sulphate [8]. Thus, the control of protein-polyelectrolytes interactions is crucial for the design of new highly specific

therapeutic agents [9]. In particular, the affinity of the cell membrane to polyelectrolytes or other biomolecules is important for understanding biological processes, such as ion transport [10], virus activation [11], or ligand-receptor interactions [12-13].

Crystalline bacterial cell surface layers (S-layers) are monomolecular arrays composed of a single (glyco)protein, and exhibit oblique, square, or hexagonal lattice symmetry, with center-to-center spacing between the morphological units in the range of 3–30 nm. S-layers are one of the most common outermost cell envelope components of prokaryotic organisms (bacteria and archaea), and represent the simplest biological membranes developed during evolution [14-15] with a thickness in the range of 5–10 nm.

Isolated S-layer subunits have the ability to self-assemble at the air-water interface [16], on lipid films [17], on liposomes [18] and on solid supports [19]. S-layers are currently used in (nano)biotechnology, diagnostics, vaccine development, biomimetics, molecular nanotechnology and controlled biomineralization [15].

The Layer-by-Layer (LbL) technique [20, 21] has been used successfully for polyelectrolyte multilayer (PEM) deposition onto planar surfaces or spheres [22-24], permitting the gradual and controlled build-up of electrostatically cross-linked films of polycation-polyanion layers. The technique results in formation of layers with thickness controlled by the number of adsorbed layers, and wettability properties determined by the outermost layer [25]. These facts, together with the possibility of building interfaces with desired properties (e.g., degree of charge, length, and hydrophobicity), represent an advantage over other supports (e.g., silicon and mica) for the recrystallization of protein layers in general.

Recently was showed that the combination of polyelectrolyte multilayer deposition and S-layer technology permits to build novel robust biomimetic surfaces and membranes.

Isolated protein subunits of the bacterial cell surface layer from Bacillus sphaericus CCM2177 (SbpA) were self-assembled on polyelectrolyte multilayer supports, with the composition of such multilayers playing a crucial role in determining the structure of the resulting supported protein layers [26]. Successful recrystallization of S-layer proteins could be achieved on the negative charged PSS terminated polyelectrolyte multilayers. This structure mimics to a certain extent the recrystallization on gram-positive bacteria, where the secondary cell wall polymer of B. sphaericus CMM2177 is negatively charged. Recrystallization of SbpA on positive charged PAH-terminated PEM was not as successful as for negative ones. In this case adsorption of S-protein could be observed, without formation of long range order.

In this chapter we present the building of a polyelectrolyte multilayer/S-layer/polyelectrolyte multilayer/S-layer by combining LbL technique and the self-assembly properties of the S-proteins, as a biomimetic sandwich-like macromolecular structure. We also address the affinity of bacterial S-layers to cationic and anionic polyelectrolytes. The surface topography and the mechanical stability of the polyelectrolyte/S-layer complex were investigated with atomic force microscopy. The wetting properties at every deposition step were proven with contact angle measurements. The thickness and the hydration (scattering length density) of the hybrid macromolecular structure were determined by neutron reflectometry.

3.2 Materials and Methods

The bacterial S-layer Protein (SbpA) was isolated from *Bacillus sphaericus* CCM2177. Growth in continuous culture, cell wall preparation, extraction of S-layer protein with 5M guanidine hydrochloride (GHCl), dyalization for 2 hours at 4º C with stirring and

further centrifugation was carried out according to procedures in the literature [27]. The SbpA monomer solution was adjusted to a concentration of 1 mg mL^{-1}.

The polyelectrolytes Poly(ethylenimine) (PEI, Mw = 750 kDa), Poly(sodium 4-styrenesulfonate) (PSS, Mw = 70 kDa) and Poly(allylamine hydrochloride) (PAH, Mw = 70 kDa) were obtained from Sigma-Aldrich (Munich, Germany). They were used as received. Calcium chloride ($CaCl_2$), hydrochloric acid (HCl) and Tris-HCl were purchased from Sigma-Aldrich (Munich, Germany). All solutions were prepared with ultrapure water (Elga Lab Water Systems, Germany) with a specific resistance of 18.2 M cm^{-1}. The same water was always used for rinsing the samples.

Silicon wafers (IMEC, Leuven, Belgium) with a native silicon oxide layer cut into pieces of 1x1cm^2 were used. They were cleaned and made hydrophilic by plasma treatment (Gala Instruments Elektronmikroscopie, Germany). The advancing contact angle of water on silicon wafers was 45±1 degrees. Silicon blocks (Siliciumbearbeitung Andrea Holm, Tann/Ndb., Germany) with dimensions of 80 x 50 x 15 mm^3 were used for neutron reflectometry experiments. They were treated with piranha solution (H_2O_2 (30%)/ H_2SO_4 conc, 1:1 v/v) for 30 min before the deposition of PEM.

Multilayer build-up. The substrates were coated with PE (from a salt free solution) using the LbL technique described in [20]. PEI was used as a precursor to enhance the stability of the alternating adsorbed PSS/PAH multilayers (from 0.5 M NaCl solutions). The polyelectrolyte concentration of the solutions was 10^{-2} M. The hydrophilic Si substrates were dipped alternatively in a beaker containing the polycation or the polyanion solution for 20 min. The substrates were rinsed for 2 minutes in 3 different beakers of water to remove excess polymer after each adsorption step. The cycle was repeated until the desired number of layers had been achieved. S-protein

recrystallization on polyelectrolytes was performed in Tris–HCl buffer (pH 9) in the presence of calcium cations as described in [26].

Atomic Force Microscopy (AFM). The two dimensional topography of the samples in liquid was imaged using multimode atomic force microscope Nanoscope III (Veeco Instruments Santa Barbara, CA). It was operated in contact mode (scan rate 4.70 Hz, at a force about 0.7-1 nN) with silicon nitride (Si_3N_4) cantilevers with nominal spring constant of 0.1 N m^{-1}. A minimum of 20 force curves between the tip and the substrate were carried out at 1000 nm s^{-1}. Scanning (and force-curve measurements) was carried out in aqueous solution (0.1 M NaCl).

Contact Angle Measurements of water on the solid supports were performed with Kruess contact angle measurement system G1 (Kruess, Hamburg, Germany). Measurements were carried out at room temperature. The size and volume of the drops were kept constant.

Neutron Reflectometry. NR experiments were conducted at the neutron reflectometer AMOR at SINQ, Paul Scherrer Institute, Villigen, Switzerland [28-29]. The measurements were performed in Time-of-Flight (ToF) mode at three angles of incidence thus covering the whole necessary Q range. A beam of rectangular cross-section focused on the sample was set by a slit system on the source side. The experiments were always performed with D_2O on the bottom of the experimental cell against a Si block above. In this case the lower medium has a higher scattering length density (SLD) than the upper one. Under these conditions, R = 1 for Q below a critical value Q_c. Above Q_c, R decays with Q and the shape of the dependence is a function of the area-averaged scattering length density profile normal to the interface. The experimentally obtained reflectivity curves were analyzed by applying the standard

fitting routine Parratt 32 [30]. It determines the optical reflectivity of neutrons from planar surfaces with a calculation based on Parratt's recursion scheme for stratified media [31]. The film is modeled as consisting of layers of specific thickness, SLD and roughness, which are the fitting parameters. The model reflectivity profile is calculated and compared to the measured one. Then the model is adjusted by a change in the fitting parameters to best fit the data. For large enough Q values, the layer thickness (d) can be estimated from the spacing of the minima of two neighboring interference fringes ΔQ by the approximation:

$$d \approx 2\pi/\Delta Q \quad (1)$$

The experiments were performed in a solid/liquid experimental cell [32]. The cell basically consists of the Si block on which the polyelectrolyte multilayers were primarily deposited and a Teflon bath tightly pressed against it. The cell allows the liquid (typical volume ~10 mL) in contact with the solid interface to be exchanged. S-protein monomers in Tris-HCl buffer (pH 9) were used for formation of S-layer on top of the previously prepared polyelectrolyte multilayers. An excess volume of the protein solution was injected slowly (15 mL in approximately 60 s) into the cell. This was followed by a delay ("incubation time") of 30 min and then an excessive rinsing with D_2O. The same procedure was used for the formation of PE layers on top of the S-layer, except that the incubation time was 20 min. All NR experiments were performed at room temperature (23 °C).

3.3 Results and Discussion

3.3.1 Building the "sandwich" structure

The hybrid polyelectrolyte multilayer/S-layer macromolecular structure was built using a "bottom-up strategy". The following multilayer structure Si/PEI/(PSS/PAH)2/PSS was used as a cushion for the first SbpA deposition. Toca-Herrera et al. showed in a previous work [26] that S-protein recrystallizes on such substrates forming defect-free domains of about 150 x 150 nm^2. The recrystallization of the protein monomers is possible due to the self-assembly properties of the S-proteins and of calcium ions contained in the solution [26]. The build-up process continued with the deposition of either PSS or PAH onto the already formed S-protein layer. Thus, the affinity of the formed protein layer to polyelectrolytes was tested. It was found that after 20 minutes, only PAH was adsorbed. Although SbpA recrystallizes on cationic PSS, the exposed S-layer surface did not seem to attract PSS, due to the slightly negative surface potential of the recrystallized S-layer under these experimental conditions [26]. Further Layer-by-Layer polyelectrolyte deposition was carried out to continue with the building of the sandwich-like structure. Therefore, cationic PAH was always used as a binding polyelectrolyte to the SbpA protein layer. Contact angle measurements were carried out in order to check the wetting properties of the layers and also to follow the assembly process. The contact angle for water droplets on samples with consecutive structures from Si/PEI/$(PSS/PAH)_2$/PSS to Si/PEI/$(PSS/PAH)_2$/PSS/S-layer/$(PAH/PSS)_3$/S-layer was measured. The value for each deposition step is presented in Figure 3.1.

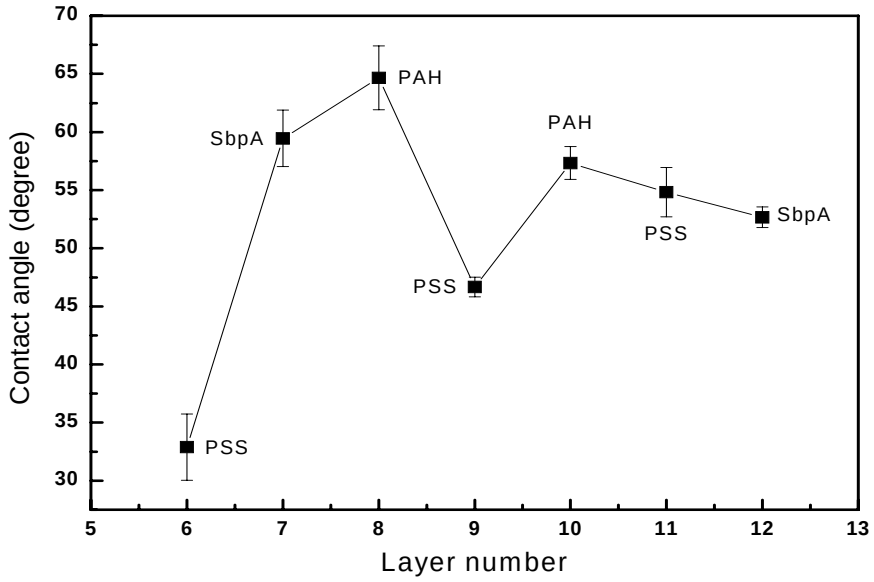

Figure 3.1. Contact angle measurements after each layer deposition. The numbers of the abscise axis refer to the sequential deposition step, while the name of the adsorbed material is indicated near the experimental points.

The saw-tooth like results showed that PE and protein adsorption took place correctly after each deposition step. The PSS interface (32.9 deg) is less hydrophobic than SbpA covered interface (59.4 deg) and the PAH (64.7 degrees) interface. However, the last SbpA protein layer (52.6 degrees) is less hydrophobic than PSS (54.8 degrees). This might be explained by i) irregular polyelectrolyte deposition takes place on the first recrystallized S-layer probably caused by irregularities and defects generated by the different nucleation sites, and ii) partial coverage of the SbpA protein on the last PSS layer (See Figure 3.5). The complexity of the inhomogeneous macromolecular structure cannot even be properly distinguished by neutron reflectometry.

Neutron reflectometry was performed in parallel to contact angle experiments to study the sandwich-like polyelectrolyte/S-layer structures. Thicker PSS terminated polyelectrolyte multilayers with the following structure Si/PEI/$(PSS/PAH)_6$/PSS was

used for this kind of experiments (necessary to perform the experiments in an accessible reflectometer Q range).

Even though a thicker PEM layer was used we assumed that the building process of the further sandwich-like structure was not affected. The experimentally obtained NR curves are presented in Figure 3.2.

The minima of the Kissig fringes of the consecutive curves were shifted to smaller Q-values which demonstrates an increase in film thickness after each deposition step.

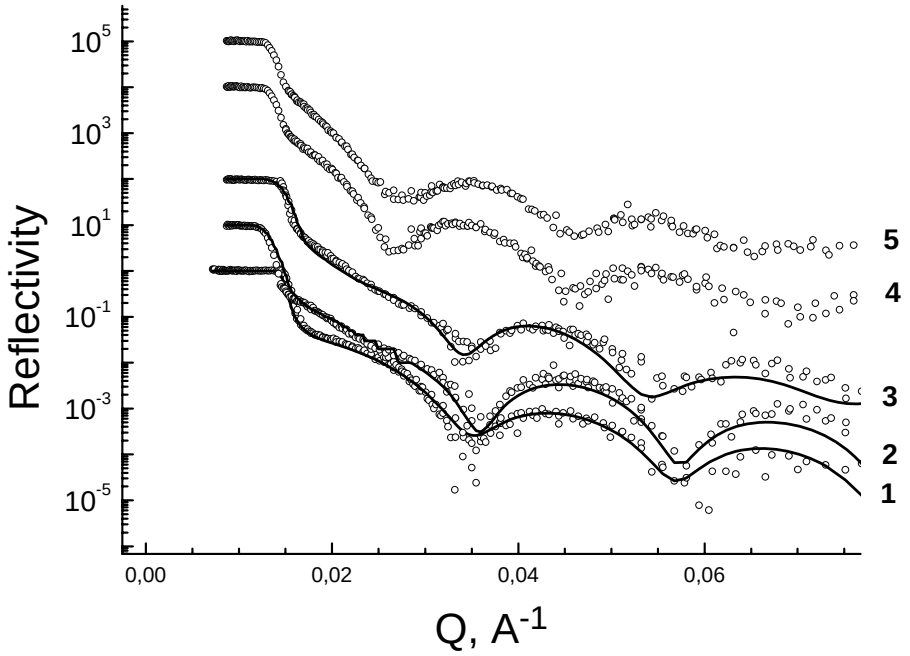

Figure 3.2. Neutron reflectivity as a function of Q for the following macromolecular structures: 1- Si/PEI/$(PAH/PSS)_6$/PSS, 2- Si/ PEI/$(PAH/PSS)_6$/PSS/SbpA, 3- Si/ PEI/$(PAH/PSS)_6$/PSS/SbpA/PAH, 4- Si/ PEI/$(PAH/PSS)_6$/PSS/SbpA/$(PAH/PSS)_2$ and 5-Si/PEI/$(PAH/PSS)_6$/PSS/SbpA/$(PAH/PSS)_2$/SbpA. Curves 2 and 3 show respectively the adsorption of SbpA on PSS and the affinity of PAH to the S-layer. Note that curves 4 and 5 are similar, meaning that no homogenous SbpA adsorption took place.

The NR data were fitted and the parameters, which gave the best fits to the experimental data, are summarised in Table 3.1.

Step No:	Sample		h, nm	SLD, $x10^{-6}Å^{-2}$
1.	Si/PEI/$(PSS/PAH)_6$/PSS	Cushion	28.0	3.60
2.	Si/PEI/$(PSS/PAH)_6$/PSS/ S-layer	Cushion	27.6	3.25
		S-layer	13.0	4.84
3.	Si/PEI/$(PSS/PAH)_6$/PSS/ S-layer/PAH	Cushion	29.4	3.85
		S-layer + PAH	16.1	5.67
4.	Si/PEI/$(PSS/PAH)_6$/PSS/ S-layer/$(PAH/PSS)_2$	Total thickness	33.4	---
5.	Si/PEI/$(PSS/PAH)_6$/PSS/ S-layer/$(PAH/PSS)_2$/ S-layer	Total thickness	33.2	---

Table 3.1. Thickness and Scattering length density of the resulting hybrid macromolecular structure for different coating steps. A two layer model is used to determine the layer thickness (h) and the scattering length density (SLD). See the text for details.

The NR curve from the bare PSS/PAH cushion was fitted with a single box model, representing the polyelectrolyte multilayer between two semi-infinite phases – Si support and bulk D_2O. The thickness and the SLD of the bare polyelectrolyte multilayer cushion are typical for the studied system. The fitting of the reflectivity curve of the recrystallized S-protein layer was possible only using two layers model. The first layer represents the polyelectrolyte multilayer cushion. The fitting parameters were similar to those of the bare polyelectrolyte multilayer. On top of it another layer was formed. The values of the thickness (ca. 13 nm) and of the scattering length density (ca. 4.84 $Å^{-2}$) were very close to that we already reported for S-layer formation [26]. The deposition of a PAH layer onto the SbpA layer led to an increase in thickness and SLD of the second layer. Precise distinction between the S-layer and the PAH layer was not possible. If one compares only the increase in thickness of the second layer it will result in an increase of around 3 nm which may be attributed to formation of a PAH layer under the experimental conditions used [34].

Another feature of this last layer is the increase of its SLD. This proves changes in the structure of the S-protein layer becoming more hydrophilic[33].Further NR experiments were performed with the samples Si/PEI/$(PSS/PAH)_6$/PSS/SbpA/$(PAH/PSS)_2$ and Si/PEI/$(PSS/PAH)_6$/PSS/SbpA/$(PAH/PSS)_2$/SbpA. The fitting of the NR curves with different and complicated multi box models did not increase the quality of the data fit. The film thickness was estimated in these cases only from the position of the minima of the Kissig fringes using Eq. (1) (see Table 3.1). It showed an increase in film thickness in the case of deposition of the polyelectrolyte layers. The deposition of a last S-protein layer was not successful; a fact confirmed by the reflectivity curves 4 and 5 in Figure 3.2.

3.3.2 Surface topography and mechanical stability of the "sandwich" structure

AFM images of the obtained nano structures are shown in Figure 3.3. The AFM deflection image showed the typical S-layer structure similar to that found in bacteria[14].

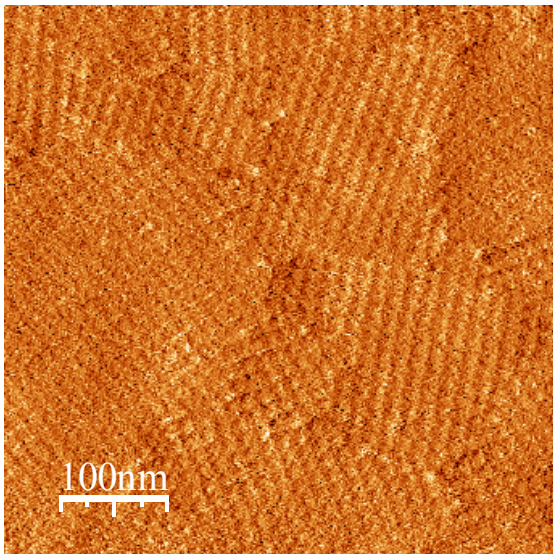

Figure 3.3. AFM deflection image (contact mode) of S-layers recrystallized on Si/PEI(PSS/PAH)$_2$/PSS (z-range: 2 nm).

The AFM tip/S-layer interaction and the mechanical properties of the recrystallized S-layer are shown in Figure 3.4.

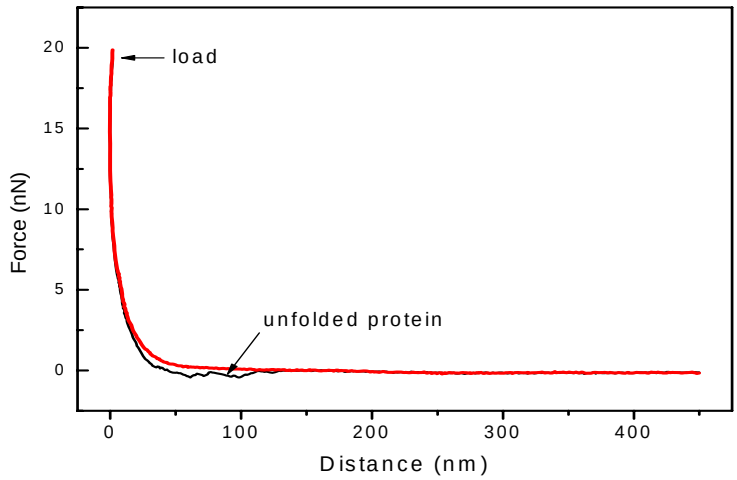

Figure 3.4. The red line of the force-distance curve shows the approach of the AFM tip, while the black line refers to the retrace curve, when the AFM tip leaves the S-layer surface. Loads of 20 nN unfold the S-layer proteins.

The red line of force-distance curve represents the tip-S-layer interaction while the tip approaches the sample. The black line, the retracing curve (the tip leaves the surface), showed that loads of 20 nN induced the unfolding of some S-protein domains of the original 2-D crystalline structure (see Figure 3.5).

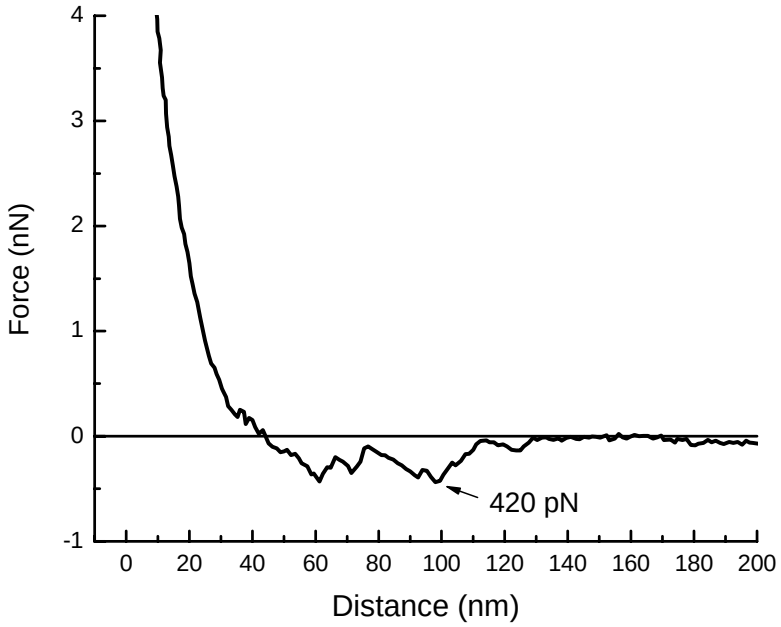

Figure 3.5. Detail of the retracing curve shown in (b). The peaks show that S-proteins unfold mechanically at about 420 pN, an order of magnitude that has been found for muscle proteins like titin [38].

Former experiments showed that S-layers on polyelectrolytes were mechanically more stable than S-layers recrystallized on silicon; it was found that loads of 15 nN were able to unfold the recrystallized S-layer on silicon, but not on PSS [26].

The affinity of the bacterial surface layer to polylectrolytes was investigated by exposing the S-layer to cationic PAH and anionic PSS. Cationic PAH was adsorbed on the S-layer after 20 min, causing the disruption of the 2-D structure (Figure 3.6). On the contrary, PSS did not adsorb. Figure 3.7 shows the intact S-layer pattern.

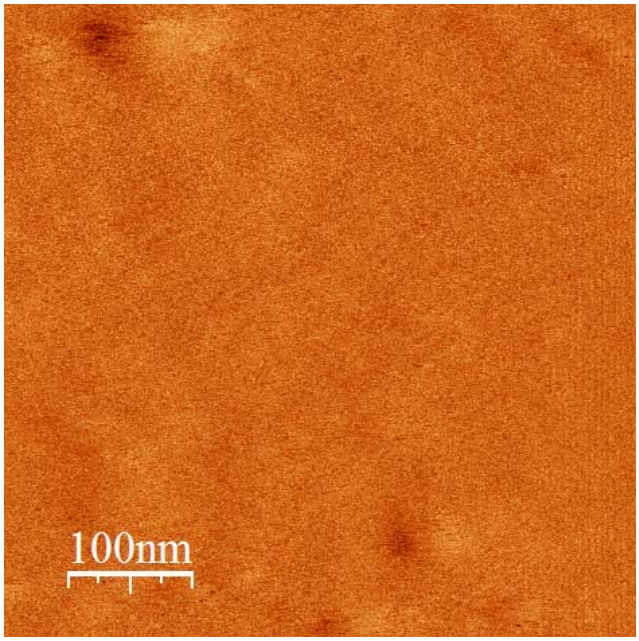

Figure 3.6. AFM deflection image of adsorbed PAH on S-layer (z-range: 2 nm).

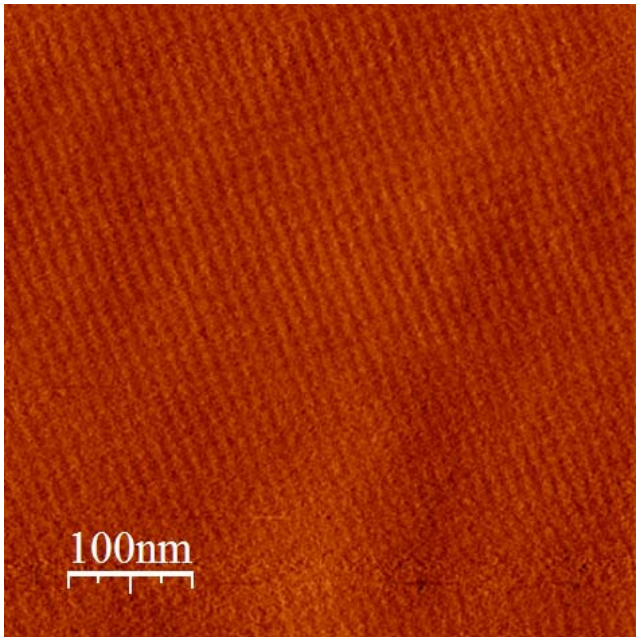

Figure 3.7. AFM deflection image after adsorbing PSS for 20 minutes, the S-layer structure remained intact (z-range: 2 nm).

This indicates that the exposed side of the S-layer does not attract negative polyelectrolytes in this time-scale. Experiments carried out in the Center of Nanobiotechnology from Vienna showed that DNA cannot be adsorbed on S-layers coated liposomes. Adsorption of DNA on S-layers can be achieved by chemical

modification with ethylendiamine, converting the negatively carboxyl groups into free amino groups (S. Küpcü, *manuscript in preparation*). The non-specificity of the S-layer surface to negative polyelectrolyte such as PSS (and DNA) may be related to the protective function of S-layer, meaning that other molecules of the cell wall drive signalling processes.

The mechanical stability of the adsorbed PAH on recrystallized S-layer is shown in Figure 3.8. The retracing curve (black line) shows that forces of about 750 pN led to the appearance of the elastic polyelectrolyte domains along to 250 nm.

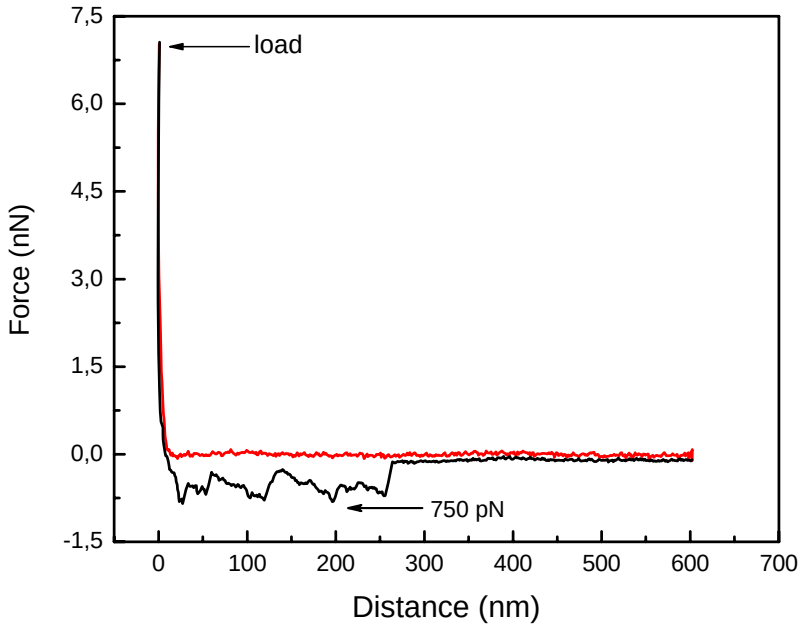

Figure 3.8. Force-distance curve showing unfolding peaks of the adsorbed PAH on S-layer.

The second adsorption of SbpA protein monomers was carried out on Si/PEI/$(PSS/PAH)_6$/PSS/S-layer/$(PAH/PSS)_2$. The final surface presented many irregularities. However, SbpA adsorption on several areas could be observed, and more important, the S-layer structure could be recognized (see Figure 3.9).

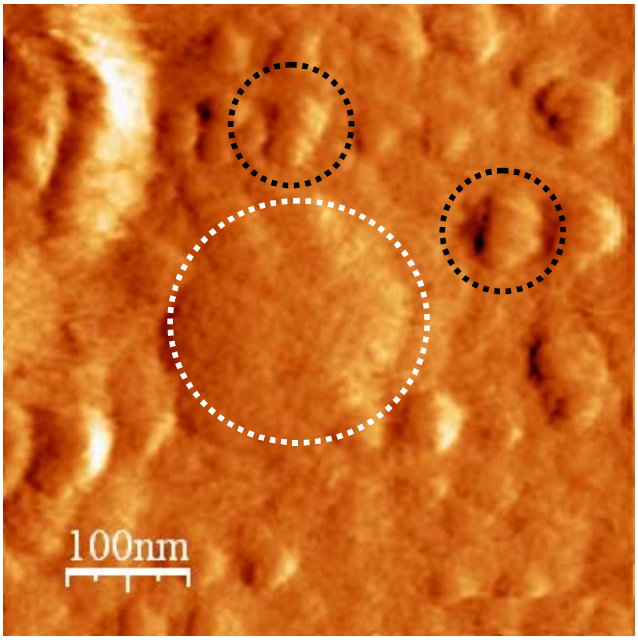

Figure 3.9. AFM deflection image measured in contact mode for the system Si/PEI/$(PSS/PAH)_2$/PSS/SbpA/$(PAH/PSS)_3$/SbpA (z-range: 1.3 nm). S-layer structure can be seen inside the white empty circle. The black empty circles show protein adsorption.

Force-distance curves (Figure 3.10) taken on the area with recrystallized S-layer showed that loads of ca. 9nN induced small adhesion peaks (Figure 3.11) of about 150 nN.

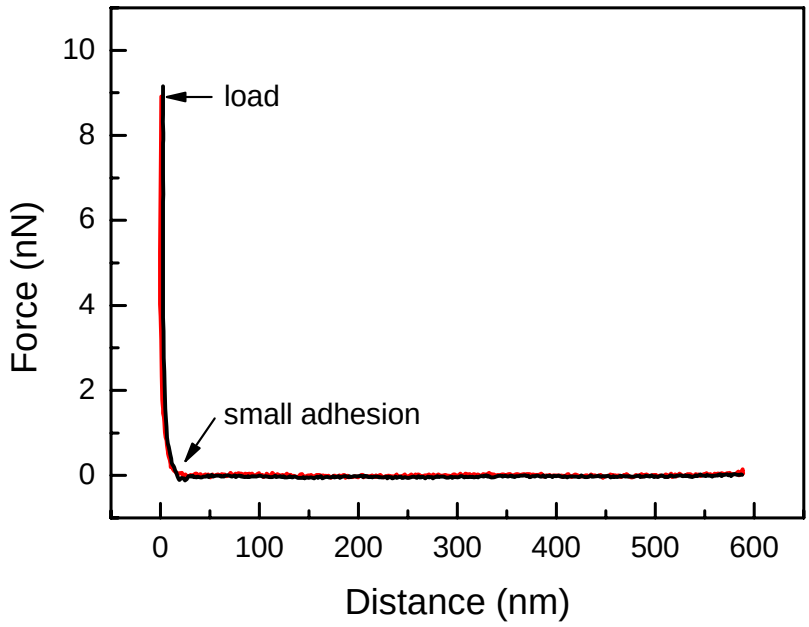

Figure 3.10. Force-distance curve taken at the center of the largest circle shows that the approaching and the retracing curves superposed each other.

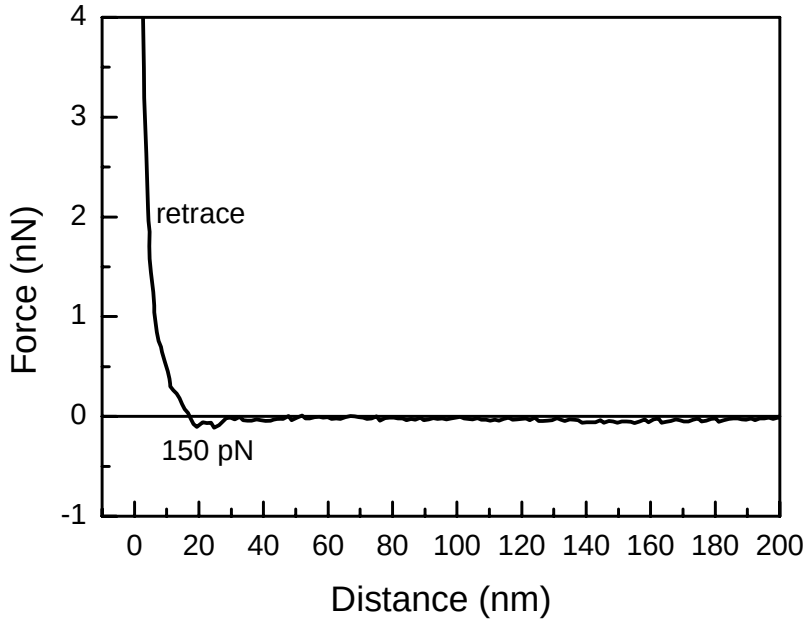

Figure 3.11. The magnification of Figure 3.10 show small adhesion peaks (around 150 pN) for a load of 9 nN. Notice that these peaks are different in length and force from the unfolding peaks shown in Figure 3.4c (both figures have the same scale for comparison).

Thus S-layers patches present a lower mechanical stability than larger S-layer domains recrystallized on PSS [26]. However, applied loads of 4 nN did not lead to adhesion peaks (additional information), which is a typical feature of robust recrystallized S-layers [26, 34, 35].

3.4 Conclusions

A sandwich-like supramolecular structure has been built by combining polyelectrolyte multilayer deposition and S-layer technology. SbpA protein recrystallization took place only on anionic PSS. However, only cationic PAH shows affinity to the exposed crystalline S-layer surface since no adsorption of anionic PSS could be observed. A

compression of 20 nN unfolds the S-layer proteins, constituting the limit of the mechanical stability of recrystallized S-layers on PSS.

Further polyelectrolyte adsorption of three polyelectrolyte bilayers PSS-terminated on S-layer was achieved. The inhomogeneity of the sandwich-like supramolecular structure induced formation of recrystallized S-layer patches after a second adsorption of SbpA monomers, with a mechanical stability of 9 nN. Our results also suggest that the S-layer surface should be chemically modified in order to attract negative polyelectrolytes. This work represents a novel strategy to build new supramacromolecular structures adsorbing S-proteins. Future work involves: i) optimization of the macromolecular building process, ii) the building of biomimetic surfaces adsorbing fusion proteins with different biological functionalities [15, 36, 37] and iii) use of polyelectrolytes with different electrical and hydrophobic properties as antibacterial surface layer agents, which is in progress in our laboratory.

References

[1] E. Kokufuta (1992). *Progress in Polymer Science* 174: 647-697.

[2] A. Griffith, A. Glidle and J.M. Cooper (1996). *Biosensors and Bioelectronics* 11: 625-631.

[3] H. Ai, S.A. Jones, Y.M. Lvov and P.R. Price (2003). *Cell Biochemistry and Biophysics* 39: 23-43.

[4] F.L.B. da Silva, L. Lund, B. Jonsson and T. Akesson (2006). *Journal of Physical Chemistry B* 110: 4459-4464.

[5] R.J. Doyle, E.E. Woodside and C.W. Fishel (1968). *Biochemistry Journal* 106: 35-40.

[6] E. Seyrek, P.L. Dubin, C. Tribet and E.A. Gamble (2003). , *Biomacromolecule*s 4: 273-282.

[7] J.M. Moss, M.P. VanDamme, W.H. Murphy and B.N. Preston (1997). *Archives of Biochemistry and Biophysics* 348: 49-55.

[8] F. Carlsson, P. Linse and M. Malmsten (2001). *Journal of Physical Chemistry B* 105: 9040-9049.

[9] Capila and R.J. Linhardt (2002). *Angewandte Chemie International Edition* 41: 390-412.

[10] D. Joseph, O. Tirmizi, X-L. Zhang, E.D. Crandall and R.L. Lubman (2002). *American Journal of Physiology: Lung Cell Molecular Physiology* 282: 675-683.

[11] T. Stegmann, F.P. Booy and J. Wilschut (1987). *Journal of Biological Chemistry* 262: 17744-17749.

[12] C.A. Helm, W. Knoll and J.N. Israelachvili (1991). *The Proceedings of the National Academy of Sciences* 88: 8169-8173.

[13] R. Merkel, P. Nassoy, A. Leung, K. Ritchie and E. Evans (1999). *Nature* 397: 50-53.

[14] U.B. Sleytr, P. Messner, D. Pum and M. Sara (1999). *Angewandte Chemie International Edition* 38: 1034-1054.

[15] U.B. Sleytr, M. Sara, D. Pum and B. Schuster (2001). *Progress in Surface Science* 68: 231-278.

[16] D. Pum and U.B. Sleytr (1996). *Landers Academic Press, Austin, TX*, 175.

[17] B. Schuster and U.B. Sleytr (2000). *Reviews of Molecular Biotechnology* 74: 233-254.

[18] S. Küpcü, M. Sara and U.B. Sleytr (1995). *Biochimica et Biophysica Acta* 1235: 263-269.

[19] D. Pum and U.B. Sleytr (1994). *Thin Solid Films* 244: 882-886.

[20] G. Decher (1997). *Science* 277: 1232-1237.

[21] Y. Lvov, G. Decher and H. Möhwald (1993). *Langmuir* 9: 481-486.

[22] X. Shi, M. Shen and H. Möhwald (2004). *Progress in Polymer Science* 29: 987-1019.

[23] E. Donath, S. Moya, B. Neu, G.B. Sukhorukov, R. Georgieva, A. Voigt, H. Baumler, H. Kiesewetter and H. Möhwald (2002). *Chemistry* 8: 5481-5485.

[24] Y. Lvov and G.B. Sukhorukov *Membr.* (1997). *Cell Biology* 11: 277-303.

[25] M. Schoenhoff (2003). *Current Opinion* in *Colloid* and *Interface Science* 8: 86-95.

[26] J.L. Toca-Herrera, R. Krastev, V. Bosio, S. Küpcü, D. Pum, A. Fery, M. Sara and U. B. Sleytr (2005). *Small* 1: 339-348.

[27] U.B. Sleytr, M. Sara, S. Küpcü and P. Messner (1986). *Archives of Microbiology* 146: 19-24.

[28] D. Clemens, P. Gross, P. Keller, N. Schlumpf and M. Konnecke (2000). Physica B 276: 140-141.

[29] http://sinq.web.psi.ch/sinq/instr/amor.html

[30] C. Braun. Parratt 32 Program for reflectivity fitting Hahn-Meitner Institute: Berlin, 1999.

[31] J.J. Ramsden, Yu.M. Lvov and G. Decher (1995). *Thin Solid Films* 254: 246-251.

[32] C. Delajon, T. Gutberlet, R. Steitz, H. Möhwald and R. Krastev (2005). *Langmuir* 21: 8509-8514.

[33] The amount of D_2O (x) in a polymer layer can be estimated from the experimental SLD value ρ_{exp} of the sample, the SLD of the sample in dry state ρ_{dry} and the SLD of D_2O, using: $\rho_{exp} = x\ \rho_{D2O} + (1\text{-}x)\ \rho_{dry}$

[34] E.S. Gyorvary, O. Stein, D. Pum and U.B Sleytr (2003). *Journal of Microscopy* 212: 300-306.

[35] J.L. Toca-Herrera, S. Moreno-Flores, J. Friedmann, D. Pum and U.B. Sleytr (2004). *Microscopy Research and Technique* 65: 226-234.

[36] N. Ilk, S. Küpcü, G. Moncayo, S. Klimt, R. Ecker, R. Hofer-Warbinek, E.M. Egelseer, U.B. Sleytr and M. Sara (2004). *Biochemistry Journal* 377: 441-448.

[37] J.L. Toca-Herrera, S. Küpcü, V. Diederichs, G. Moncayo, D. Pum and U.B. Sleytr (2006). *Biomacromolecules* 12: 3298-3301.

[38] R.B. Best, S.B. Fowler, J.L. Toca-Herrera, A. Steward, E. Paci and J. Clarke (2003). *Journal of Molecular Biology* 330: 867-877.

Chapter 4

Thermal stability, mechanical properties and water content of bacterial protein layers recrystallized on polyelectrolyte multilayers

4.1 Introduction

Among many biomolecular structures, bacterial surface layers (S-layers) represent an important biopolymer in nature with great potential for the building of nanostructured biomimetic surfaces [1]. A crucial biological issue regarding S-layers and other proteins such as whey milk protein [2], hen egg-white lysozyme [3] or spectrin of human red blood cells [4] is their stability in different solvents or under temperature change.

Crystalline bacterial cell surface layers (S-layers) are monomolecular arrays composed of a single (glyco)protein, and exhibit oblique, square, or hexagonal lattice symmetry, with center-to-center spacings between the morphological units in the range of 3–30 nm. S-layers represent the simplest biological membranes developed during evolution with a thickness in the range of 5–10 nm [5]. Isolated S-layer subunits have the ability to self-assemble at the air-water interface [6], on lipid films [7], on liposomes [8] and on polyelectrolyte supports [9], making them an important tool for biophysical and technological studies [10]. A complete description of the S-protein self assembly can be found in references [11] and [12].

It is accepted that S-layers contribute to bacterial protection against adverse conditions and display an unusual physical and chemical stability [13]. Therefore it is interesting to investigate and understand how such persistent protein structures developed by bacteria respond to environmental stress conditions. Previous work carried out on S-layers from mesophilic (optimum growth temperatures 20-45°C) and thermophilic [14] (optimum growth temperatures from 55°C to 100°C) microorganisms has shown to be thermostable at very high temperatures. S-layer of *Comamonas acidovarans* retains its native folding to about 90ºC [15] and S-layer of *Campylobacter fetus* is stable up to 100ºC [16]. Most thermophilic bacteria contain S-layer, suggesting that such two-dimensional nanostructures play an important role in membrane integrity at high temperature and, therefore, in cell viability [17].

Former results showed that recrystallization of S-proteins (from *Bacillus sphaericus*) on secondary cell wall polymer (SCWP), its natural support in bacteria, enhanced its thermal stability in comparison with S-layers recrystallized on silicon wafers [18]. However, that study did not address either the S-protein adsorbed mass, after the self-assembly process that leads to the protein crystal structure, or the water volume fraction of the protein layer, facts that play an important role in the stabilization of the tertiary and quaternary structure as well as in the interactions between the macromolecules.

Quartz microbalance with dissipation (QCM-D) has been used in the last decade to investigate protein adsorption [19] or antibody-antigen kinetics [20]. More recently, QCM-D has been combined with i) ellipsometry and atomic force microscopy to follow lipid vesicle deposition on mica [21], ii) optical waveguide lightmode spectroscopy to investigate the density, the refractive index and the structure of adsorbed native and denatured proteins layers [22], and iii) surface plasmon resonance to show that the water mass sensed by the quartz microbalance is not only originated from water entrapped

within supramolecular assemblies and from water dynamically entrapped between adsorbed biomacromolecules [23].

Neutron reflectometry has been used to monitor the in-situ adsorption of phospholipid layers at the solid liquid interface [24] and has been combined with atomic force microscopy to study the affinity of polyelectrolytes to the bacterial surface layer [25].

Quartz microbalance with dissipation monitoring, atomic force microscopy and neutron reflectometry have been combined to investigate the recrystallization and structure of bacterial cell surface layers (SbpA proteins from *Bacillus sphaericus* CCM2177) on anionic terminated polyelectrolyte multilayer (PEM) cushion. Quartz microbalance with dissipation measures the adsorbed mass coupled to the surface of a piezoelectric device, therefore it has been used to estimate the S-protein mass adsorption on polyelectrolyte multilayers. The surface topology of the polyelectrolyte/S-layer system for different temperatures and the mechanical properties of the protein layer have been studied with atomic force microscopy. Thus, the critical denaturation temperature (T_{cd}) for recrystallized SbpA proteins on a PEM cushion has been determined. The film thickness of the hybrid/S-protein system has been determined by NR, while its water content could be determined by combining NR and QCM-D.

4.2 Materials and Methods

Chemicals. Poly(ethylenimine) (PEI, Mw = 750 kDa), Poly(sodium 4-styrenesulfonate) (PSS, Mw = 70 kDa) and Poly(allylamine hydrochloride) (PAH, Mw = 70 kDa) were obtained from Sigma-Aldrich (Munich, Germany) and used as received. Perdeuterated poly(sodium 4-styrenesulfonate) (dPSS, Mw = 80 kDa) was purchased from Polymer Standards Service (Mainz, Germany). Deuterium oxide (D_2O) with min. 99.9% isotope

enrichment was purchased from Sigma-Aldrich (Germany). The aqueous solutions were prepared with ultrapure water from a Milli-Q Plus 185 water generation system (Millipore, resistivity >18.2 MΩ cm).

Silicon wafers (IMEC, Leuven, Belgium) with a native silicon oxide layer were cut into pieces 1x1cm^2 in size, cleaned and made hydrophilic by plasma treatment (Gala Instruments Elektronmikroscopie, Germany).

Silicon blocks (Siliciumbearbeitung Andrea Holm, Tann/Ndb., Germany) of 8x5 x1.5 cm^3 were used for neutron reflectometry experiments. They were cleaned with piranha solution (H_2O_2 (30%)/ H_2SO_4 conc, 1:1 v/v) for 30 min and then thoroughly washed with ultrapure water before the deposition of polyelectrolyte multilayers (PEM).

SbpA bacterial cell surface layer protein (S-layer) was isolated from *Bacillus sphaericus* CCM2177. Growth in continuous culture at 30º, cell wall preparation, extraction of S-layer protein with 5M guanidine hydrochloride (GHCl), dyalization and further centrifugation were carried out according to literature procedure [26]. The SbpA monomer solution used for recrystallization experiments was adjusted with Milli-Q water to a concentration of 1 mg mL^{-1}.

SbpA recrystallization on polyelectrolyte multilayers (PEM). Prior to S-layer deposition, silicon wafers and blocks were coated with PEM using the Layer-by-Layer technique [27]. The deposition was performed from polyelectrolyte solutions with a concentration of 10^{-2} M based on the monomer unit and a NaCl concentration of 0.5 M. Coated silicon wafers had the structure: Si/PEI/$(PSS/PAH)_2$/PSS. The coated silicon blocks for NR studies were with the structure Si/PEI/$(dPSS/PAH)_6$dPSS. SbpA protein recrystallization experiments on Si wafers were carried out in mini Petri dishes (30 mm diameter, 5 mL volume). The wafers were immersed and kept overnight in buffer

solution containing protein monomers (the protein:buffer volume ratio was 1:9). The buffer consisted of 0.5 mM Tris-HCl, pH 9, with 10 mM $CaCl_2$. The samples with recrystallized protein were washed with Milli-Q water before starting the experiments.

For neutron reflectometry experiments, S-layer recrystallization was performed in a home-made solid/liquid experimental cell [28]. The experimental cell permits the liquid exchange (typical volume ~ 10 mL) in contact with the solid interface, thus deposition of the protein layers can be followed in-situ. The protein in recrystallizing H_2O buffer solution was used for the formation of the S-layer on top of the previously prepared PEM. An excess volume of the solution was injected slowly (15 mL in approximately 60 s) into the cell. This was followed by a delay ("incubation time") of 60 min and then extensively rinsed with D_2O. All neutron reflectometry experiments were performed against D_2O, thus assuring high scattering intensity.

Quartz Crystal Microbalance with Dissipation Monitoring (QCM-D). Adsorption and viscoelastic studies on S-proteins adsorbed on PEM were carried out with a QE401 (electronic unit)/QFM401 (flow module) instrument from Q-sense AB (Gothenburg, Sweden). The QCX301 gold crystals (Q-Sense AB, Gothenburg, Sweden) were cleaned before surface preparation by immersion in a 6:1:1 (vol/vol) solution of H_2O:NH_3(25%):H_2O_2 (30%) at 70ºC for 10 min followed by rinsing with Milli-Q water and drying in a stream of nitrogen gas. Before mounting the crystals in the flow chamber they were treated with UV/ozone for 30 min. A volume of 0.5 ml of temperature-equilibrated polyelectrolyte or SbpA protein solution was pumped through the measurement chamber in order to study the PEM deposition and S-layer protein adsorption processes by continuously recording the sets of resonances frequencies and dissipation factors. The QCM-D data were analyzed with Q-Tools (software provided by Q-Sense).

Atomic Force Microscopy (AFM). The surface topography of recrystallized and denatured S-proteins was imaged in aqueous solution (0.1 M NaCl), operating at room temperature in contact mode (scan rate 4.70 Hz, at a scanning force of about 0.7-1 nN) with a Nanoscope III multimode (Veeco Instruments, Santa Barbara, CA). Silicon nitride (Si_3N_4) cantilevers with nominal spring constant of 0.1 N m^{-1} were used. The thermal experiments were carried out as follows: the protein layer was exposed for 10 minutes to water at different temperatures ranging from 25ºC to 60ºC, after that, the samples were allowed to reach room temperature and were imaged. AFM images were treated using the WSxM program [29].

Neutron Reflectometry (NR). Prior to the NR experiments the silicon blocks were coated with polyelectrolytes. The last layer was PSS. The NR experiments started with in-situ deposition of S-protein layer onto the reference bare polyelectrolyte layer. Thus, silicon/polyelectrolyte/S-layer complex were prepared at 25 °C. The formation of the S-layer was performed in H_2O. The H_2O subphase was exchanged to D_2O after the formation of the S-layer. All further NR experiments were performed only against D_2O. The temperature was risen from 25 °C up to 60 °C with a step of 5 °C and then was gradually decreased down to room temperature. NR curves were collected at each step. Experiments were carried out in Time-of-Flight (ToF) mode at the neutron reflectometer instrument AMOR at SINQ, Paul Scherrer Institute, Villigen, Switzerland at three angles of incidence [30, 31]. The experimentally obtained reflectivity curves were analyzed by applying standard fitting routine.

4.3 Results and Discussion

The build-up process of the polyelectrolyte multilayer and the adsorption of S-layer protein were continuously monitored using QCM-D as shown in Figure 4.1.

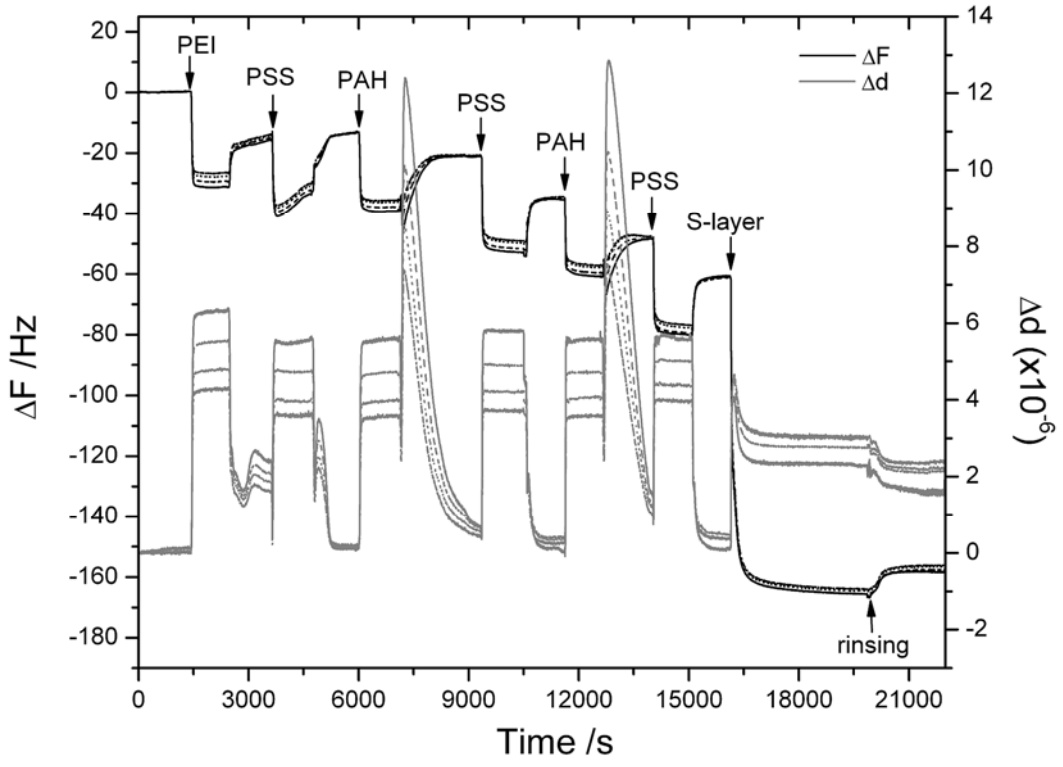

Figure 4.1. Representative measurement of the changes in frequency (ΔF- black line) and dissipation (ΔD- grey line) for polyelectrolyte multilayer deposition and further S-layer protein adsorption as a function of time. The overtones shown are: 5^{th}, 7^{th}, 9^{th} and 11^{th}. Note that the different overtones for ΔF are closed to each other, while there is a slightly separation for ΔD. However, the amount of adsorbed protein on the polyelectrolyte multilayer can be calculated with the Sauerbrey equation.

At t = 1400 s, the gold surface is exposed to the PEI solution, resulting in a decrease in frequency (f) and an increase in the dissipation (d). At t = 2500 s, polyelectrolyte deposition is interrupted by exchange to Milli-Q water. At t = 3600 s, Milli-Q water is changed to PSS solution. The polyelectrolyte multilayer formation continued with the

deposition of PAH, PSS, PAH and PSS. Finally, S-layer protein solution was injected in the experimental cell at t = 16000 s and was let for adsorption at least during one hour, and afterwards the excess of protein was removed with Milli-Q water. The changes in frequency and dissipation as a function of polyelectrolyte multilayer deposition and S-layer proteins adsorption after washing with Milli-Q water are shown in Figure 4.2.

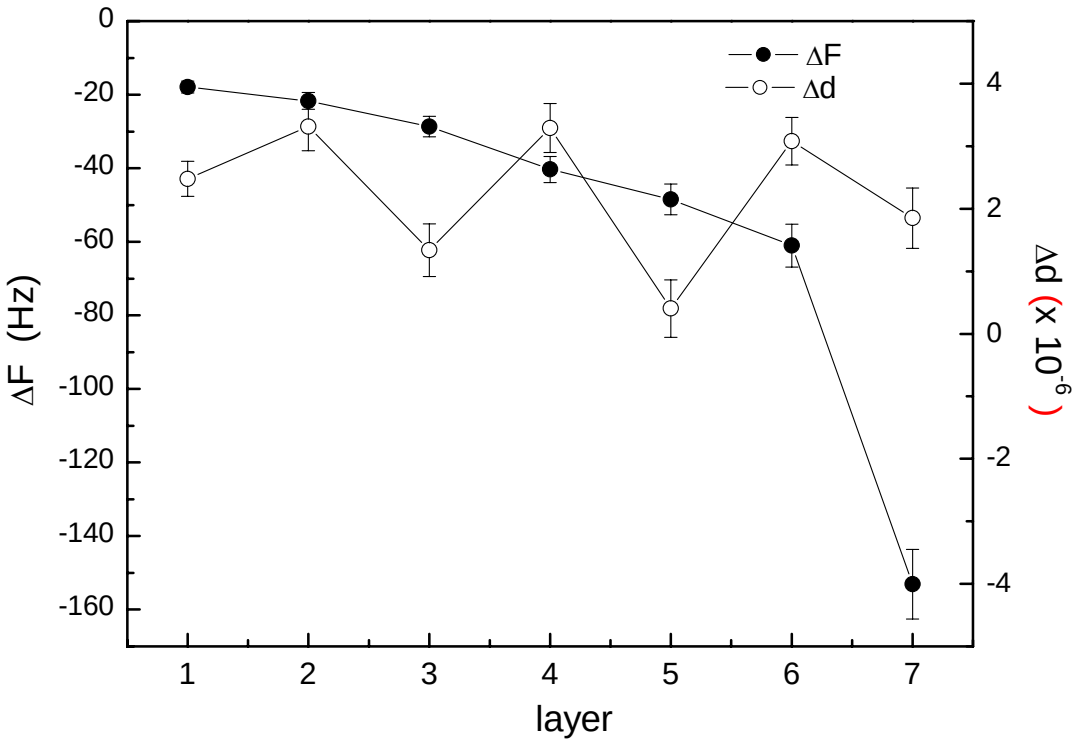

Figure 4.2. Changes in frequency (filled circles) and dissipation (empty circles) equilibrium values measured in water after removing the polyelectrolyte and protein solutions for the 5th overtone. The polyelectrolyte deposition induces a monotonous decay (of about 9 Hz) while for S-protein adsorption is more pronounced (ca. 92 Hz).

A uniform decrease in the frequency is noticed after every polyelectrolyte layer deposition (see Figure 4.2), due to the adsorbed polyelectrolyte mass [32].

The decrease in the frequency (92 Hz) due to the adsorption of S-proteins corresponds to a surface mass of about 1600 ng/cm^2 according to Sauerbrey equation [33, 34]:

$$\Delta m = C\frac{\Delta f}{n}$$

Where, Δf is the shift of the resonance frequency, C = 17.7 ng cm^{-2} Hz (at f=5 MHz) is the mass sensitivity constant and n (=1, 3, 5, . . .) is the overtone number (the data shown in the manuscript are already divided by the overtone number, which is a feature of the Q-Tools software). The Sauerbrey equation, that considers the film as rigid, is an appropriate approximation when $\Delta D/\Delta f < 0.2 \times 10^{-6}$ Hz^{-1} as explained in the work of Glasmäster et al. (2002) [35].

Figure 4.2 shows (for the 5th overtone) that PSS adsorption decreases the dissipation in comparison with PEI. Further deposition of PAH led to an increase in the dissipation compared to PSS. Finally, the adsorption of S-layer proteins was followed by an increase in the dissipation comparing with PSS.

Once the adsorption of S-proteins on anionic terminated polyelectrolyte multilayers took place, atomic force microscopy was used to investigate the sample surface topography as a function of temperature.

Figure 4.3 shows a typical 2-D structure of S-layer recrystallized on PSS-terminated polyelectrolyte multilayers at 25ºC, with lattice parameters a = 14.3±1 nm, b = 13.4±1 nm and γ = 94.1±0.8 degree, similar to those reported previously [9].

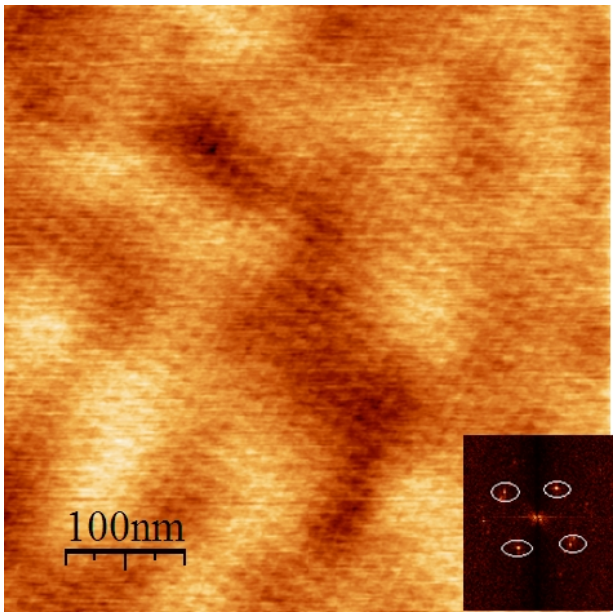

Figure 4.3. AFM height image of S-layers recrystallized on Si/PEI(PSS/PAH)$_2$/PSS (z-range: 2 nm, roughness: 0.27 nm), performed at 25ºC in 100 mM NaCl aqueous solution. Note the large extension of the recrystallized S-layer, ca. 1 x 1 μm^2, and the square lattice P4 (see text) structure typical for SbpA. The Fourier transform of the S-layer nanostructure is shown down at the right corner.

A force-distance curve (load 10 nN) is shown in Figure 4.4. The empty circles represent the AFM-tip/S-layer interaction while the tip approaches the sample and the filled circles correspond to the retracing curve (the tip leaves the protein surface layer). The approaching curve does not show the typical curvature of the electrostatic repulsion. Neither adhesion nor protein unfolding events are observed in the retracing curve; this is a common feature for recrystallized S-layer at these applied loads (approaching and retracting curves superpose each other) [18].

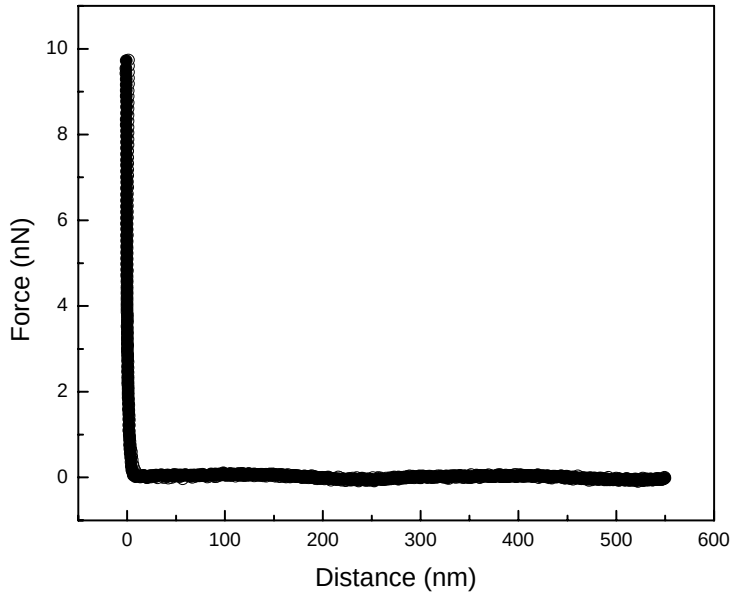

Figure 4.4. Force-distance curve measured in 100 mM NaCl aqueous solution. The approaching curve (empty circles) shows the AFM tip-S-layer interaction. Since the Debye-length is 0.96 nm a possible electrostatic repulsion is screened. The retracting curve (filled circles) indicates that no unfolding events are observed at loads of 10 nN. It is difficult to distinguish both curves because they superpose each other.

The samples were gradually heated up to 60 ºC and the AFM experiments were performed at each step. It was found that at 55ºC, the 2-D crystalline S-layer structure was lost (see Figure 4.5), with the characteristic square symmetry (P4) vanishing into a more amorphous phase, as shown by the Fourier transform.

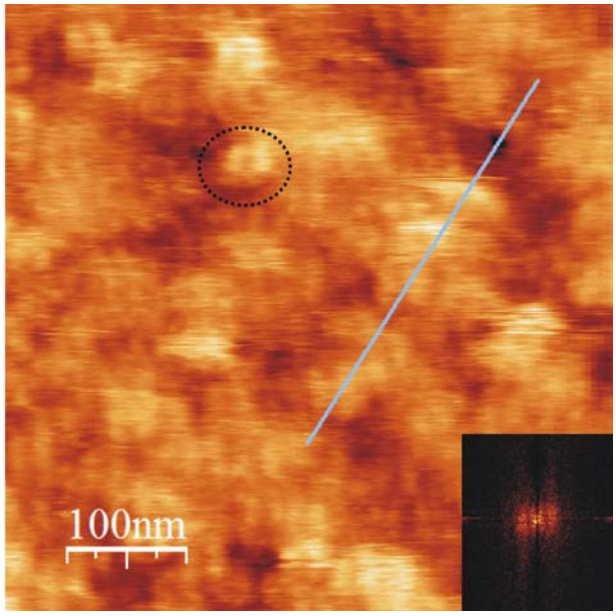

Figure 4.5. AFM height image of S-layers recrystallized on Si/PEI(PSS/PAH)$_2$/PSS after thermal treatment at 55ºC (z-range: 8 nm, roughness: 1 nm), The measurement was carried out at room temperature in 100 mM NaCl aqueous solution. The 2-D crystalline structure of the S-layer is lost as the Fourier analysis shows (located down in the picture at the right corner). The former protein crystal lost its structure forming protein aggregates (see black circle).

Denatured S-proteins, with elliptical shapes of about 100 nm length, and hilly protein aggregates (of thickness ca. 8 nm) can be distinguished on the sample surface, as the surface profile analysis shows in Figure 4.6.

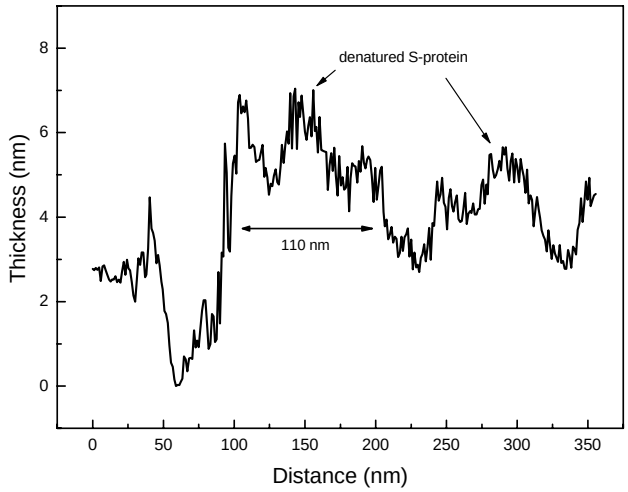

Figure 4.6. Surface profile analysis of the protein layer along the line. The largest thickness is about 8 nm, while the length of the aggregates is around 100 nm.

A representative force-distance curve taken after exposing the S-layer to 55ºC is shown in Figure 4.7 (applied load: 10 nN).

The approaching curve (empty circles) shows that no strong repulsion between the tip and the surface occurred. The retracting curve (black line) shows that protein unfolding events occurred at forces ranging from 0.2 - 0.70 nN, indicating the presence of soft material in the sample, as can be seen in more detail in the inset of Figure 4.7.

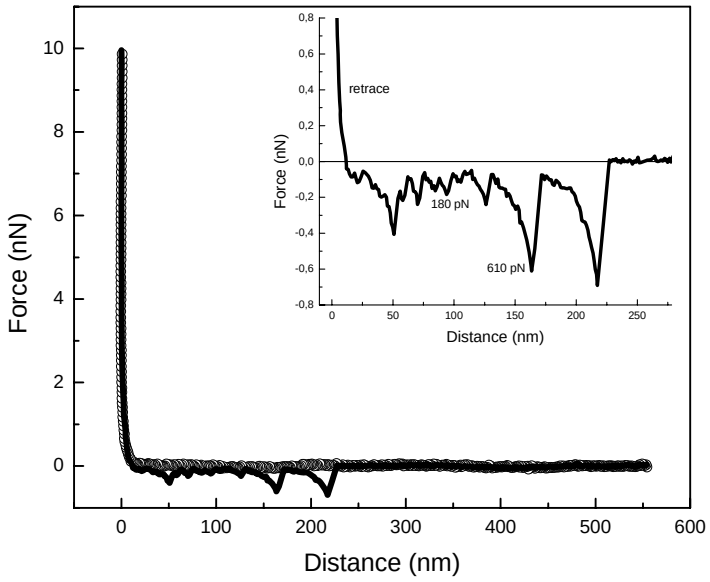

Figure 4.7. Force-distance curve measured in 100 mM NaCl aqueous solution after thermal treatment at 55 ºC. The main difference with the retracting curve of Figure 4.4 is the appearance of unfolding peaks of denatured S-proteins after applying loads of 10 nN; a feature commonly found in denatured S-proteins. Inset: magnification of the retracting force-distance curve. S-protein domains unfold at forces ranging from 200 pN to 700 pN.

The samples that lost the crystalline nanostructure were introduced overnight in recrystallizing buffer solution (0.5 mM Tris-HCl buffer, pH 9, with 10 mM $CaCl_2$). Figure 4.8 shows a height AFM picture of a denatured sample treated with recrystallizing buffer solution.

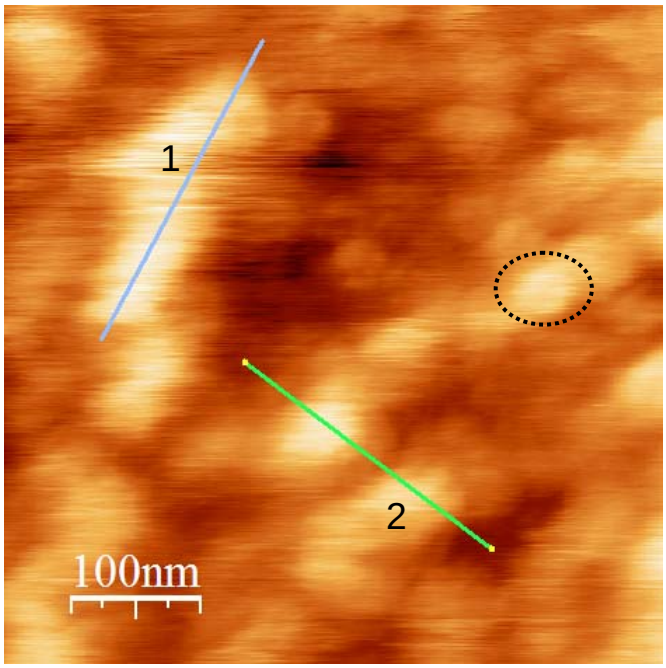

Figure 4.8. AFM height image of S-layer treated with recrystallizing buffer (pH 9) after thermal exposure at 55 ºC. (z-range: 18 nm, roughness: 2.85nm). The measurement was performed at room temperature in 100 mM NaCl aqueous solution. The recrystallization buffer is not able to recover the crystalline protein layer; it builds protein aggregates that can be seen on the surface (black circle).

The sample surface had a 2.85 nm roughness and many protein aggregates could be found. The 3-D image of Figure 4.8 is shown in Figure 4.9, it can be observed that the hybrid polyeletrolyte-protein surface presents a mountain-like profile with large variation in thickness.

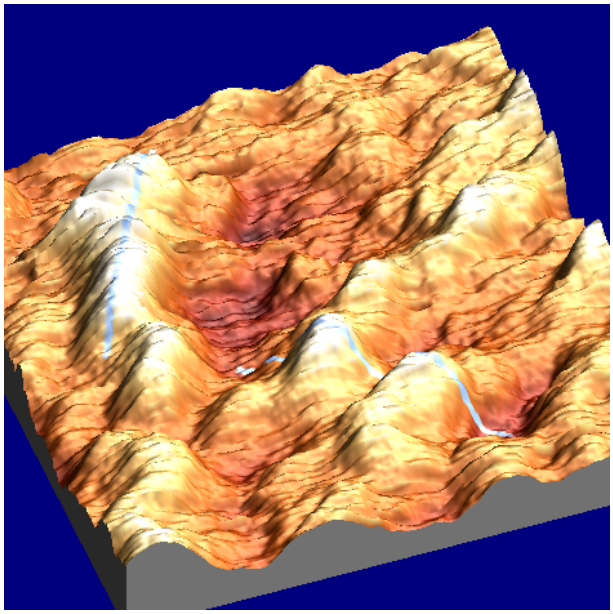

Figure 4.9. Corresponding 3-D image (dimension: 500 nm x 500 nm). The profile polyelectrolyte/protein system is very inhomogeneous presenting many aggregates.

Further analysis of the surface indicates that the aggregates presented thickness values from 8 nm to 13 nm and lateral lengths ranging from 60 nm to 130 nm (Figure 4.10).

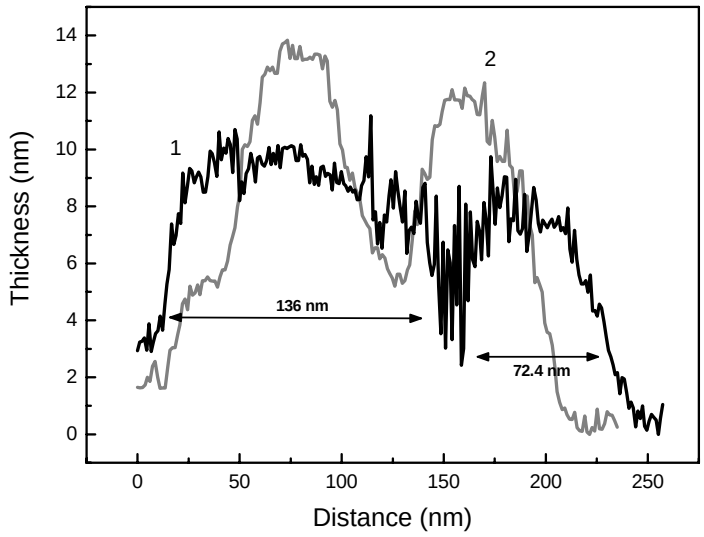

Figure 4.10. Quantification of the surface profile of Figures 4.8 and 4.9 taken along two different directions (line 1 and 2). The vertical analysis shows that the height varies from 8 nm to 13 nm, while the horizontal analysis indicates that the protein aggregates vary from 70 nm to 130 nm.

No recovery of the S-layer crystalline structure after buffer treatment is observed, thus thermal denaturation is an irreversible process.

NR experiments were performed to obtain information about changes in the film thickness and hydration in the direction normal to the solid/liquid interface. Figure 4.11 shows the NR curves as a function of temperature.

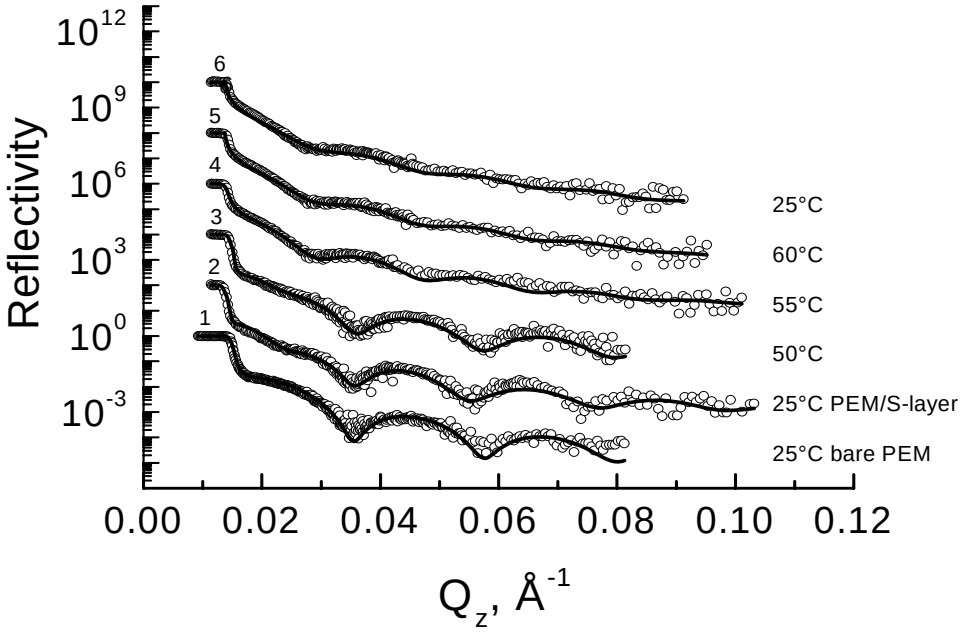

Figure 4.11. Reflectivity curves for Si/PEI/$(PSS/PAH)_6$/PSS/S-layer at different temperatures. 1) Bare support at 25°C, 2) Si/PEI/$(PSS/PAH)_6$/PSS/S-layer at 25°C, 3) at 50°C, 4) at 55°C, 5) at 60°C and 6) after cooling down at 25°C.

Bare Si/PEI/$(PSS/PAH)_6$/PSS at 25°C is shown in curve 1. Afterwards, adsorption of SbpA protein monomers on PSS, forming S-layer, at 25°C is shown in curve 2. The position of the fringes moves to smaller Q value which indicates increase in the film thickness. Curve 3 refers to the supramolecular structure Si/PEI/$(PSS/PAH)_6$/PSS/S-layer at 50°C. NR results showed that up to 55°C, no significant changes in the

reflectivity are induced. The sample was exposed at 55°C and 60°C and the reflectivity was measured (curves 4 and 5 in Figure 4.11). The corresponding NR curves show a shift of the fringe to the left of about 0.007 $Å^{-1}$ and present a flatter profile than the curves 1, 2 and 3. Qualitatively, this proves the formation of new film structure. No difference can be observed between the fringes of the curves 4, 5 and 6. The decrease of the temperature down to 25ºC (curve 6) does not induce any change in the NR curve; this can be explained by the fact that the system does not recover to the initial state represented in curve 2.

More quantitative information about the thickness and SLD can be obtained by fitting the NR data. The information that can be extracted in a single NR experiment includes the film thickness, *d*, the scattering length density profile, ρ(*z*), across the film, and the surface roughness, σ, between the different layers.

The scattering length density (SLD) is defined as the product of the number density n_i of the i^{th} atom and of its scattering length b_i $\rho(z) = \sum_i n_i b_i$ and it is highly dependent on the isotopic nature of the studied compounds and their concentration (density) in the film.

The experimentally obtained reflectivity curves were analyzed by applying the standard fitting routine, Parratt 32 [36]. It determines the optical reflectivity of neutrons from planar surfaces using a calculation based on Parratt's recursion scheme for stratified media [37]. The film is modelled as consisting of layers of specific thickness, scattering length density, and roughness, which are the fitting parameters. The model reflectivity profile is calculated and compared to the measured one and then the model is adjusted by a change in the fitting parameters to best fit the data. For large enough $Q = \frac{4\pi}{\lambda}\sin(\theta)$ (where l is the wavelength of the neutrons and q is the angle of

incidence), values the layer thickness, can be estimated from the spacing of the minima of two neighbouring interference fringes ΔQ by the approximation $d \approx \frac{2\pi}{\Delta Q}$. Our fitting strategy was always to use the simplest physically reasonable model to describe the experimental data. We began with one-layer models for the film and then added additional layers to improve the fit. The complexity of the model was increased with the addition of new layers to describe the different film regions until a reliable fit to the experimental data was obtained. The results shown represent the best fits of the data using simple, insightful models. Large variations in parameter space were allowed, but we restricted our models to those that generated reasonable results based on the known number of deposited layers and scattering length densities of the components.

The best fitting parameters are summarised in Table 4.1 and shown as solid lines on Figure 4.11.

Step No:	Temperature, °C		h, nm	SLD, x10^{-6}Å^{-2}	□, nm
1.	25	bare cushion	27.7	3.98	1.0
2.	25	PEM cushion	28.8	4.06	0.5
		S-layer	14.1	4.97	0.5
3.	35	PEM cushion	28.3	4.06	1.2
		S-layer	14.7	4.96	0.5
4.	45	PEM cushion	28.7	4.10	0.5
		S-layer	14.7	5.19	0.5
5.		PEM cushion	27.8	4.29	0.5

	50	S-layer	13.7	5.39	3.7
6.	55	PEM cushion	29.0	4.24	0.5
		S-layer	12.3	5.29	0.5
7.	60	Total thickness	33.5	3.13	2.0
8.	65	Total thickness	33.7	2.93	2.3
9.	55	Total thickness	33.4	2.82	2.2
10.	45	Total thickness	34.2	2.65	2.1
11.	25	Total thickness	33.1	2.63	1.8

Table 4.1. Thickness, scattering length density and roughness of the interface between the recrystallized S-layers and D_2O subphase for different temperature steps

The thickness and the SLD of the bare polyelectrolyte multilayer cushion are typical for the studied system [24]. The fitting of the reflectivity curve of the recrystallized S-protein layer was possible using a two-layer model. The first layer represents the polyelectrolyte multilayer cushion, while the second one takes into account the S-protein layer. The values obtained for the thickness (ca. 14.1 nm) and the scattering length density (ca. 4.97 x 10^{-6} $Å^{-2}$) were very close to those already reported for the formation of such protein layers [9]. A small oscillation (ca. 0.4 nm) in the thickness of S-layer was noticed in the temperature range 25-50°C. A rise in the scattering length density (ca. 0.42 x $10^{-6}Å^{-2}$) was observed by increasing the temperature for the same

interval. The S-layer thickness decreased at 55°C in ca. 1.8 nm comparing with the thickness of freshly formed S-layer at 25°C. At temperatures above 55°C, NR could not distinguish between the S-layer and the polyelectrolyte cushion and best fitting to the experimental points is only possible using a single box model. Cooling down to 25°C, the reflectivity signal indicated no recovery of the initial structure. The small value of the SLD of the S-layer after temperature decreasing at 25°C suggests the formation of a densely packed polymer-protein layer, which incorporates a smaller amount of D_2O, the S-protein layer becoming more hydrophobic. Precise discrimination between the S-layer and the PEM was not possible for temperatures higher than 55°C.

The roughness of the remaining S-protein layer treated at 55°C was similar to the roughness of the recrystallized S-layer under normal conditions (25°C). It increased at temperatures above 55°C. This increase in the roughness can be explained by the presence of diffuse borders between S-layer and polyelectrolyte multilayer due probably to protein denaturation and further interpenetration into the polyelectrolyte multilayer.

The measured change in the frequency Δf in the QCM experiments permits the estimation of the adsorbed amount of S-protein by using the Sauerbrey equation, which is valid only under the assumption that the adsorbed S-protein layer behaves non-elastically when deposited on the QCM crystal. Combining the adsorbed mass per unit area given by QCM with the thickness of the S-layer obtained from the NR data (14.1 nm, see Table 4.1), a density of M = 1.16 g/cm^3 is obtained. This value (M) is the sum of the contributions of the adsorbed protein and bound water:

$$M = \alpha D_{Slayer} + (1-\alpha) D_{H_2O} \qquad (2)$$

here α is the volume of the protein and D_{Slayer} and D_{H2O} is the mass density of the protein and the water respectively; α is the volume of the S-protein in the film, or its volume fraction when volume unit is considered.

The measured SLD of the S-protein layer in water[¶] (ρ_{exp}) is a volume fraction weighted sum of the SLD of the individual components, which build the film. These components are in our case the pure S-protein with SLD ρ_{Slayer} and the D_2O with SLD ρ_{D2O}.

$$\rho_{\exp} = \alpha\rho_{Slayer} + (1-\alpha)\rho_{D_2O} \qquad (3)$$

The SLD of the S-protein is related to its mass density and the scattering length b_i of the atoms by the equation:

$$\rho_{Slayer} = \frac{\sum_i b_i \, D \, N_A}{M_w} \qquad (4)$$

where N_A is the Avogadro's number and M_w is the molecular weight of the protein. Solving the system of equations (2) and (3) and considering eq. (4)[†] the volume fraction of the S-protein in the adsorbed layer can be calculated. The SLD of the pure S protein layer was calculated to be $\rho_{Slayer} = 2.02 \text{ x } 10^{-6}$ Å^{-2}. Values of $\alpha = 0.32$ and $D_{Slayer} = 1.48$ g/cm^3 were obtained. These numerical results show that S-proteins form very loosely packed layers on solid supports, which incorporate around 68% water.

The purpose of this study was to report on the building of bacterial protein crystals on anionic polyelectrolyte multilayers, the influence of the temperature on the stability of the 2D protein crystal structure, as well as the estimation of the amount of protein and water present in the hybrid macromolecular structure. Toca-Herrera et al. showed previously [18] that the P4 crystalline structure of S-layer recrystallized on secondary

[¶] NR experiments were performed in heavy water D_2O instead of light water H_2O. Small discrepancy between the QCM and NR data is possible because of the different strength of interactions between the S-protein and the two isotope forms of the water.

[†] The molecular weight of the SbpA protein is $M_w = 132062$ [38] with scattering length of 29846.2 Å.

cell wall polymer (SCWP) was irreversibly lost at 70°C. Atomic force micrographs show that the crystalline structure of S-layer is lost at 55°C. This temperature can be considered as a denaturation temperature since only the correct folding of SbpA proteins can reproduce (within error) the P4 structure found in bacteria [5]. The secondary cell wall polymer is quite difficult to purify or synthesize, therefore synthetic available polyelectrolytes with similar negative charge and hydrophobic behaviour were used as a cushion for the S-layer recrystallization. This study shows that the anionic polyelectrolyte PSS cannot provide better thermal stability for recrystallized S-layers than the secondary cell wall polymer. The thermal stability of the S-layer on its natural environment, the secondary cell walls polymer, is 15ºC higher.

The first question to address is if the difference in the denaturation temperature can be attributed to changes in the polyelectrolyte multilayer structure. Since PEM systems are stable at temperatures up to 60°C [39], the decrease in thermal stability might be due to the lack of the lectin-protein interaction that takes place between SbpA and SCWP in their natural environment (in bacteria). However, the use of anionic PSS as cushion for protein recrystallization improves the thermal stability by 10°C as shown by differential scanning calorimetry experiments: SbpA proteins present a phase transition at 45.8°C with a change in enthalpy of 1814.6 kJ/mol.

Although neutron reflectometry results show no significant change in the roughness of S-layer exposed to temperature above 55 °C comparing with S-layer formed at 25°C, an increase in the roughness was registered at temperatures higher than 55°C. Precise discrimination between the S-layer and the polyelectrolyte multilayer was not possible for temperatures above 55°C, meaning that both, the denatured S-proteins and the polyelectrolyte multilayer might have similar “optical” density for the neutron beam.

Taking also into account that AFM experiments show no evidence loss of protein mass, we conclude that denatured S-proteins interpenetrate into the PEM forming protein aggregates of about 7 nm thickness. Furthermore, the difference of 5.4 nm between the thickness of Si/PEI/$(PSS/PAH)_6$PSS/S-layer after cooling down at 25°C (33.1 nm) and the thickness of bare Si/PEI/$(PSS/PAH)_6$PSS (27.7 nm) at 25°C does not correspond to the typical S-layer thickness of ca. 14 nm [9]. Addition of recrystallization buffer (pH 9) containing calcium ions produces conformational surface changes in the hybrid S-protein/PEM leading to large protein aggregates. We have shown in earlier work [9] that divalent cations (in Tris buffer) are necessary to recrystallize SbpA monomers, in our case the denatured nature of the protein on the polyelectrolyte multilayer does not permit to rebuild a crystalline protein layer.

An important result of this study is the quantification of the ratio protein/water in the hybrid polyeletrolyte/S-layer system. A previous study [40] carried out with X-ray reflectivity and grazing incidence diffraction reported that the protein volume fraction of recrystallized S-proteins on the zwitterionic lipid dipalmitoylphosphatidylethanolamine reached a maximum of 60% in two horizontal sections of the S-layer, close to the lipid monolayer and close to the free subphase, determined on the basis for the volume determined for recrystallized amino acids [41], corrected for a reduction in packing density of the molecules in the protein. In our case, the combination of the adsorbed mass per unit area, the protein thickness and the properties of heavy water (translated as scattering length density in our data) values allowed to estimate the amount of protein and water in the hybrid system. Our calculations show that, before denaturation, the S-protein forms a very loosely packed layer on polyelectrolyte multilayers with water content of about 68% water. Thermal denaturation causes the irreversible loss of the 2-D crystalline S-layer structure, which

cannot be recovered by treatment with recrystallizing buffer, results that have been shown for similar systems [18].

As a final remark it has to be said that, this work has not addressed how the surface roughness affects the response of the QCM-D in liquid, which would give information about the water of hydration layers and the trapped water [42]. These experiments might be combined in the near future with surface plasmon resonance and ellipsometry measurements, to complement the study of mass adsorption and water content of bacterial fusion proteins recrystallized on different supports.

4.4 Conclusions

The adsorption of the bacterial S-protein SbpA on anionic terminated polyelectrolyte multilayers as a function of time has been monitored by quartz microbalance with dissipation. An adsorption time of one hour with a change in frequency of 92 Hz leads to the formation of S-protein layer that is softer than PSS. Atomic force microscopy and neutron reflectometry showed that the protein layer presented a 2-D structure with lattice parameters ($a = 14.3 \pm 1$ nm, $b = 13.4 \pm 1$ nm and $\gamma = 94.1 \pm 0.8$) and a thickness of 14 nm, which loses its crystalline regularity at 55°C, forming protein aggregates. This critical denaturation temperature (Tcd) is about 10°C higher than denaturation in solution. The crystalline structure of the S-layer cannot be recovered either by decreasing the temperature or with recrystallization buffer. The difference in thickness after decreasing the temperature may indicate that the denatured S-protein domains interpenetrate in the polyelectrolyte multilayer. The mechanical properties of the S-proteins are also changed by temperature: force distance curves show that aggregates of

denatured proteins unfold at lower loads than the proteins that constitute the 2D crystal. Typical unfolding forces for protein motifs are in the range from 200 pN to 700 pN.

The combination of the adsorbed mass per unit area measured with the quartz microbalance with dissipation and the S-layer thickness obtained with neutron reflectometry allows to calculate the S-layer density (M = 1.16 g/cm^3), with a scattering length density of (2.02 x 10^{-6} Å^{-2}) for pure S-protein. These results show that the recrystallization of S-proteins builds very loosely packed layers on polyelectrolyte multilayers incorporating around 68% water. We have shown that the combination of atomic force microscopy, quartz microbalance with dissipation monitoring and neutron reflectometry is able to deliver information about the water volume fraction around the S-protein layer.

References

[1] U.B. Sleytr, N. Ilk, E.M. Egelseer, D. Pum and B. Schuster (2006). *FEBS Journal* 274: 323-334.

[2] N. Parris, C.M. Hollar, A. Hsieh and D. Cockley (1997). *Journal of Dairy Science* 80: 19-28.

[3] K. Sasahara and K. Nitta (2006). *Proteins* 63: 127–135.

[4] G.M. Artman, Ch. Kelemen, D. Porst, G. Buldt and S. Chien (1998). *Biophysical Journal* 75: 3179-3183.

[5] U.B. Sleytr, P. Messner, D. Pum and M. Sara (1999). *Angewandte Chemie Inernational Edition* 38: 1034-1054.

[6] D. Pum and U.B. Sleytr, *Landers Academic Press*, 1996, Austin, TX. 175-209.

[7] B. Schuster and U. B. Sleytr (2000). *Reviews of Molecular Biotechnology* 74: 233-254.

[8] S. Küpcü, M. Sara and U.B. Sleytr (1995). *Biochimica et Biophysica Acta* 1235: 263-269.

[9] J.L. Toca-Herrera, R. Krastev, V. Bosio, S. Küpcü, D. Pum, A. Fery, M. Sara and U.B. Sleytr (2005). *Small* 1: 339–348.

[10] U.B. Sleytr, M. Sara, D. Pum and B. Schuster (2001). *Progress in Surface Science* 68: 231-278.

[11] U.B. Sleytr, M. Sára, D. Pum and B. Schuster, in: Supra-molecular Polymers, Second Edition, ed. A. Ciferri, CRC Press, Taylor & Francis Group, Boca Raton, FL. 2005. pp.583-616.

[12] U. B. Sleytr, M. Sára, D. Pum, B. Schuster, P. Messner and C. Schäffer, in: Biopolymers, ed. A. Steinbüchel and S. Fahnestock, Wiley-VCH, Weinheim, Germany. 2002, Vol. 7 pp. 285-338.

[13] H. Engelhardt and J. Peters (1998). *Journal of Structural Biology* 124: 276-302.

[14] Wm. Bridge Cooke (1957). *Ecology* 38: 185-186.

[15] P. Rehaber, Ph.D. Thesis, University of Regensburg, 1992.

[16] Z. Pei, R. Ellison, R. Lewis and M.J. Blaser (1988). *Journal of Biological Chemistry* 263: 6416-6420.

[17] L.A. Fernandez-Herrero, G. Olabarria, J.R. Caston, I. Lasa and J. Berenguer (1995). *Journal of Bacteriology* 177: 5460-5466.

[18] J.L. Toca-Herrera, S. Moreno-Flores, J. Friedmann, D. Pum and U. B., Sleytr (2004). *Microscopy Research and Technique* 65: 226–234.

[19] F. Höök, M. Rodahl, B. Kasemo and P. Brzezinski (1998). *Proceedings of the National Academy of Sciences* 95: 12271-12276.

[20] F. Höök, M. Rodahl, P. Brzezinski and B. Kasemo (1998). *Langmuir* 14: 729-734.

[21] R. P. Richter and A. R. Brisson (2005). *Biophysical Journal* 88: 3422-3433.

[22] J. Vörös (2004). *Biophysical Journal* 87: 553-561.

[23] E. Reimhult, C. Larsson, B. Kasemo and F. Höök (2004). *Analytical Chemistry* 76: 7211-7220.

[24] T. Gutberlet, B. Klösgen, R. Krastev and R. Steitz (2004). A*dvanced Engineering Materials* 6: 832-836.

[25] M. Delcea, R. Krastev, Th. Gutlebert, D. Pum, U.B. Sleytr and J.L. Toca-Herrera (2007). *Journal of Nanoscience and Nanotechnology* 7: 4260-4266.

[26] U.B. Sleytr, M. Sara, S. Kupcu and P. Messner (1986). *Archives of Microbiology* 146: 19-24.

[27] G. Decher (1997). *Science* 277: 1232-1237.

[28] C. Delajon, Th. Gutberlet, R. Steiz, H. Möhwald and R. Krastev (2005). *Langmuir* 21: 8509-8514.

[29] I. Horcas, R. Fernandez, J.M. Gomez-Rodriguez, J. Colchero, J. Gomez-Herrero and A.M. Baro (2007). *Review of Scientific Instruments* 78: 013705-1-013705-8.

[30] D. Clemens, P. Gross, P. Keller, N. Schlumpf and M. Konnecke (2000). *Physica B* 276: 140-141.

[31] http://sinq.web.psi.ch/sinq/instr/amor.html

[32] J.J. Ramsden, Y.M. Lvov and G. Decher (1995). *Thin Solid Films* 254: 246-251.

[33] G. Sauerbrey (1959). *Zeitschrift für Physik* 155: 206-222.

[34] K.K. Kanazawa and J.G. Gordon (1985). *Analytical Chemistry* 57: 1770-1771.

[35] K. Gläsmäster, Ch. Larsson, F. Höök, and B. Kasemo (2002). *Journal of Colloid and Interfaces Science* 246: 40-47.

[36] C. Braun, Parratt 32 Program for reflectivity fitting Hahn-Meitner Institute: Berlin, 1999.

[37] L.G. Parratt (1954). *Physical Review* 95: 359-369.

[38] N. Ilk, C. Voellenkle, E.M. Egelsser, A. Breitwieser, U.B. Sleytr and M. Sara (2002). *Applied Environmental Microbiology* 68: 3251-3260.

[39] Y.M. Lvov, G. Decher and H. Möhwald (1993). *Langmuir* 9: 481-486.

[40] M. Weygand, B. Wetzer, D. Pum, U.B. Sleytr, N. Cuvillier, K. Kjaer, P.B. Howes and M. Lösche (1999). *Biophysical Journal* 76: 458-468.

[41] S.J. Perkins, in Modern Physical Methods in Biochemistry, Part B. A. Neuberger and L.L.M.V. Deenen, editors. Elsevier, Amsterdam. 1988, pp. 143-265.

[42] L. Macakova, E. Blomberg, P.M. Claesson (2007). *Langmuir* 23: 12436-12444.

Chapter 5

How the pH influences the surface properties of recrystallized bacterial surface layer protein

5.1 Introduction

Proteins are fragile biomolecules which require suitable conditions for normal maintenance of their structure and function. Many of the interactions that stabilize the 3-D conformation of the protein are relatively weak and sensitive to various environmental factors including high temperature, low or high pH and ionic strength.

Many protein functions like catalysis and binding, are dependent on the protein charge groups explaining the fact that proteins are not created with a pI closer to the pH where they should normally perform their function [1]. It is known that changes in pH influence cell membrane processes, such as: SseB protein secretion in Salmonella [2], epithelial ion transport [3], or virus activation [4] and the structural integrity of bacterial and archaeal surface layers.

Crystalline bacterial cell surface layers (S-layers) are one of the most common cell envelope components of prokaryotic organisms (*Archaea* and *Bacteria*). S-layers are monomolecular arrays composed of a single protein or glycoprotein and represent the simplest biological membranes developed during evolution [5]. The nanobiotechnological interest of isolated S-layer subunits is their ability to self-

assemble at the air-water interface [6], on lipid films [7], on liposomes [8], on polyelectrolyte supports [9]. We have combined here polyelectrolytes and S-layer technology to study the surface properties of bacterial SbpA protein recrystallized on positively and negatively charged polyelectrolyte at pH in the range 4-8. This studies supply information about the hydrophobicity of the protein surface layer on different substrates and might have application in antifouling by removing or preventing the accumulation of living microorganisms.

In this work, the structural properties of recrystallized S-layer on polyelectrolyte have been investigated as a function of pH and were monitored by atomic force microscopy (AFM). The wetting properties of the SbpA protein recrystallized on different substrates (hydrophilic silicon wafers and polyelectrolytes) have been measured by contact angle. The deposition of polyelectrolytes, the adsorption of SbpA protein and its viscoelastic properties and also the influence of the pH on the structure of S-layer were monitored by quartz crystal microbalance with dissipation monitoring (QCM-D). We report for the first time about the stability of liquid films on S-layers as a function of pH. The recrystallization of S-layer on poly(ethylenimine), a positively charged polyelectrolyte, is also reported for the first time.

5.2 Materials and Methods

Bacterial S-layer Protein. The bacterial S-layer protein (SbpA) was isolated from *Bacillus sphaericus* CCM2177. Growth in continuous culture, cell wall preparation, extraction of S-layer protein with 5M guanidine hydrochloride (GHCl), dyalization for 2 hours at 4º C with stirring and further centrifugation was carried out according to Sleytr et al. [10]. The protein concentration of the clear supernatant containing the

disassembled S-layer subunits was adjusted with Milli-Q water to a final concentration of 1 mg/mL and used for all recrystallization experiments. SbpA protein presents a pI value of 4.2 as determined by isoelectrical focusing.

Polyelectrolytes (PEs). Poly(ethylenimine) (PEI, Mw = 750 kDa), Poly(sodium 4-styrenesulfonate) (PSS, Mw = 70 kDa), Poly(allylamine hydrochloride) (PAH, Mw = 70 kDa) were obtained from Sigma-Aldrich (Munich, Germany) and were used as received. PEI and PAH are polycationic and PSS is polyanionic.

Other chemicals. Calcium chloride ($CaCl_2$), citric acid-monohydrate ($C_6H_8O_7.H_2O$), disodium hydrogen phosphate ($Na_2HPO_{4)}$ and Tris-HCl, hydrochloric acid (HCl), sodium hydroxide (NaOH), sodium dodecyl sulfate (SDS), hydrogen peroxide (H_2O_2) and ammonium hydroxide (NH_4OH) were obtained from Sigma-Aldrich (Munich, Germany). The Milli-Q water used had a specific resistance of 18.2 MΩ cm^{-1} (Elga Lab Water Systems, Germany).

Buffer solutions. 1 mM citric acid-monohydrate ($HOC(COOH)(CH_2COOH)_2 \cdot H_2O$) and 2 mM disodium hydrogen phosphate (Na_2HPO_4) buffer solutions were adjusted to different pHs. 0.5 mM Tris-HCl buffer with 10 mM $CaCl_2$ was adjusted at pH 9 and used for SbpA protein recrystallization.

Silicon wafers. Silicon wafers (IMEC, Leuven, Belgium) with a native silicon oxide layer cut into pieces of 1x1cm^2 were used. They were previously cleaned and made hydrophilic by oxygen plasma treatment (Gala Instruments Elektronmikroscopie, Germany).

Multilayer build-up. Hydrophilic silicon wafers were coated with polyelectrolyte multilayer (PEM) using Layer-by-Layer technique [11]. Samples were dipped alternatively in a beaker containing the polycationic or the polyanionic solution for 20

min. PEI was used to recrystallize SbpA protein and as a precursor for PSS/PAH multilayers. The concentration of the polyelectrolyte solution was 10^{-2} M based on the monomer unit, with a NaCl concentration of 0.5 M. The substrates were rinsed for 3 minutes in 3 different beakers of Milli-Q water in order to remove the excess polymer after each adsorption step. Six layers of polyelectrolyte were deposited, knowing that at six layers and above the influence of the substrate is lost [12]. The last deposited layer, in most of the experiments, was PSS, negatively charged, because SbpA protein does not recrystallize on positively charged PAH [9].

S-layers recrystallization. Recrystallization experiments were carried out in mini Petri dishes (30 mm diameter, 5 mL volume). Substrates were immersed and kept overnight in buffer solution containing protein monomers. The protein/buffer volume ratio was 0.1/1 for every sample. The samples with recrystallized protein were washed with Milli-Q water before starting the experiments.

Atomic force microscopy (AFM). The two-dimensional topography of recrystallized S-layer was measured in aqueous solution (0.1 M NaCl) at room temperature in contact mode (scan rate 4.70 Hz, at a force about 0.7-1 nN) with silicone nitride (Si_3N_4) cantilevers with a nominal spring constant of 0.1 N m^{-1} using a multimode atomic force microscope Nanoscope III (Veeco Instruments Santa Barbara, CA).

Contact angle measurements. The contact angle of buffer solutions on solid support, on substrates coated with polyelectrolytes and SbpA protein were measured at room temperature with a Kruess Drop Shape Analysis System (Kruess, Hamburg, Germany). The size (within a fraction of a mm) and the volume (1 µl) of the drops were kept constant since it is known that variations in the volume of the drops can lead to

inconsistent contact angle measurements [13, 14]. At least three different drops were measured for every sample.

Quartz Crystal Microbalance with Dissipation Monitoring (QCM-D). The adsorption of polyelectrolyte and SbpA protein, the viscoelasticity of the systems were investigated as a function of pH using a QE401 (electronic unit)/QFM401 (flow module) instrument from Q-sense AB (Gothenburg, Sweden). Silicon and gold crystals were used. The QSX303 silicon dioxide 50 nm crystals (Q-Sense AB, Gothenburg, Sweden) were immersed for 30 min in a 2% sodium dodecyl sulfate (SDS) solution, while the QCX301 gold crystals (Q-Sense AB, Gothenburg, Sweden) were immersed for 10 min in a 6:1:1 (vol/vol) solution of H_2O:NH_4OH(25%):H_2O_2(30%) at 70ºC. Both types of crystals were rinsed with Milli-Q water, dried in a stream of nitrogen gas and 30 min UV/ozone treated before mounting the crystals in the flow chamber. A volume of 0.5 ml of temperature-equilibrated polyelectrolyte or SbpA protein solution was pumped through the measurement chamber in order to study the PEM deposition and S-layer protein adsorption processes by continuously recording the sets of resonances frequencies and dissipation factors. The presented results correspond to the 5^{th} overtone. The QCM-D data were analyzed with Q-Tools (software provided by Q-Sense).

5.3 Results and Discussion

The recrystallization of SbpA protein on different positively and negatively polyelectrolytes has been previously reported [9]. However, we report for the first time the recrystallization of SbpA on poly(ethylenimine), a positively charged polyelectrolyte. AFM deflection images (Figure 5.1) showed that SbpA protein recrystallizes on PEI and the structure of S-layer is not affected by pH in the range 4-8.

The square lattice parameters obtained by 2D Fourier transforms are a = 15 ± 1 nm; b = 15 ± 1.5 nm and γ = 83 ± 15; similar values as reported in [9].

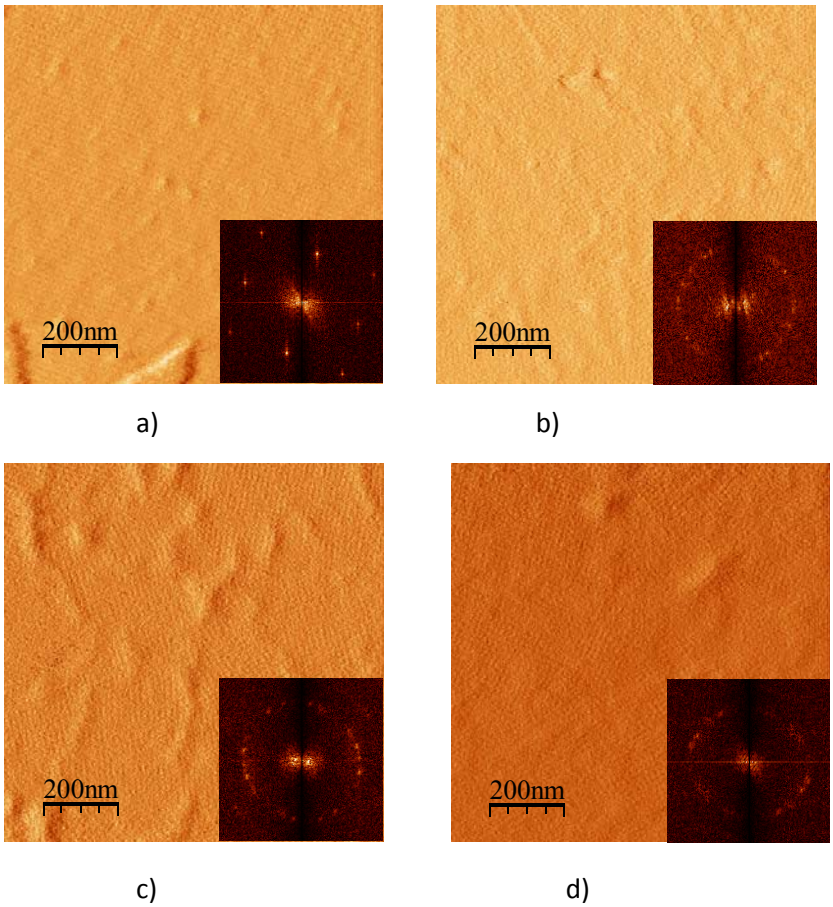

Figure 5.1. AFM deflection images of SbpA protein recrystallized on PEI at different pHs and the corresponding 2-D Fourier transformations down at the right corners. (a) pH 8, (b) pH 6, (c) pH 5 and (d) pH 4. The S-layer lattice parameters do not change at different pHs.

The adsorption of PEI on silicon and the adsorption of S-layer protein on top and the effect of the pH on the structure of adsorbed S-protein were monitored by QCM-D (see Figure 5.2). At t = 1120 s, the silicon surface is exposed to PEI solution, resulting in a decrease in frequency of 13 ± 1 Hz and an increase in dissipation of about 1.32 x 10^{-6}. At t = 1810 s, polyelectrolyte deposition is interrupted by exchange to Milli-Q water. At t = 2410 s, the surface is exposed to SbpA protein solution, resulting in an increase in

the dissipation of about (11 ± 2) x 10^{-6} and a decrease in frequency of 154.5 ± 3.5 Hz according to Sauerbrey equation [15].

$$\Delta f = \frac{-1}{nC}\Delta m \quad (1)$$

where, Δf is the change in the resonance frequency, or frequency shift, and 1/C = the mass sensitivity of quartz, with C = 17.7 ng/(cm^2 Hz), for a 5 MHz crystal, n = the overtone number (the data shown in the manuscript are already divided to the overtone number by Q-Tools software).

At t = 6400 s, the adsorption of SbpA protein is interrupted by exchange with Milli-Q water. At t = 8400 s, the Milli-Q water is changed to buffer with pH 4, 6 and 8, respectively. At t = 10 500 s, the buffer was changed to Milli-Q water. After exposure to pH 8, an increase in the frequency of 42 Hz and a decrease in the dissipation of 4.40 x 10^{-6} were noticed. Treatment at pH 6 results in an increase of the frequency of 96 Hz and a decrease in dissipation of 9.2 x 10^{-6} while the pH 4 let to an increase in frequency of 87 Hz and a decrease in dissipation of 5.42 x 10^{-6}.

After pH treatment, the loss of mass per unit area approximately 56% for pH 4, 62% for pH 6 and 27% for pH 8. Treatment at pH 6 showed the highest loss of mass and an increase in the rigidity of the layer. Although the QCM-D is able to register changes in mass and viscoelasticity, AFM measurements show no structural changes.

A remaining question that is beyond this study is the clarification of the nature of the loss of mass, work is going on.

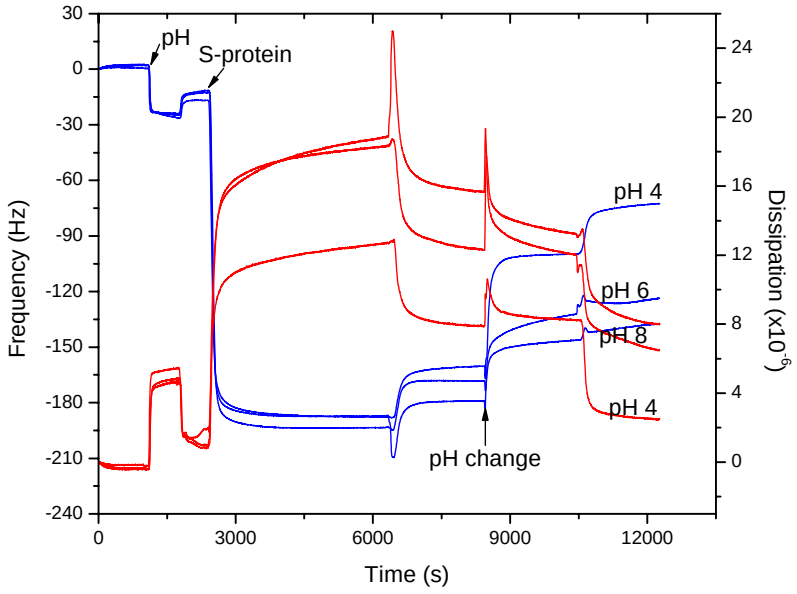

Figure 5.2. Representative measurement of the changes in frequency and dissipation for PEI deposition, S-layer protein adsorption and further pH treatment as a function of time.

The polyelectrolyte multilayer/S-layer macromolecular structure was built using "bottom-up strategy". The following multilayer structure Si/PEI/(PSS/PAH)2/PSS was used as a cushion for the recrystallization of SbpA protein. The recrystallization of the protein monomers takes place due to the self-assembly properties of S-proteins and of calcium ions contained in the buffer solution [9].

Buffer solutions with different pH values were used to study the 2-D structural and electrical properties of recrystallized S-layer. At pH 3, the former protein crystal lost its structure forming protein aggregates. (data not shown). The recrystallization of SbpA protein on PSS-terminated PEM has been already reported [9].

AFM deflection images (Figure 5.3) showed that SbpA protein recrystallizes on PSS-terminated PEM forming domains with typical square symmetry (see the Fourier transforms placed at the bottom corners) and the two-dimensional structure is not affected by pH in the range of 4-8. The square lattice parameters obtained by 2D Fourier

transforms are a = 14 ± 1 nm and b = 15± 1 nm. The S-crystals form angles of 89º ± 5 between them.

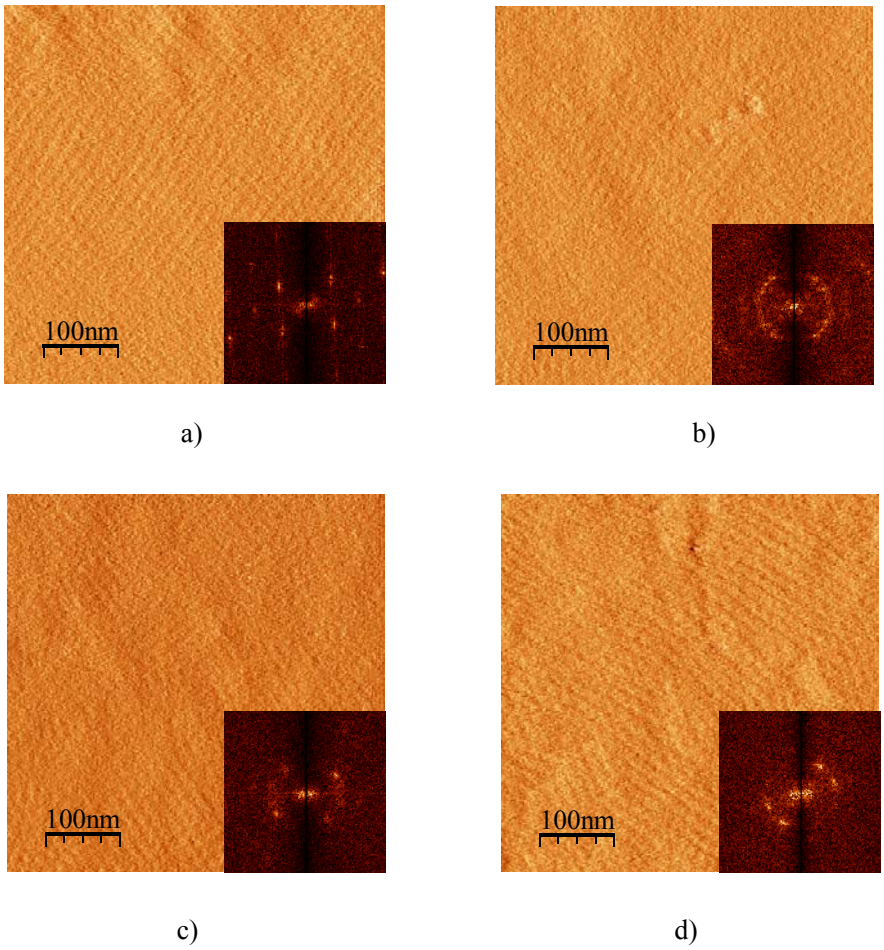

Figure 5.3. AFM deflection images of SbpA protein recrystallized on PSS-terminated polyelectrolyte multilayers at different pHs and the corresponding 2-D Fourier transformations down at the right corners. (a) pH 8, (b) pH 6, (c) pH 5 and (d) pH 4.

The PSS-terminated polyelectrolyte multilayer build-up and the adsorption of S-layer protein on top, monitored by QCM-D was already reported [10].

Figure 5.4 presents the changes in the dissipation as a function of polyelectrolyte multilayer deposition, S-layer proteins adsorption and treatment at pH in the range 4-8.

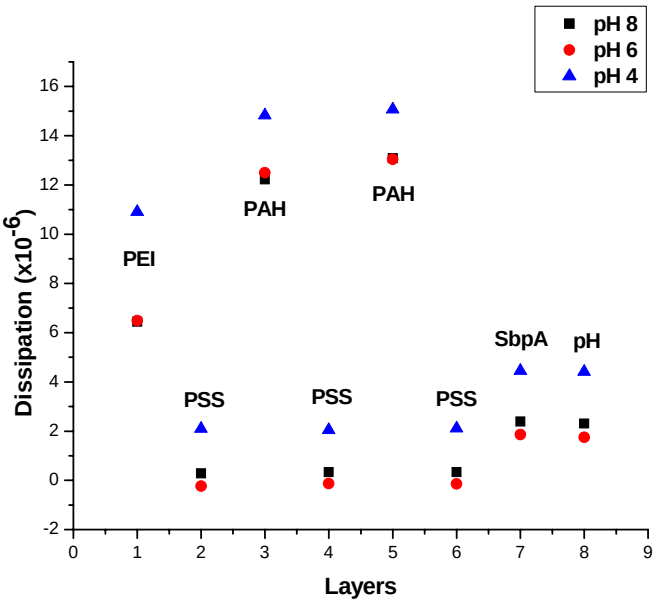

Figure 5.4. Dissipation equilibrium values measured in water after removing the polyelectrolyte, protein solutions and the buffer solution at different pHs

PSS adsorption decreases the dissipation ((7.24 ± 1.34) x 10^{-6}) in comparison with PEI, PSS forms a more compact layer than PEI. Further deposition of PAH led to an increase in the dissipation compared to PSS ((12.47 ± 0.2) x 10^{-6}). Finally, the adsorption of S-layer proteins was followed by an increase in the dissipation ((2.14 ± 0.18) x 10^{-6}) comparing with PSS, which indicates that the final protein layer (S-layer) is more viscoelastic than PSS. An insignificant decrease in the dissipation ((0.08 ± 0.04) x 10^{-6}) was registered after the exposure of SbpA protein at different pHs. This indicates that the pH in the range 4-8 does not affect significantly the viscoelastic properties of S-layer.

Wetting properties of the SbpA protein recrystallized on different substrates (silicon, PEI, PSS). The wettability of surfaces is a subject of great interest in the past few decades. The surface energy of a sample determines if a given liquid drop will roll

up or spread when deposit on it. Surface roughness can enhance repelling or wetting properties [16], resulting in “superhydrophobic” or “superhydrophilic” textures.

Figure 5.5 shows the contact angle of a buffer solution drop deposited on different substrates and of SbpA protein recrystallized on substrates with different physico-chemical properties as a function of pH. The substrates used for SbpA recrystallization were: hydrophilic silicon wafers, silicon wafers coated with one positively charged polyelectrolyte layer (PEI) and silicon wafers coated with six layers of polyelectrolyte, PSS-terminated, negatively charged.

Contact angle measurements showed that substrates alone are highly hydrophilic at any pH. For silicon wafers, contact angle was in the range 0-15 degrees, silicon wafers coated with PEI had a contact angle in the range 8-24 degrees, while silicon coated with PSS presented a contact angle between 25 and 29 degrees. No significant difference was noticed with the pH (see Figure 5.5). Silicon wafers were more hydrophilic than silicon wafers coated with PSS and PEI. The highest hydrophobicity was registered for silicon wafers coated with PSS.

The recrystallized S-layer (on all the substrates) was more hydrophobic comparatively with the surface of the substrates alone. In the case of the substrates covered with SbpA protein, the contact angle varies between 48 in 82 degrees for silicon/SbpA system, 20 and 34 for silicon/PEI/SbpA system and between 44 and 93 degrees for silicon/PSS/SbpA system. For all the substrates, SbpA protein conferred more hydrophobicity to the substrates. Silicon/SbpA and silicon/PSS/SbpA systems were more hydrophobic at pH 4 and 5 comparing with pH 6 and 8.

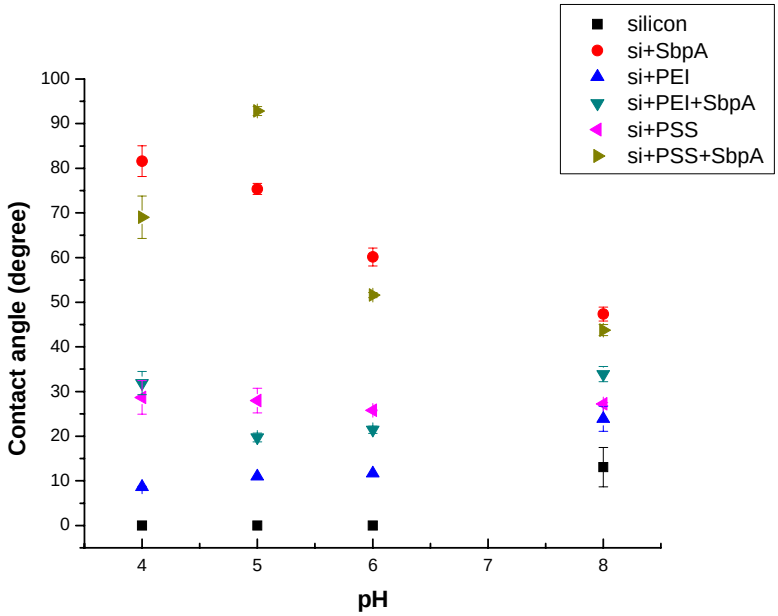

Figure 5.5. Contact angle measurements for different substrates and for SbpA protein recrystallized on different substrates. Note that SbpA has always a behavior more hydrophobic that its support.

However, the contact angle is a macroscopic measurement and possible defects of S-layer array (protein surface domains) could have an influence in the final values.

Water film stability on recrystallized SbpA protein. The water film stability on recrystallized SbpA protein on different substrates was microscopically time-monitored as a function of pH, at room temperature by depositing drops with a constant volume (1 μL) on the surface of recrystallized SbpA protein. The contact angle was measured every 60 s until the drop disappeared (see Figure 5.6).

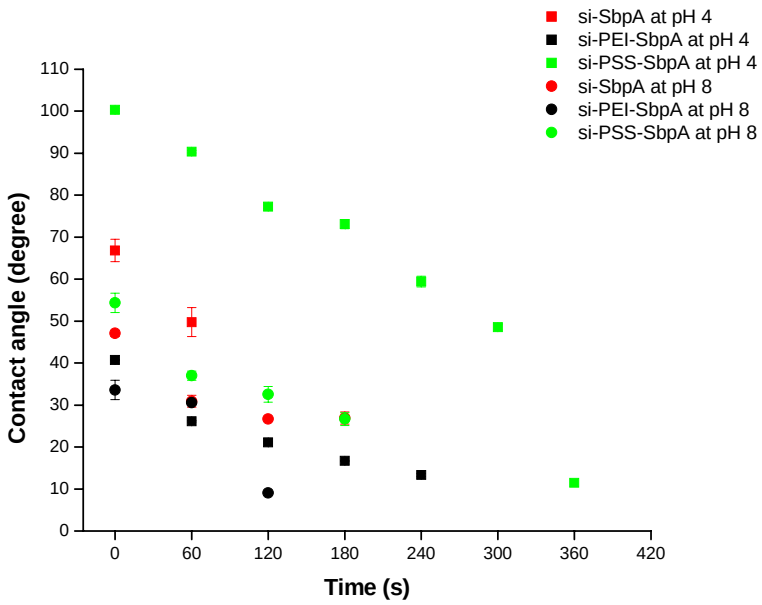

Figure 5.6. Water drop stability on recrystallized SbpA protein on different substrates at pH 4 and 8 as a function of time.

At pH 4, the water thin film on SbpA protein surface of the system silicon/SbpA was less stable and dried faster (60s) than the silicon/PEI/SbpA system (240s) and the silicon/PSS/SbpA system (360s). At pH 8, the silicon/PEI/SbpA system dries after 120s, while the silicon/PSS/SbpA system and the silicon/SbpA system dry in 180s.

Ciunel and co-workers showed that depending on the surface charge of the substrate, the water films are stable on negatively charged surfaces or rupture rapidly on positively charged surfaces [17]. At pH 4 the surface charge of the S-layer becomes less negative than a pH 8, decreasing the initial repulsive force between the S-layer and the water/air interface (negatively charged).

The attractive interaction between SbpA protein layer and the air/water interface induces instability in the water thin film producing its disruption. At pH higher than 4, the electrostatic repulsion between S-layer and air/water interface makes the water thin

film more stable. This phenomenon does not occur on recrystallized S-layers on polyelectrolyte multilayers.

5.4 Conclusions

In this work, we have studied the surface properties of SbpA protein recrystallized on hydrophilic silicon wafers, PEI and PSS-terminated polyelectrolyte multilayers as a function of pH, by combining atomic force microscopy, contact angle measurements and quartz crystal microbalance with dissipation monitoring.

The recrystallization of SbpA protein on positive poly(ethylenimine) (PEI) was reported here for the first time. The pH influence on the SbpA protein layer structure on PEI was also monitored. AFM micrographs do not show significant influence of pH in the range 4-8 on the global structure of the protein layer recrystallized on silicon wafers, on silicon coated with PEI and on PSS-terminated polyelectrolyte multilayers.

However, pH has an influence on the wetting properties of the protein layer. Contact angle measurements showed that the surface of recrystallized SbpA on hydrophilic silicon wafers is more hydrophobic than a two-dimensional crystal on polyelectrolyte.

The water film on SbpA protein surface is not stable and dries faster at lower pH, possibly due to the charge inversion of the protein layer (+) facing the water/air interface (-). SbpA protein confers hydrophobicity to the substrates and the system silicon/PEI/SbpA looses more mass than the system silicon/SbpA and silicon/PSS/SbpA after treatment at pH 4.

Future work concerning the variation in thickness of the hybrid PEM/SbpA system and the influence of the support on the water film stability on recrystallized S-layers should be carried out.

References

[1] S. Lindman, W-F. Xue, O. Szczepankiewicz, M.C. Bauer, H. Nilsson and S. Linse (2006). *Biophysical Journal* 90: 2911-2921.

[2] R.B. Caldwell and C.T. Lattemann (2004). *Applied Environmental Microbiology* 70: 610-612.

[3] D. Joseph, O. Tirmizi, X-L. Zhang, E.D. Crandall and R.L. Lubman (2002). *American Journal of Physiology Lung Cellular and Molecular Physiology* 282: L675-L683.

[4] T. Stegmann, F.P. Booy and J. Wilschut (1987). *Journal of Biological Chemistry* 262: 17744-17749.

[5] U.B. Sleytr, M. Sara, D. Pum and B. Schuster (2001). *Progress in Surface Science* 68: 231-278.

[6] D. Pum and U.B. Sleytr (1996). *Landers Academic Press*, Austin, TX, pp. 175-209.

[7] B. Schuster and U.B. Sleytr (2000). *Reviews in Molecular Biotechnology* 74: 233-254.

[8] S. Küpcü, M. Sara and U.B. Sleytr (1995). *Biochimica et Biophysica Acta* 1235: 263-269.

[9] J.L. Toca-Herrera, R. Krastev, V. Bosio, S. Kupcu, D. Pum, A. Fery, M. Sara and U.B. Sleytr (2005). *Small* 1: 339-348.

[10] U.B. Sleytr, M. Sara, S. Küpcü and P. Messner (1986). *Archives of Microbiology* 146: 19-24.

[11] G. Decher (1997). *Science* 277: 1232-1237.

[12] M. Schönhoff (2003). *Journal of Physics: Condensed Matter* 15: R1781-R1808.

[13] A. Marmur (1994). *Advances in Colloid and Interface Science* 50: 121-141.

[14] A. Marmur (1998). *Colloids and Surfaces A* 136: 209-215.

[15] G. Sauerbrey (1959). *Zeitschrift für Physik* 155: 206-222.

[16] J. Bico, U. Thiele and D. Quere (2002). *Colloids and Surfaces A* 206: 41-46.

[17] K. Ciunel, M. Armelin, G.H. Findenegg and R. von Klitzing (2005). *Langmuir* 21: 4790-4793.

Chapter 6

On the interaction of lipid-bacterial proteins and membrane formation through S-layer recrystallization on lipid layers

6.1 Introduction

Phospholipids are amphiphilic molecules representing the major components of biological membranes. In the last decades they have gained interest in many fields such as biochemistry, chemistry and polymer science. When a suspension of phospholipids is mechanically dispersed in aqueous solution several types of lipid membrane model systems can be formed: i) phospholipid vesicles [1, 2]; ii) phospholipid monolayers [3-6]; iii) free standing foam films, formed by two monolayers of surfactant molecules [7,8] and, iv) supported phospholipid bilayers [9, 10].

Lipid membranes with associated or integral proteins have attracted lively interest in the last decades [11, 12]. Lipid bilayers have been extensively used as matrix for protein adsorption or insertion, some examples are annexin A5 [13], streptavidin [14], histidine-tagged (His-tagged) membrane proteins [15]. Also, different approaches and molecules have been used to functionalize a lipid monolayer, such as biotinylated amphiphile-streptavidin system [16], protein A [17], lipid linkers [18].

Bacterial surface layer proteins (S-layers) are two-dimensional protein lattices forming the outermost cell envelope component in a broad spectrum of bacteria and archaea [19-

20]. They are composed of a single protein or glycoprotein species and exhibit either oblique, square or hexagonal lattice symmetry with center-to-center units in the range 3-30 nm. Bacterial S-layers are 5 to 10 nm thick and have pores of uniform morphology and size in the range 2-8 nm [21]. S-layer proteins are able to crystallize onto lipid monolayers [22-24], solid-supported membranes [25, 26] or liposomes [27, 28]. S-layer supported lipid membranes have been optimized for billions of years of evolution in most extreme habitats. They are biomimetic structures mimicking the supramolecular building principles of archaeal cell envelope and are promising candidates used for structure-function studies on reconstituted integral proteins and also, in the membrane protein-based molecular nanotechnology.

In this work, saturated and unsaturated lipids with different head groups and charge have been used to study the interaction of the SbpA protein from *Lysinibacillus sphaericus* CCM 2177 (former *Bacillus sphaericus*) with liposomes, and lipid bilayers and monolayers. We have also studied the influence of lipid mixtures on SbpA recrystallization. In particular, the lipids used were phosphatidylcholine (PC), phosphatidylserine (PS) and phosphatidylglycerol (PG). It is known that phosphatidylcholine (PC) and phosphatidylserine (PS) phospholipids are required for normal cellular structure and function. On one hand, saturated PC (phosphatidylcholine) phospholipids have gained the interest in the pharmaceutical branch because they promote metabolism through the cell membrane. On the other hand, unsaturated PC lipids might be important in the formation of a lipid reservoir, in the initial adsorption of lipids to the interface or in the regulation of surface tension during the respiratory cycle. PC lipids are uncharged, therefore we have used an anionic phospholipid, phosphatidylglycerol (PG), which is one of the major membrane phospholipids and

assist in translocation of proteins across membranes and initiation of DNA replication [29-31].

In addition, a more complex biomimetic supramolecular structure consisting of the following steps: i) polyelectrolyte multilayers (PEM) on silicon, ii) 1,2-dimyristoyl-sn-glycero-3-phosphocholine (DMPC) on PEM and iii) SbpA protein adsorption on DMPC, have been also investigated.

6.2 Materials and Methods

***Lipids**:* All lipids used in this work were purchased from Avanti Lipids. The corresponding structures and transition temperatures (Tm) are shown in Figure 6.1.

DOPC: 1,2-dioleoyl-sn-glycero-3-phosphocholine Tm = -20ºC

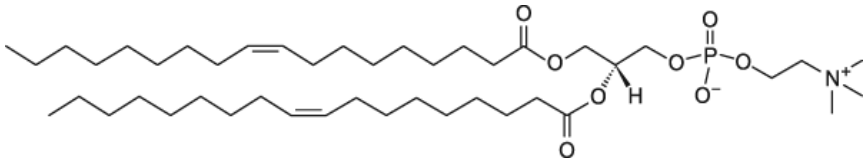

DMPC: 1,2-dimyristoyl-sn-glycero-3-phosphocholine Tm = 23ºC

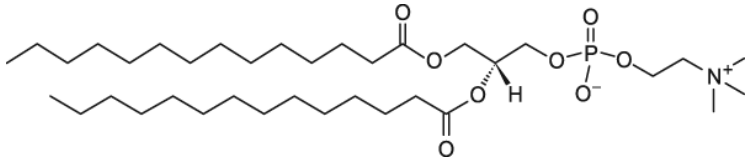

DMPG: 1,2-dimyristoyl-sn-glycero-3-[phospho-rac-(1-glycerol)] Tm = 23ºC

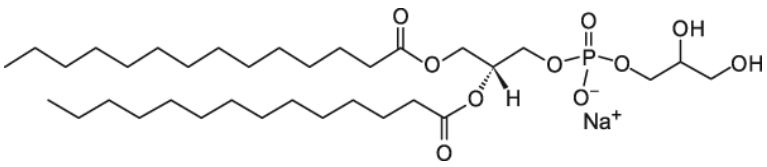

DPPC: 1,2-dipalmitoyl-sn-glycero-3-phosphocholine Tm = 41ºC

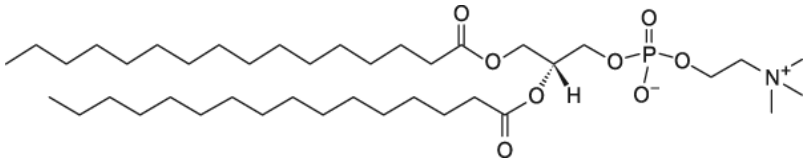

DOPS:1,2-Dioleoyl-*sn*-Glycero-3-[Phospho-L-Serine] Tm = -11ºC

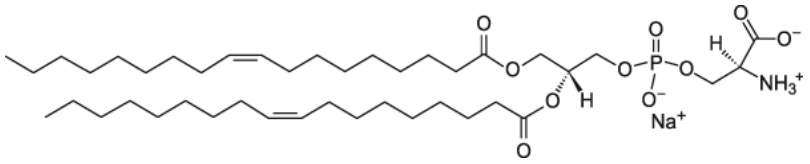

Figure 6.1. Chemical structures and transition temperatures (Tm) of the lipids used in this work.

Polyelectrolytes*:* Poly(ethylenimine) (PEI, Mw = 750 kDa), Poly(sodium 4-styrenesulfonate) (PSS, Mw = 70 kDa), Poly(allylamine hydrochloride) (PAH, Mw = 70 kDa) were obtained from Sigma-Aldrich (Munich, Germany) and were used as received. PEI and PAH are polycationic and PSS is polyanionic.

Buffer solutions*:* Two buffer solutions were used in this work: Tris buffer (0.5 mM Tris-HCl, 10 mM $CaCl_2$, pH 9), and HEPES buffer (10 mM HEPES, 2 mM $CaCl_2$, 150 mM NaCl, pH 7.4).

Substrates*:* 5 MHz QCX303 silicon dioxide coated quartz crystals (Q-Sense AB, Gothenburg, Sweden) were cleaned before surface preparation by immersion in a 6:1:1 (vol/vol) solution of H_2O:NH_3(25%):H_2O_2 (30%) at 70ºC for 10 min followed by rinsing with Milli-Q water and drying in a stream of nitrogen gas. Before mounting the crystals in the flow chamber they were treated with UV/ozone for 30 min.

High quality Ruby Muscovite mica grade V-4, was purchased from SPI Supplies, USA.

SbpA bacterial cell surface layer protein (S-layer) was isolated from *Lysinibacillus sphaericus* CCM 2177 (former *Bacillus sphaericus*). Growth in continuous culture, cell wall preparation, extraction of S-layer protein with 5M guanidine hydrochloride (GHCl), dyalization and further centrifugation were carried out according to literature procedure [32]. The SbpA monomer solution used for recrystallization experiments was adjusted with Milli-Q water to a concentration of 1 mg mL^{-1}. Tris buffer containing protein monomers (protein: buffer volume ratio of 1:9) was used for recrystallization experiments.

Lipid vesicles preparation*:* The lipids used in this work were dissolved in chloroform and a film of lipid molecules was formed after the evaporation of the organic solvent under nitrogen stream and dried under vacuum for more than 1h. The obtained film was hydrated with HEPES buffer under vortexing in order to accelerate lipids to come in suspension. The lipids were then assembling with the hydrophobic part inside, forming multilamellar liposome vesicles (MLVs). In order to prepare large unilamellar vesicles (LUVs), MLVs solution was extruded several times through a polycarbonate membrane (100 nm diameter pores size) mounted in an extruder, at a temperature higher than the transition temperature (Tm) of the used lipid.

Dynamic light scattering (DLS) measurements were carried out with a Nano ZS ZEN 3600 Zetasizer from Malvern Instruments.

Electrophoretical mobility of the formed liposomes was measured with a Nano ZS ZEN 3600 Zetasizer from Malvern Instruments using Smolukowski approximation [33]. All measurements were carried out in HEPES solution.

Quartz Crystal Microbalance with Dissipation Monitoring (QCM-D)*:* Adsorption and viscoelastic studies on S-proteins adsorbed on lipidic systems were carried out with a

QE401 (electronic unit)/QFM401 (flow module) instrument from Q-sense AB (Gothenburg, Sweden) at 25ºC.

Atomic Force Microscopy (AFM) measurements were performed in aqueous solution (0.1 M NaCl), operating at room temperature in tapping mode (scan rate 1 Hz) with a Nanoscope V multimode (Veeco Instruments, Santa Barbara, CA). Silicon nitride (Si_3N_4) cantilevers with nominal spring constant of 0.1 N m^{-1} were used.

Nuclear Magnetic Resonance (NMR) studies were performed with a Bruker Avance 500MHz spectrometer equipped with a 5 mm double resonance inverse probe. One pulse experiments were recorded with 15 seconds of recycled delay and 64 transients. The proton spectral width of 8000 Hz and a total of 64k points were used with 90 degree pulse of 7.5 μs. The data was zero-filled to 128k points and then it was Fourier transformed. All the spectra were processed with Bruker TOPSPIN software.

Langmuir-Blodgett (LB) film preparation: The monolayers were prepared with a Langmuir trough from R&K (Riegler & Kirstein), Berlin. Lipids dissolved in chloroform in total concentration 0.25 mg/mL were spread onto Tris buffer subphase and left for solvent evaporation for 10 min. The lipid monolayer was compressed using a constant barrier speed of 12 Å $molecule^{-1}$ min^{-1} to a pressure at which the monolayer does not reach the collapse. SbpA protein solution (1 mg mL^{-1}) was injected under the lipid monolayer and left overnight for recrystallization.

Transmission Electron Microscopy (TEM) studies were performed with a JEM-2100F /UHR Pole Piece (JEOL, Japan) microscope with a 2k x 2k U-1000 CCD camera (GATAN, UK). The S-layer/lipid system prepared in the Langmuir-Blodgett trough was transferred onto formvar/carbon electron microscope grids. The grids were carefully placed onto the interface and removed after several seconds and then protein films were

chemically cross-linked with 0.5% glutaraldehyde solution (in 0.1 M potassium phosphate buffer, pH 7.2) for 15 min and negatively stained with 0.1 % uranyl acetate in water for 15 min [34].

6.3 Results and Discussion

6.3.1 The interaction of DOPC with SbpA protein

The first studied case was the interaction of SbpA protein with the zwitterionic unsaturated 1,2-dioleoyl-sn-glycero-3-phosphocholine (DOPC). It is known that this lipid is able to form a fluid lipid bilayer when adsorbs on SiO_2 substrate [35].

DOPC vesicles were prepared as described in *Material and Methods* section and their size and apparent charge were characterized by dynamic light scattering and electrical mobility measurements, respectively. It was found that the vesicle size was in the range of (148.0±1.3) nm; while the zeta potential, calculated from the electrophoretic mobility using the Smolukowski approximation [33] took a value of about (0.20±0.06) mV.

The purity of DOPC lipid and its ability to form vesicles have been studied by NMR spectroscopy. Figure 6.2 presents ^{1}H NMR spectrum of pure DOPC lipid in chloroform. The spectrum is free of any impurities and shows signal arising from $–CH_3$ groups marked by red bullets near to 1 ppm and also signal from $-CH_2-$ groups marked by blue bullets between 1-1.5 ppm. Figure 6.2 presents also signals corresponding to $–CH_3$ groups (red color) and $-CH_2-$ groups (blue color). The increase in line width corresponds to an increase in size of the molecules. This can be due to the aggregation of lipid molecules. Also, the decrease in the signals is due to the lack of molecules mobility. In addition, DOSY (diffusion order spectroscopy) experiments showed that

the 2 signals come from a bigger molecule than from a single lipid molecule (data not shown).

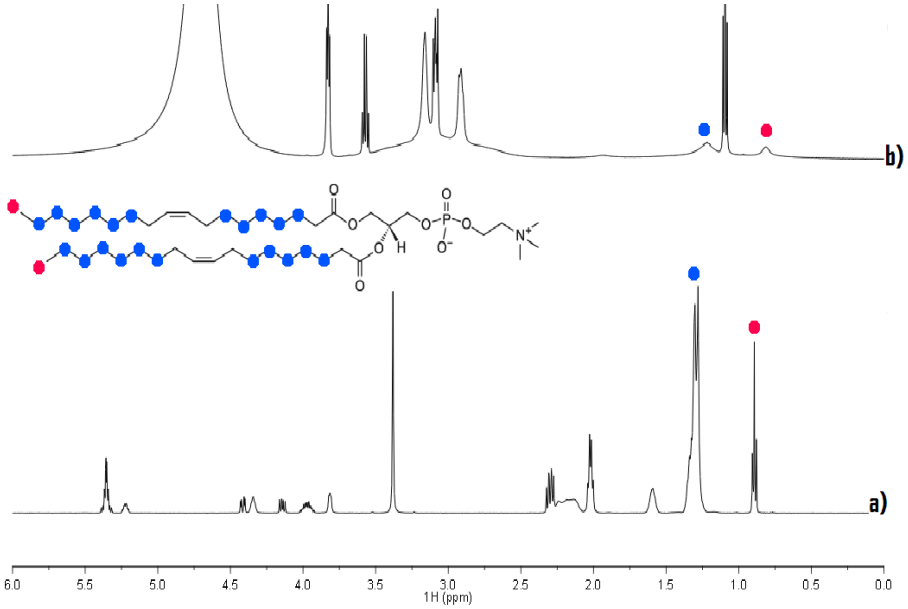

Figure 6.2. The ^{1}H NMR spectrum of DOPC lipid in chloroform (a) and DOPC vesicles in HEPES buffer (b).

The adsorption of DOPC vesicles on silicon crystals have been monitored using QCM-D as can be seen in Figure 6.3. At t = 1230s, DOPC vesicle solution (0.1 mg/mL) is injected. Vesicle adsorption induces a decrease in frequency (f) of 31 Hz. Vesicle rupture occurs after approximately 50 sec causing a final change in frequency up to 23 Hz, which is typicall for lipid bilayer formation. Simultaneously to the frequency variation, the change in the dissipation (D) was recorded. When the vesicles were adsorbed, the dissipation increased to 4 x10^{-6}, decreasing to about 0.66 x10^{-6} after bilayer formation. This shows that the formed lipid bilayer is more rigid than the lipid vesicles. At t = 2050s, HEPES buffer was injected and f and D remain stable upon rinsing indicating that the vesicles are adsorbed in a stable manner. Further, the next experimental step was the adsorption of S-layer protein on a DOPC bilayer. At t = 2680s, S-layer protein solution was introduced and left for adsorption during 30 min.

After rinsing step, an insignificant decrease in frequency (1 Hz) took place; while the dissipation increased with 1 x10^{-6}.

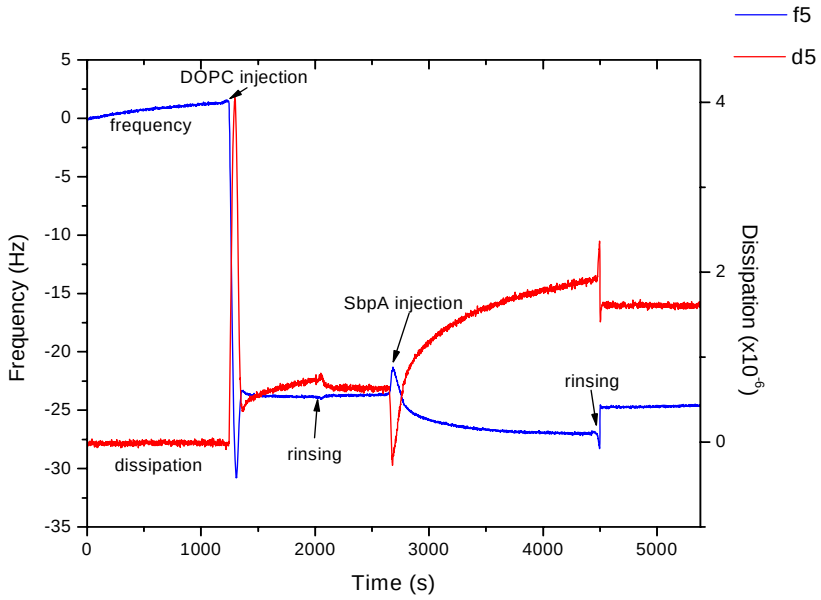

Figure 6.3. Representative measurement of the changes in frequency (blue line) and dissipation (red line) for DOPC vesicle adsorption and further S-layer protein adsorption as a function of time. The measurement shows bilayer formation after vesicles rupture and no significant S-protein adsorption. The 5th overtone is shown here.

We can conclude that no SbpA protein adsorption on DOPC took place. A possible explanation could be that the DOPC lipid bilayer is to fluid (soft) at 25ºC presenting no available binding sites for protein deposition. From other studies, it is known that SbpA will absorb on "hard" surfaces, which confer little or none translational freedom of the molecules responsible for protein binding, such as positive liposomes [27], polyelectrolyte multilayers [36] or mica [38].

The QCM samples were characterized with AFM. Figure 6.4 shows a height AFM image of QCM sample (a), while the recrystallization of SbpA protein on silicon wafers (this can be considered as control experiment) is presented in (b). As can be seen, SbpA recrystallization is characterized by p4 crystalline structure [36] as shown by Fast

Fourier Transform (FFT, placed at the bottom right corner). On the contrary, sample from QCM experiment does not show protein recrystallization.

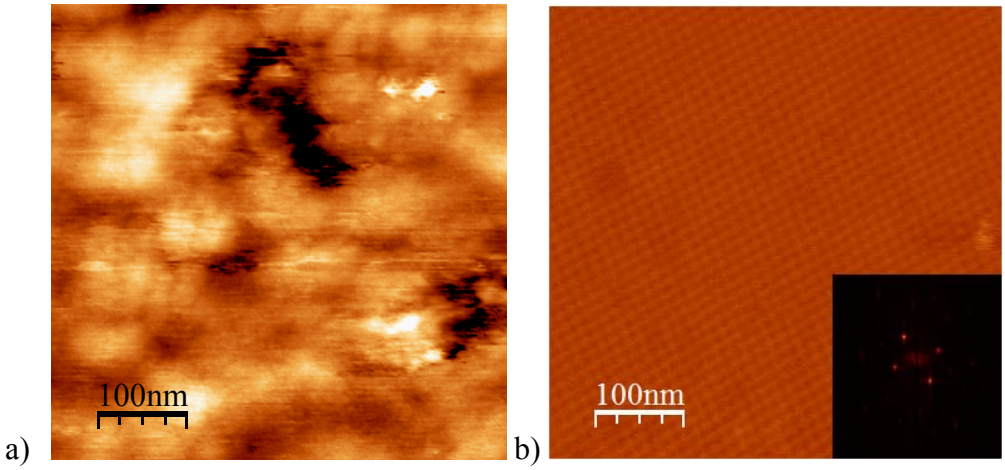

Figure 6.4. (a) Height AFM image of QCM sample (b) height AFM image of SbpA protein adsorbed on silicon and the corresponding FFT (at the right corner). The vertical scale of both images is 15 nm.

Since silicon crystals did not provide satisfactory results, another support (mica) has been used. Mica is a well-known substrate for lipids and S-layer adsorptions [37, 38].

In a similar way to the QCM experiment, bilayer formation and S-protein adsorption were monitored by AFM as a function of time (see Figure 6.5). The bare mica surface, which has a surface roughness of 0.27 nm.

DOPC vesicle solution (0.1 mg/mL) was injected and left for adsorption for 30 min. Afterwards, the topography of the sample was imaged (a). The roughness of the system increased slightly, being 0.36 nm. Surface profile analysis (see green line in (b)) shows that the difference in thickness between the mica support and the adsorbed lipid is about 5 nm, which should correspond to a lipid bilayer. After proving the lipid bilayer formation, the last step was to introduce the bacterial protein to the system. SbpA protein was injected and left for adsorption for 1h. The AFM picture shows that the typical S-pattern corresponding to S-layer formation is present all over the surface (c).

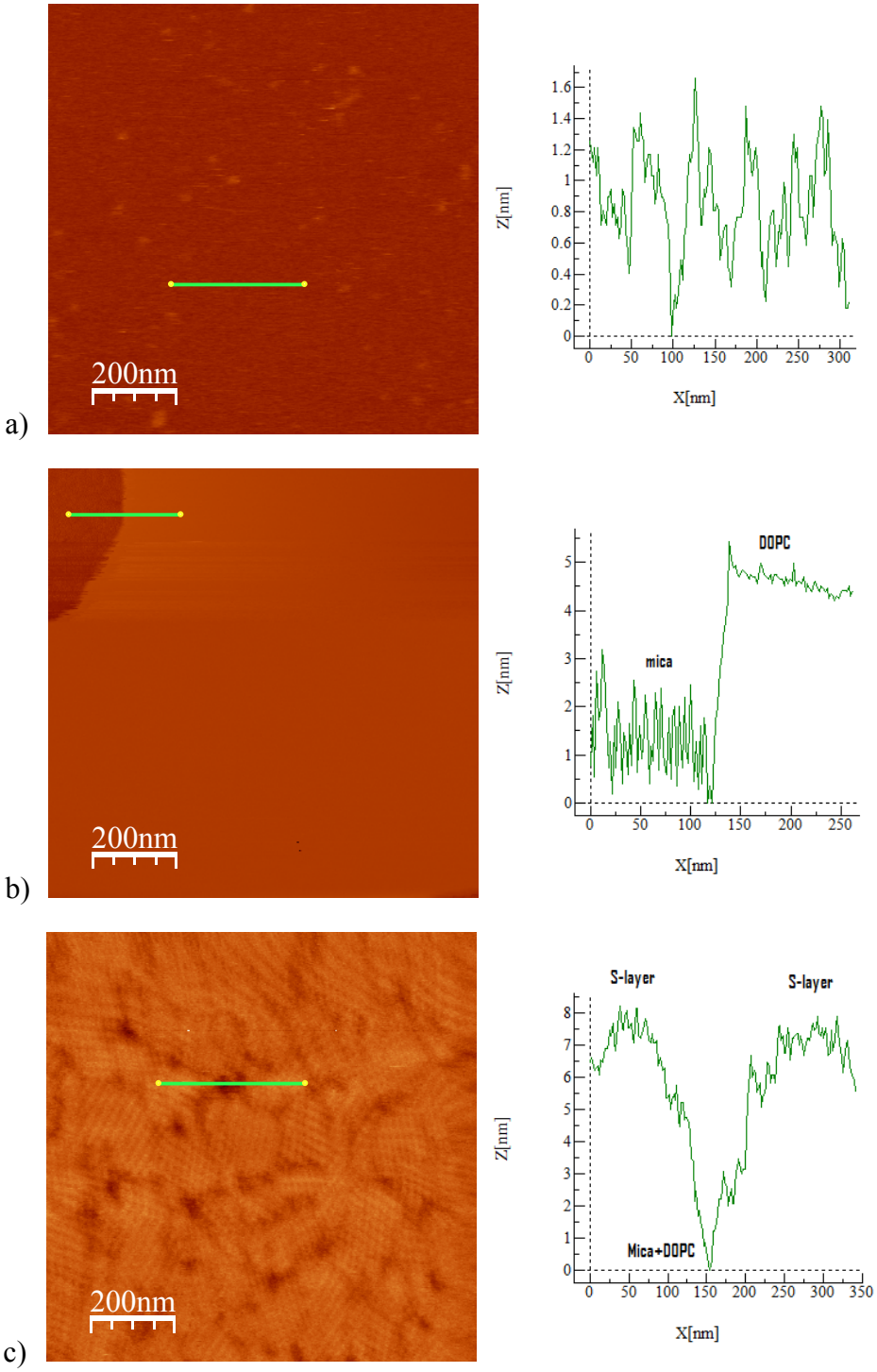

Figure 6.5. (a) Height AFM image and surface profile analysis (right side) of mica surface at t=0; (b) Height AFM image and surface profile analysis of mica covered with DOPC at t=30 min; (c) Height AFM image and surface profile analysis of SbpA protein adsorbed on DOPC bilayer at t=90 min. All images have the vertical scale of 15 nm.

Thus, we can conclude that the recrystallization of SbpA protein on top of DOPC bilayer formed on mica was successful. The roughness of the SbpA protein adsorbed on mica covered with DOPC was 0.57 nm, higher than for mica and mica covered with

DOPC. Surface profile analysis (see green line in (c) shows that the difference in thickness between the DOPC support and the adsorbed SbpA protein is about 8 nm, which should correspond to a protein monolayer.

Both silicon and mica supports allow the formation of DOPC bilayer on top of them, but SbpA protein adsorption occurs only on DOPC adsorbed on mica. Since silicon and mica are hydrophilic and negatively charged under our experimental conditions, the difference in surface chemistry and roughness (1.3 nm for silicon crystal) should influence how the lipid is adsorbed; and therefore the availability of the lipid substrate for the protein. Taken into account that the protein will need a system with less degree of freedom (lower lipid mobility) to form a stable layer, this result will imply that the lipid on mica is less mobile than on silicon.

6.3.2 The interaction of DMPC with SbpA protein

After using an unsaturated lipid, like DOPC, we used an zwitterionic saturated lipid: 1,2-dimyristoyl-sn-glycero-3-phosphocholine (DMPC). As can be seen, both lipids share the headgroup structure, which is of zwitterionic nature. As in the previous section, the size and the electrophoretic mobility of the vesicles were characterized. Freshly formed DMPC liposomes had size in the range of (106.0±0.5) nm, while the zeta potential took a value of (0.33±0.09) mV, which corresponds to the zwitterionic nature of the lipid. It is important to mention that we used polyelectrolyte multilayers (PEM) as direct lipid support because the PEM-lipid system has been proposed as a biomimetic membrane in the last decade. In this way, we introduce (PSS) poly(sodium 4-styrenesulfonate) in the system, a surface with a more hydrophobic behaviour than mica and silicon, maintaining the negative charge of the surface.

The coupling of lipid molecules to polymer components in a planar biomimetic model membrane made of DMPC lipid bilayer supported by polyelectrolyte multilayers was studied by neutron reflectometry [39].

In this work, we have monitored the adsorption of DMPC (0.1 mg/mL) on polyelectrolyte multilayer (PEM) and further SbpA protein adsorption by QCM-D (see Figure 6.6). At t = 800s, the silicon surface is exposed to the Poly(ethylenimine) (PEI) solution, resulting in a decrease in frequency (f) and an increase in the dissipation (D). At t = 847s, polyelectrolyte deposition is interrupted by exchange to Milli-Q water. At t = 1617s, Milli-Q water is changed to Poly(sodium 4-styrenesulfonate) (PSS) solution. The polyelectrolyte multilayer deposition continued with the injection of Poly(allylamine hydrochloride) (PAH) solution at t = 2340s, PSS solution at t = 3100s, PAH at t = 3780s and again PSS at t = 4500s. A uniform decrease in the frequency is noticed after every polyelectrolyte layer deposition. At t = 5140s, DMPC solution was injected and left for adsorption and then was changed to HEPES buffer at t = 9895s. DMPC vesicles adsorb and remain intact on PSS-terminated PEM as can be deduced from the decrease in the frequency (158 Hz) and the increase in dissipation of about $30x10^{-6}$. According to Sauerbrey equation [40], the decrease in the frequency corresponds to a surface mass of about 2797 ng/cm^2 due to DMPC vesicle adsorption.

Finally, S-layer protein solution was injected in the experimental cell at t = 11762s and was left for adsorption during one hour. No remarkable SbpA protein adsorption took place; the decrease in frequency of about 23 Hz corresponds to a surface mass of 407 ng/cm^2. In a previous work, it has been reported that SbpA protein layer formation induces a change in frequency of about 92 Hz [41], therefore we can conclude that SbpA protein adsorbs randomly on DMPC vesicles without forming a protein monolayer or bilayer. The adsorption of S-layer proteins also produces an increase in

the dissipation (ca. 5 x10^{-6}), which indicates that the final hybrid-protein layer is more viscoelastic than DMPC vesicles.

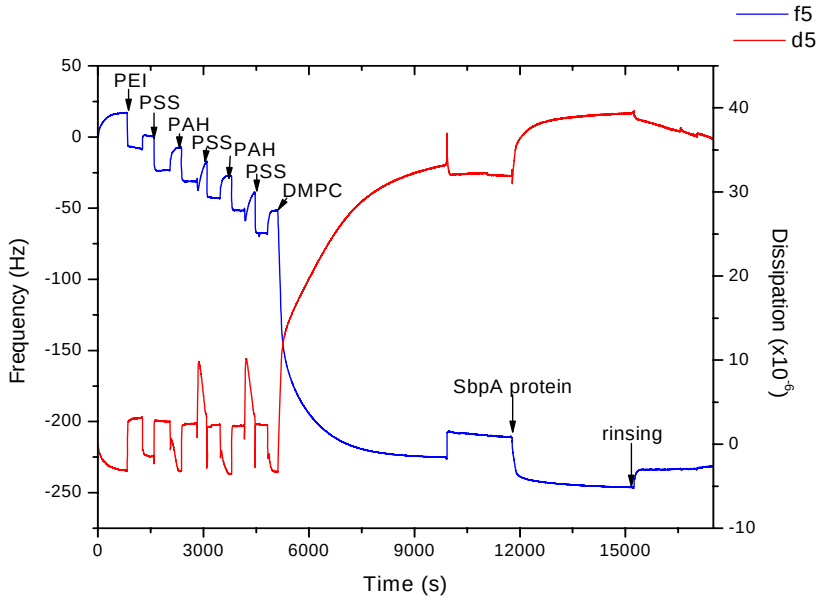

Figure 6.6. Representative measurement of the changes in frequency (blue line) and dissipation (red line) for DMPC vesicles adsorption on PEM and further S-layer protein adsorption as a function of time. Note the monotonous decrease in frequency due to PEM formation followed by the strong decrease in frequency caused by DMPC vesicles adsorption (158 Hz) and the slight decrease in frequency (23 Hz) due to SbpA protein adsorption. The strongest change in dissipation is produced by the lipid-protein system. The 5th overtone is shown here.

6.3.3 The interaction of DPPC with SbpA protein

The difference between DMPC and 1,2-dipalmitoyl-sn-glycero-3-phosphocholine (DPPC) is the alkyl chain length. DPPC has two more -CH_2- groups which imply a higher melting temperature (41ºC) than DMPC (23ºC). When we performed the DMPC experiments at room temperature, the lipids were in a fluid phase since the alkyl chains are disordered, while in the experiments performed in this section, DPPC was in a gel phase. In this way, we were able to check if the thermodynamic state of the lipid influences the lipid-protein interaction since the lipid headgroup remain the same.

The size and the apparent charge of the freshly formed DPPC liposomes were measured by DLS and electrophoretic mobility. DPPC liposomes presented a size of (155.0±2.1) nm and the zeta potential was close to zero (0.8±0.03) mV, so we consider them uncharged.

The adsorption of DPPC vesicles on silicon crystals was monitored using QCM-D as can be seen in Figure 6.7. At t = 920s, a DPPC vesicle solution (0.1 mg/mL) was injected. A decrease in frequency of 310 Hz was recorded; this can be interpreted as DPPC vesicles adsorption on silicon, remaining intact with time. This value is higher than the one obtained for DMPC vesicle adsorption on PSS-terminated PEM. This is not unexpected since DPPC vesicles are larger than DMPC vesicles and DPPC molecule is heavier than DMPC. Vesicle adsorption is correlated with an increase in dissipation which took a value of 20 $x10^{-6}$. At t = 1990s, HEPES buffer was injected and f and D remain quite stable upon rinsing indicating that the adsorbed vesicles are stable. Further, we introduced S-layer protein solution in the system at t = 3475s. The system was equilibrated for 1h. Protein adsorption induces a decrease in frequency of 52 Hz, and an increase in dissipation of about 15 $x10^{-6}$. However, after the rinsing step, the frequency and the dissipation reached similar values as for DPPC vesicles adsorption.

This measurement is a proof that SbpA protein is removed after rinsing step and therefore, does not have strong affinity to DPPC.

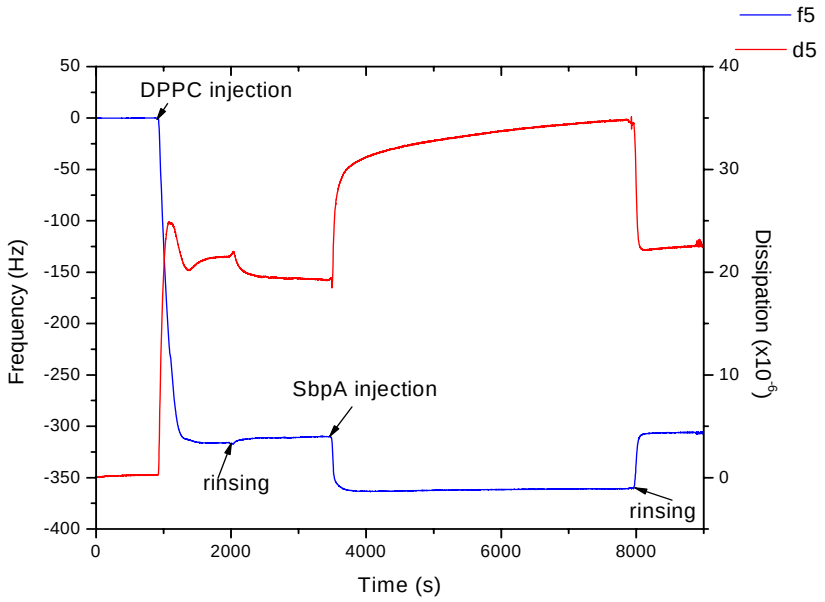

Figure 6.7. Representative measurement of the changes in frequency (blue line) and dissipation (red line) for DPPC vesicles adsorption and further S-layer protein adsorption as a function of time. From the measurement it can be clearly stated that DPPC vesicles adsorb strongly on silicon crystals. It can be also observed that SbpA protein desorption occurred during washing step. The 5th overtone is shown here.

In order to clarify the absence of protein on DPPC vesicles, AFM experiments were carried out. Figure 6.8 shows that DPPC vesicles (see white empty circles) of diameter 200 nm are adsorbed on silicon crystals.

The adsorption of DPPC vesicles (200 nm diameter) on silicon produces a deformation of the vesicles. This could be deduced from surface profile analysis (see green line) which shows a difference in height between the vesicles and the silicon substrate between 50-80 nm. No crystalline S-protein structure could be observed on the vesicle surface.

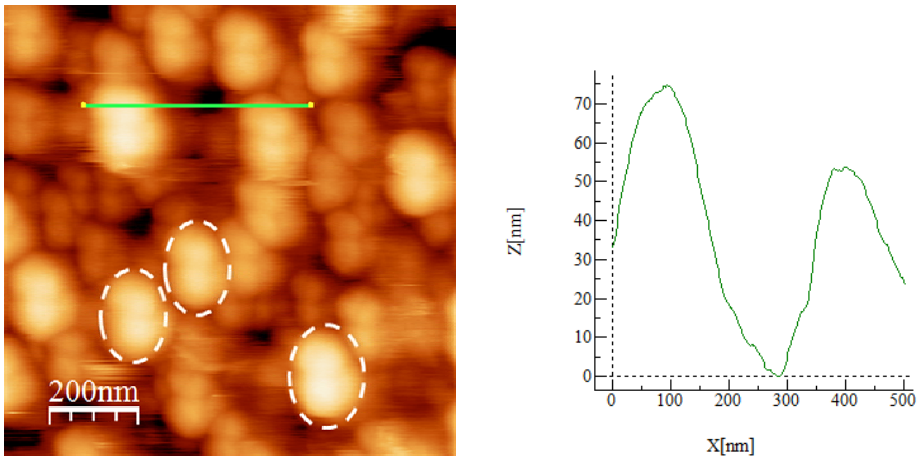

Figure 6.8. On the left: height AFM image of DPPC vesicles (white circles) adsorbed on silicon. Neither S-protein, nor typical S-layer pattern could be observed. The vertical scale of the image is 77 nm. On the right: a profile analysis (along the green line) shows that the height of the vesicles is from 50 to 70 nm.

This AFM result correlates with QCM results. Both experimental techniques confirmed that SbpA protein has no affinity for DPPC vesicles. In this case, we have proved that the variation of the thermodynamic state of the alkyl lipid chain maintaining the same headgroup (PC) does not lead either to SbpA protein adsorption or to protein crystal formation.

6.3.4 The interaction of DMPG with SbpA protein

Untill now we have used uncharged lipids (due to zwitterionic nature of PC). In this section, we are using (DMPG) 1,2-dimyristoyl-sn-glycero-3-[phospho-rac-(1-glycerol)], a saturated lipid, with the same chain length as DMPC but different (charged) headgroup. DMPG as a saturated anionic phospholipid constitutes one of the major membrane phospholipids.

Freshly formed DMPG liposomes had a size in the range of (105.0±2.2) nm and were negatively charged (-26.3±1.8) mV as measured by dynamic light scattering and electrophoretic mobility. The presence of DMPG liposomes was also confirmed by

TEM as is shown in Figure 6.9. Vesicles with size in the range 100-200 nm were observed.

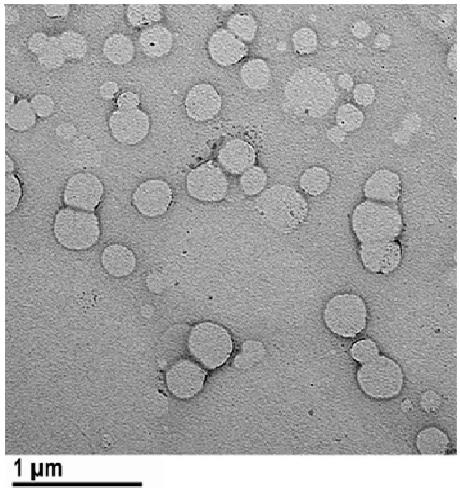

Figure 6.9. TEM image of DMPG vesicles deposited on carbon grids and negatively stained with uranyl acetate. The size range of the DMPG vesicles is in agreement with DLS measurements within error.

The purity of DMPG lipid and the presence of the vesicles have been studied by NMR spectroscopy. Figure 6.10 presents ^{1}H NMR spectrum of DMPG lipid in chloroform. The spectrum is free of any impurities shows signals arising from $–CH_3$ groups marked by red bullets near to 1 ppm and also signals from $-CH_2-$ groups marked by blue bullets between 1-1.5 ppm. The signal at 1.55 ppm is given by the deuterated water present in chloroform. Figure 6.10 presents also signals corresponding to $–CH_3$ groups (red color) and $-CH_2-$ groups (blue color). The increase in line width corresponds to an increase in size of the molecules. This can be due to the aggregation of lipid molecules. Also, the decrease in the signals is due to the lack of molecules mobility. In addition, DOSY (diffusion order spectroscopy) experiments showed that the 2 signals come from a bigger molecule than from a single lipid molecule.

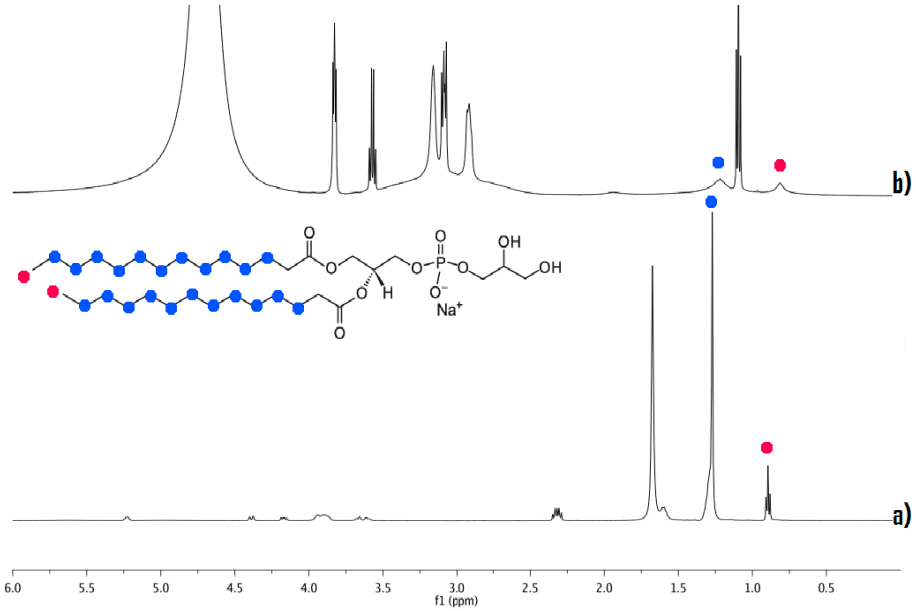

Figure 6.10. The ^{1}H NMR spectrum of DMPG lipid in chloroform (a) and DMPG vesicles in HEPES buffer (b).

Vesicle adsorption on silicon crystals was monitored by QCM-D as can be seen in Figure 6.11. At t = 2000s, DMPG vesicles solution (0.1 mg/mL) was injected, causing a decrease in frequency of 20 Hz and an increase in dissipation up to 8 $x10^{-6}$. This change in frequency indicates a bilayer lipid formation at one step, a different mechanism from the DOPC case. At t = 5420s, HEPES buffer was injected and f and D remained quite stable upon rinsing indicating that the vesicles are adsorbed in a stable manner. Finally, S-layer protein was introduced in the system. At t = 6320s, S-layer protein solution was injected and left for adsorption during more than 1h. It can be clearly seen in Figure 6.11 that SbpA protein adsorption induces a change in frequency of 93 Hz which, applying Sauerbrey equation corresponds to a surface mass of 1646 ng/cm^2. This value is in agreement with results obtained for SbpA adsorption on PEM and silanes [41, 42]. The adsorption of SbpA protein increased slightly the dissipation (2 $x10^{-6}$), conferring the lipid-protein system a higher viscoelasticity than the lipid layer itself.

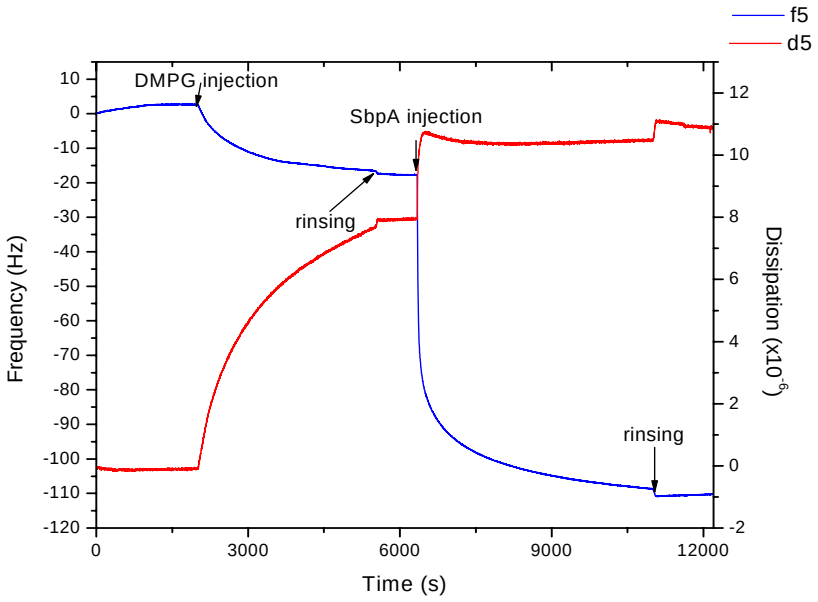

Figure 6.11. Representative measurement of the changes in frequency (blue line) and dissipation (red line) for DMPG vesicles adsorption and further S-layer protein adsorption as a function of time. A decrease in frequency of 20 Hz is related to DMPG bilayer formation. More remarkable is the change in frequency (93 Hz) after SbpA protein injection which means a very strong protein-lipid interaction. The 5th overtone is shown here.

After adsorbing bacterial protein on a DMPG bilayer we proceed to study the SbpA interaction with DMPG vesicles. Mica was the appropriate support for DMPG vesicle adsorption. A lipid solution of 0.1 mg/mL was adsorbed on mica during 30 min. Afterwards, SbpA protein was injected into the system, which equilibrated for 1h.

Height AFM measurements give an overview image of the system SbpA-covered vesicles, the diameter of the vesicles being in the range of 100-200 nm (a). However, from this picture it is not possible to distinguish if the protein is covering the vesicles. In order to elucidate this question, we made a zoom of (a). Height AFM image (b) shows the presence of crystalline structure of SbpA protein on DMPG vesicles.

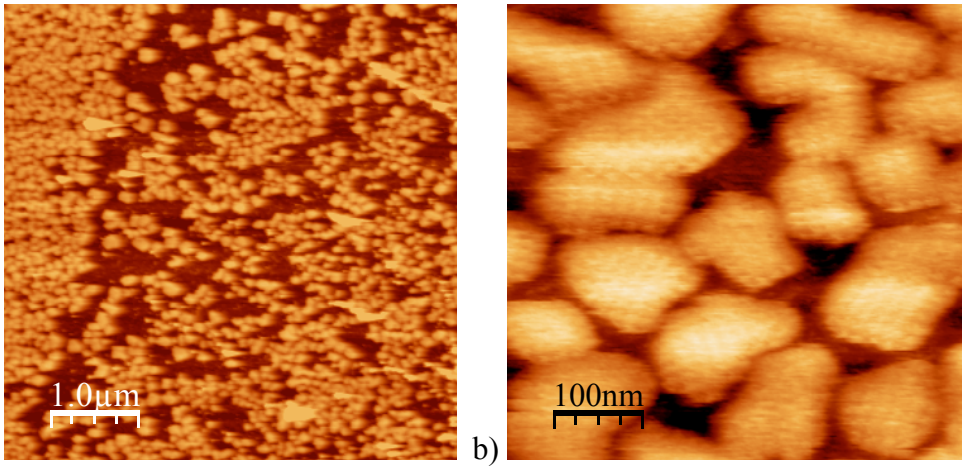

Figure 6.12. Height AFM images of: (a) DMPG vesicles possibly coated with SbpA protein; (b) a zoom of picture a shows recrystallized SbpA protein on DMPG vesicles. The vertical scale of the images is 20 nm.

6.3.5 The interaction of DOPC/DOPS (4:1) mixture with SbpA protein

In the last sections, we have studied the interaction between protein and lipid layers composed of a single type of phospholipids. However, this is not the normal situation in biological membranes, since they are composed of lipid mixtures, proteins, etc.

In this section, we study the SbpA protein interaction with phospholipid mixtures. These mixtures will allow us to vary not only the exposed lipid surface charge to the protein but also the lipid headgroup size and the fluidity of the lipid layer.

The first lipid mixture used consisted of DOPC (1,2-dioleoyl-sn-glycero-3-phosphocholine) and DOPS (1,2-Dioleoyl-*sn*-Glycero-3-[Phospho-L-Serine]) in a molar ratio 4:1. It has to be said that both lipids are unsaturated, DOPC being uncharged, while DOPS has negative charge due to serine group (see Figure 6.1).

Another reason to use this lipid mixture is that it forms a lipid bilayer on silicon or mica substrates [43]. The size and the apparent charge of DOPC/DOPS (4:1) liposomes were characterized by DLS and electrophoretic mobility. Liposomes had size in the range of (130±3) nm and the zeta potential was (-12.0±0.3) mV, that is slightly negatively charged as expected from DOPS molecules.

The adsorption of DOPC/DOPS (4:1) vesicle mixture on silicon was monitored using QCM-D as can be seen in Figure 6.13. At t = 765s, vesicle mixture solution (0.1 mg/mL) was injected. A decrease in frequency of 70 Hz and an increase in dissipation of 8 x10^{-6} were recorded as a consequence of vesicle adsorption. Vesicle rupture led to bilayer formation as the final change in frequency shows (26 Hz), while the dissipation reached a value close to zero.

Finally, at t = 4240s, SbpA protein solution was injected. The system was left 1h for equilibration. After rinsing, the final decrease in frequency of about 72 Hz and increase in dissipation of about 14 x10^{-6} was registered.

The change in frequency after SbpA protein adsorption corresponds to a surface mass of 1274ng/nm, which is a bit lower than a S-protein bilayer and slightly larger than a protein monolayer. This measurement shows that the addition of negative lipid is enough to force SbpA protein adsorption on the DOPC/DOPS (4:1) lipid mixture bilayer comparing with the DOPC bilayer.

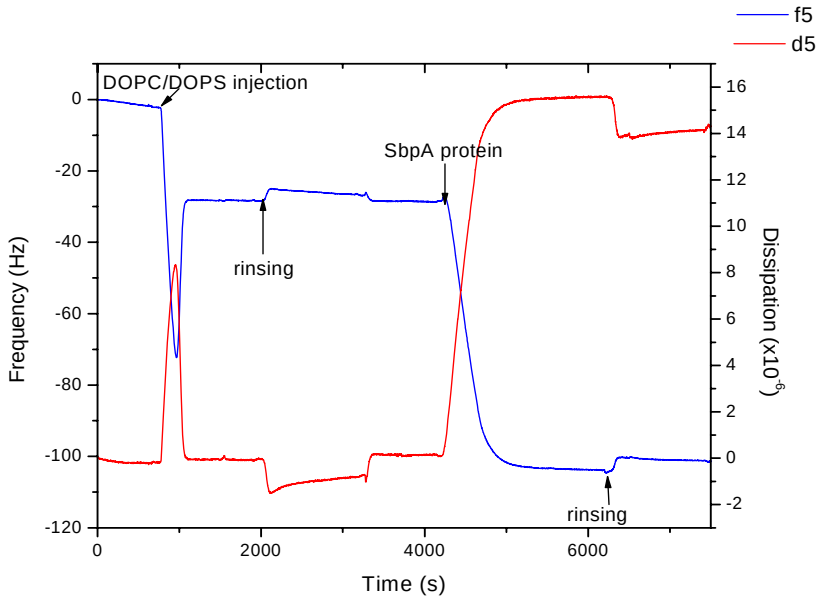

Figure 6.13. Representative measurement of the changes in frequency (blue line) and dissipation (red line) for DOPC/DOPS (4:1) vesicles mixture adsorption and further S-

layer protein adsorption as a function of time. Bilayer formation occurs after vesicle rupture. SbpA protein adsorbs on the formed bilayer. A charge ratio of DOPC/DOPS (4:1) is enough to adsorb SbpA protein. The 5th overtone is shown here.

Structural information of the protein/lipid mixture system was studied by AFM. Figure 6.14 shows a height AFM image and the corresponding surface profile analysis of SbpA protein adsorbed on DOPC/DOPS mixture. It can be seen that protein adsorption did not lead to a regular crystalline layer (Fast Fourier Transform at the top right corner shows no regularity). The measurement shows a non-homogeneous surface with a roughness of 1.5 nm, likely composed of protein-lipid mixture. Regular spots (white empty circles) of about 50 nm in diameter can be observed; taking into account that the vesicle size was about 130 nm, we do not consider these structures as vesicles. Surface profile analysis (see green line) shows that the largest thickness is about 4-5 nm (the thickness of a lipid bilayer), while the length of the aggregates is around 50-100 nm.

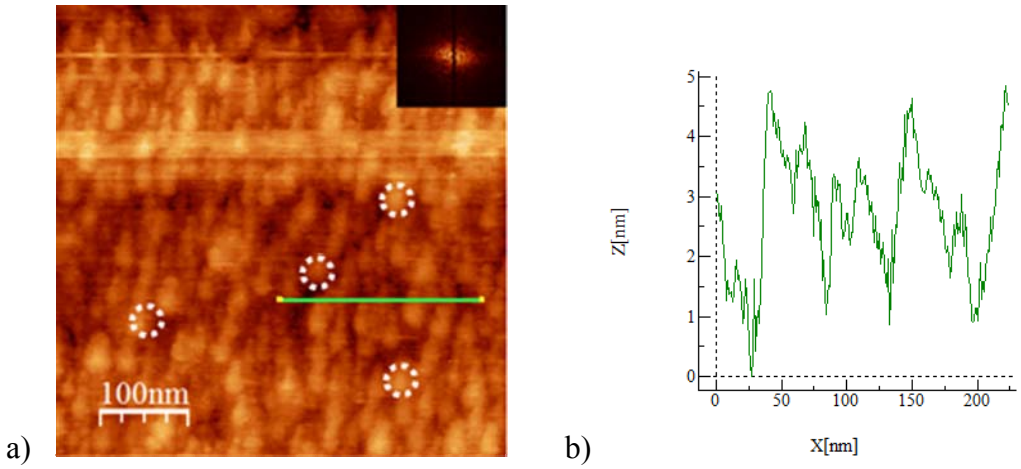

Figure 6.14. (a) Height AFM image of SbpA protein adsorbed on DOPC/DOPS (4:1) mixture and the corresponding FFT at the top right corner, showing no crystalline protein structure. The vertical scale of the image is 20 nm. (b) Surface profile analysis (along the green line) shows a thickness difference of about 4-5 nm, and aggregates around 50-100 nm in length.

Although a DOPC/DOPS (4:1) mixture and DOPC form a lipid bilayer on silicon, only the mixture is able to attract SbpA proteins without obtaining a crystalline protein layer.

SbpA protein adsorption can be due to the negative nature of the lipid bilayer since the viscoelastic properties of DOPC bilayer and the lipid mixture bilayer are similar as shown by QCM (see Figure 6.3 and Figure 6.13).

6.3.6 The interaction of DOPC/DMPG (1:1) mixture with SbpA protein

The introduction of negative charge in a lipid mixture composed of unsaturated DOPC and DOPS led to the adsorption of SbpA protein, although the viscoelastic properties of both type of bilayers were similar.

In this section, we use a lipid mixture that changes simultaneously the surface charge and the rigidity of the lipid layer. This mixture is composed of DOPC (1,2-dioleoyl-sn-glycero-3-phosphocholine) and DMPG (1,2-Dioleoyl-*sn*-Glycero-3-[Phospho-L-Serine]) in a molar ratio of 1:1. Previously it has been shown that DOPC vesicles led to a lipid bilayer formation, while DMPG vesicles attracted SbpA proteins (see section 6.3.4).

The size and the apparent charge of DOPC/DMPG (1:1) liposomes were characterized by DLS and electrophoretic mobility. Liposomes had a size in the range of (186±3) nm and a zeta potential of (-16.0±0.3) mV. This value is very similar to the zeta potential of DOPC/DOPS mixture.

The adsorption of the DOPC/DMPG vesicles on silicon was monitored by QCM-D as can be seen in Figure 6.15. At t = 740s, vesicle mixture solution (0.1 mg/mL) was injected. A decrease in frequency of 66 Hz and an increase in dissipation of 5 $x10^{-6}$ indicate vesicle adsorption. At that point, the system remained in an intermediate state for approximately 1500s until vesicle rupture occurred and a lipid bilayer was formed as the changes in frequency (38 Hz) and dissipation (3 $x10^{-6}$) show. The usual values for bilayer formation are around 25 Hz and 1 $x10^{-6}$ for the change in frequency and dissipation respectively. Finally, at t = 3320s, SbpA protein solution was injected. The

system was left for equilibration during 1h. No significant change in frequency was noticed, meaning that no significant SbpA adsorption on DOPC/DMPG (1:1) mixture took place.

Although, it has been shown that DMPG vesicles attracts SbpA proteins, the ability of DMPG to attract SbpA protein is lost when DMPG is mixed with DOPC in a lipid bilayer.

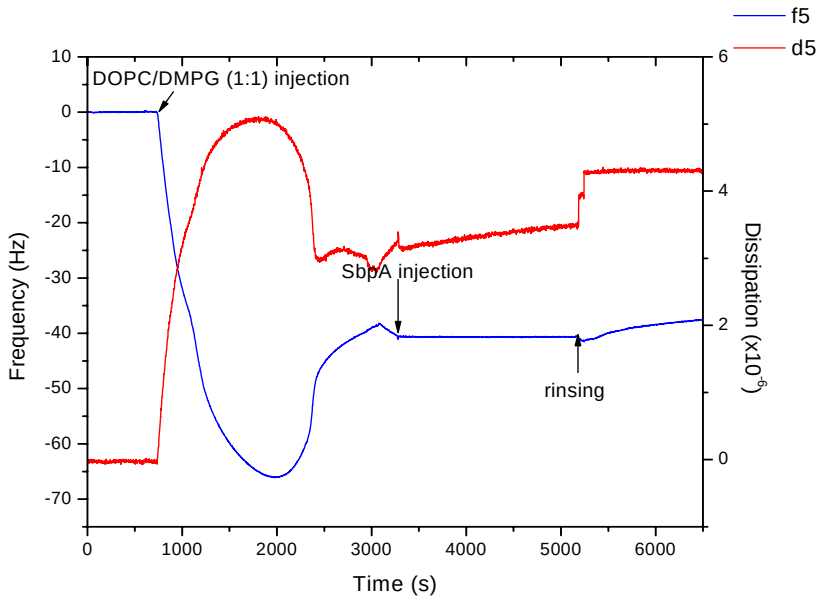

Figure 6.15. Representative measurement of the changes in frequency (blue line) and dissipation (red line) for DOPC-DMPG (1:1) vesicle adsorption. At 2000s, a minimum in the frequency is observed. However, the shape of the minimum is wider than the minimum observed for DOPC vesicle adsorption and DOPC-DOPS (4:1) vesicle adsorption. This is connected to the kinetic behavior of vesicle rupture that in this case is slower. This slow kinetics ends with the formation of an intermediate state composed of vesicles and a lipid bilayer. The frequency and dissipation show that SbpA protein does not adsorb on a DOPC-DMPG (1:1) lipid mixture. The 5th overtone is shown here.

Structural studies of SbpA protein adsorbed on a DOPC/DMPG (1:1) mixture were investigated by AFM (see Figure 6.16). Since the mixture DOPC/DMPG on silicon did not lead to SbpA adsorption, another support (mica) was used for vesicle adsorption. DOPC/DMPG (1:1) lipid suspension (0.1 mg/mL) was left to adsorb on mica surface

for 30 min. Afterwards, SbpA protein (0.1 mg/mL) was introduced in the system which was left 1h for equilibration. Figure 6.16 shows the topography of the protein-lipid mixture. Two different structures can be observed: the first one consists of patches with the regular protein structure (roughness of 0.6 nm), and the second one, consisting of very flat lipid domains (roughness of 0.3 nm) (bright areas). This argument is supported by surface profile analysis (see the green line in Figure 6.16), which shows a difference in thickness between the two structures of about 3-3.5 nm, a value that can be attributed to the thickness of a lipid bilayer.

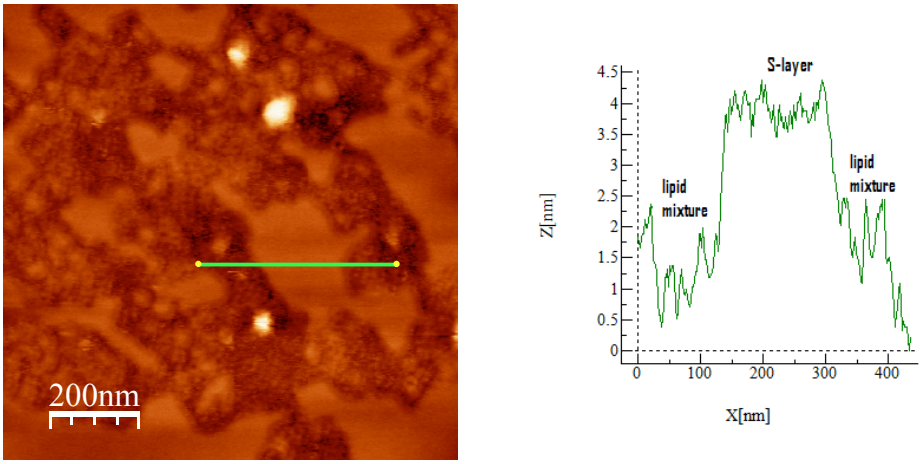

Figure 6.16. Height AFM image and surface profile analysis of the SbpA protein/(DOPC/DMPG) lipid system on mica. Note the hybrid nature of the system, consisting of adsorbed protein and flat lipid domains which are likely adsorbed on top of the protein layers. This result is an unexpected phenomenon, since indicates that the protein removed the adsorbed lipid layer, and opens a new question regarding the adsorption kinetics (competition) of SbpA protein and DOPC/DMPG (1:1) on mica substrate. The vertical scale of the AFM image is 15 nm.

Further characterization of the protein/lipid mixture surfaces was carried out performing force-distance curves measurements different areas. Figure 6.17 shows a force-distance curve carried in the bright areas. The approaching curve shows a slight repulsion regime of about 5 nm range, before touching the surface. The load increases until a kink of about 5 nm appears. This means that the AFM tip has indented the lipid layer [44]. The

retracting curve shows a small adhesion peak, which is related to the interaction between the AFM tip and the lipid molecules, reaching the zero force level of about 10 nm distance. Note that the picture presents an offset for the deflection error (zero force level) of -24 nm (the force is the deflection of the cantilever multiplied by its spring constant). Figure 6.18 shows a force-distance curve carried out in the protein areas. The approaching and retracting curves coincide; this is typical for S-layer structure [36]. The approaching curve shows that no indentation event takes place for loads four times higher than the previous case.

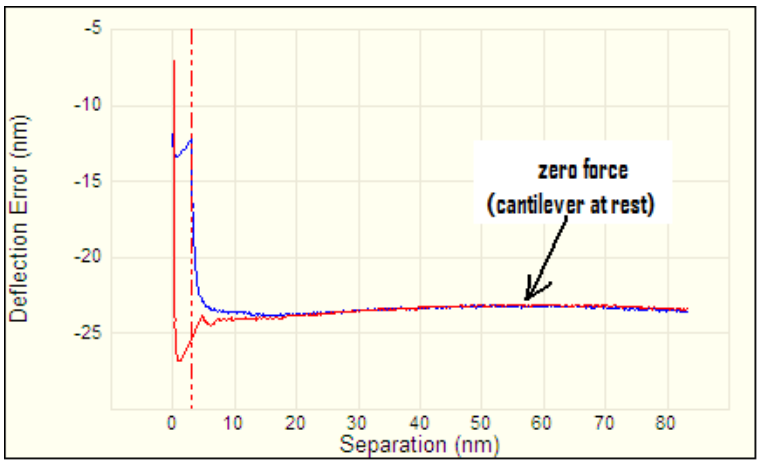

Figure 6.17. Representative force-distance curve taken on bright areas of Figure 6.16. The kink observed in the approaching curve is a measure of a bilayer thickness (5nm)

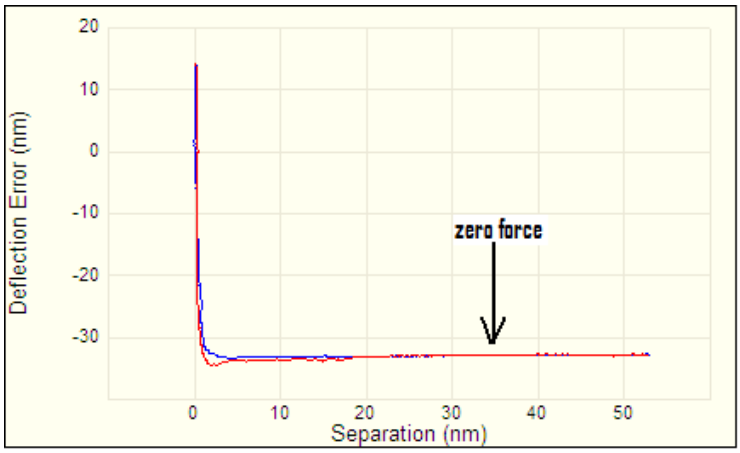

Figure 6.18. Representative force-distance curve taken on the regular protein structure in Figure 6.14. In this case, no indentation event is observed. The overlapping of

approaching and retracting curves shows that the material is not viscoelastic (no hysteresis occurs). Furthermore, no protein unfolding events are observed.

Surface profile analysis together with force-distance measurements proof the presence of a lipid bilayer on top of S-layer structure. A hypothesis could be that SbpA proteins remove the lipid molecules during the protein self-assembly process on the mica surface.

6.3.7 The interaction of lipid monolayers with SbpA protein

In the previous sections, bilayer formation or vesicle adsorption was led by the interaction between the lipid molecules and the substrate. However, we could not control either the thermodynamic state of the lipid, or the amount of the adsorbed lipid. In this section, we will work with lipid monolayers on a Langmuir trough. This will allow us to control the lipid phase behaviour and the amount of the lipid present at the air/water interface. An advantage of this technique is that one can change and control the thermodynamic state of the lipid at air/water interface by compressing the layer with two barriers. Lipid monolayers were obtained after spreading the lipids at the air/water interface when the two barriers were far away from each other (maximum available surface). At this moment, the lipids are in a gas phase (there are no collisions between lipid molecules). By moving the barriers, the lipid molecules are forced to occupy a smaller available area. In this way, there is a moment when the lipid molecules start to interact with each other, and a surface pressure is measured. When this type of experiment is carried out at constant temperature, it is called isotherm. From former experiments it is known that SbpA protein adsorbs on solid supports like silicon wafers, mica, and “hard” well-organized surfaces, such as lipid monolayers, disulphides or

silanes [42, 45]. Therefore, in this section, we will prepare three "hard" well-organized lipid layers.

In order to achieve this goal, surface pressure-area (π-A) isotherms were measured in a aqueous subphase (0.5 mM Tris-HCl, 10 mM $CaCl_2$, pH 9 buffer) at 25ºC, for the following lipid systems: DPPC, DPPC/DOPS (1:1) and DPPC/DMPG (1:1). Representative isotherms are shown in Figure 6.19. The first isotherm (a) corresponds to uncharged DPPC monolayer. This isotherm is very well known [46]. The DPPC lipid monolayer isotherm presents a plateau region at a surface pressure of 8 mN/m between molecular areas of 100-150$Å^2$, reaching a more condensed state for molecular areas bellow 100 $Å^2$. This condensed phase means that the lipid is well-packed being a suitable candidate support for SbpA protein adsorption. Therefore, the chosen surface pressure for SbpA protein to adsorb was 30 mN/m (the lipid molecules are well-packed).

The second isotherm (b) corresponds to the DPPC/DOPS (1:1) lipid mixture. The addition of charged DOPS eliminates the fluid-crystalline coexistence phase (plateau region). The surface pressure remains zero until a molecular area of about 135$Å^2$ is reached. At that molecular area, lipid molecules start to interact with each other; this can be seen in the monotonous increase in the surface pressure with molecular area decreasing. Since at 28 mN/m, for a molecular area of 60 $Å^2$, the lipid molecules are well-packed, this surface pressure was chosen to adsorb SbpA protein on the lipid monolayer.

The last isotherm (c) corresponds to a lipid mixture of DPPC/DMPG (1:1).

The addition of charged DMPG also removes the plateau region of the DPPC isotherm. The surface pressure remains zero until a molecular area of about 150 $Å^2$ is reached and

increased monotonously until 16 mN/m, which is almost half of the surface pressure of the two previous isotherms. SbpA adsorption was carried out at this surface pressure.

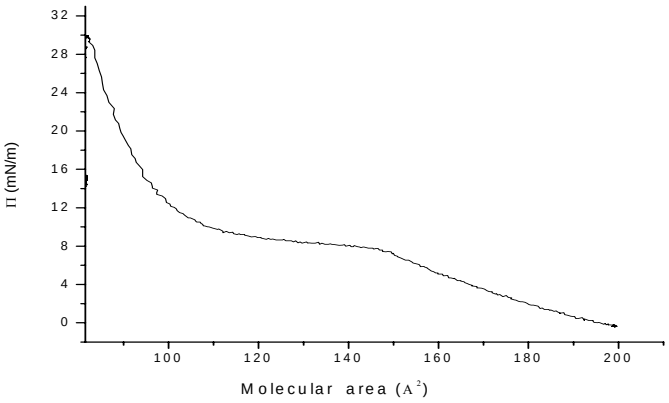

a)

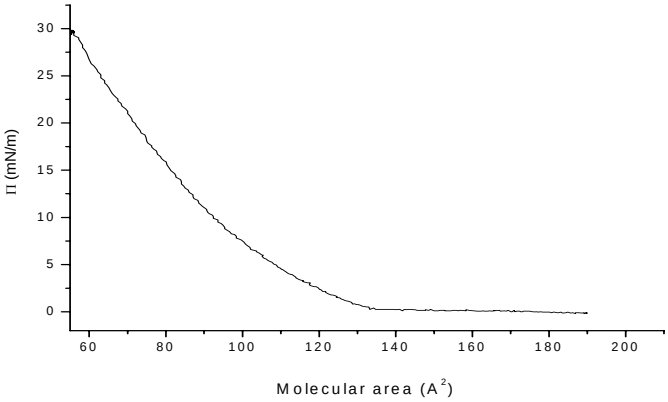

b)

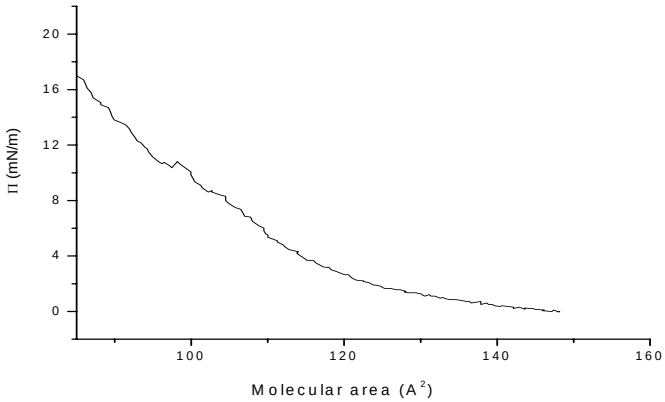

c)

Figure 6.19. π-A isotherms of the following lipid systems: (a) DPPC, (b) DPPC/DOPS (1:1) and (c) DPPC/DMPG (1:1). Tris buffer was used as aqueous surface. The temperature was kept constant at 25ºC.

After lipid monolayer formation, SbpA protein solution (3 mL) was injected under the lipid monolayer. Protein adsorption experiments were carried out overnight. Finally, lipid/protein system was transferred to a formvar carbon grid. The structure of the protein/lipid system was investigated with TEM. EM-micrographs of SbpA protein adsorbed onto lipid monolayers are shown in Figure 6.20.

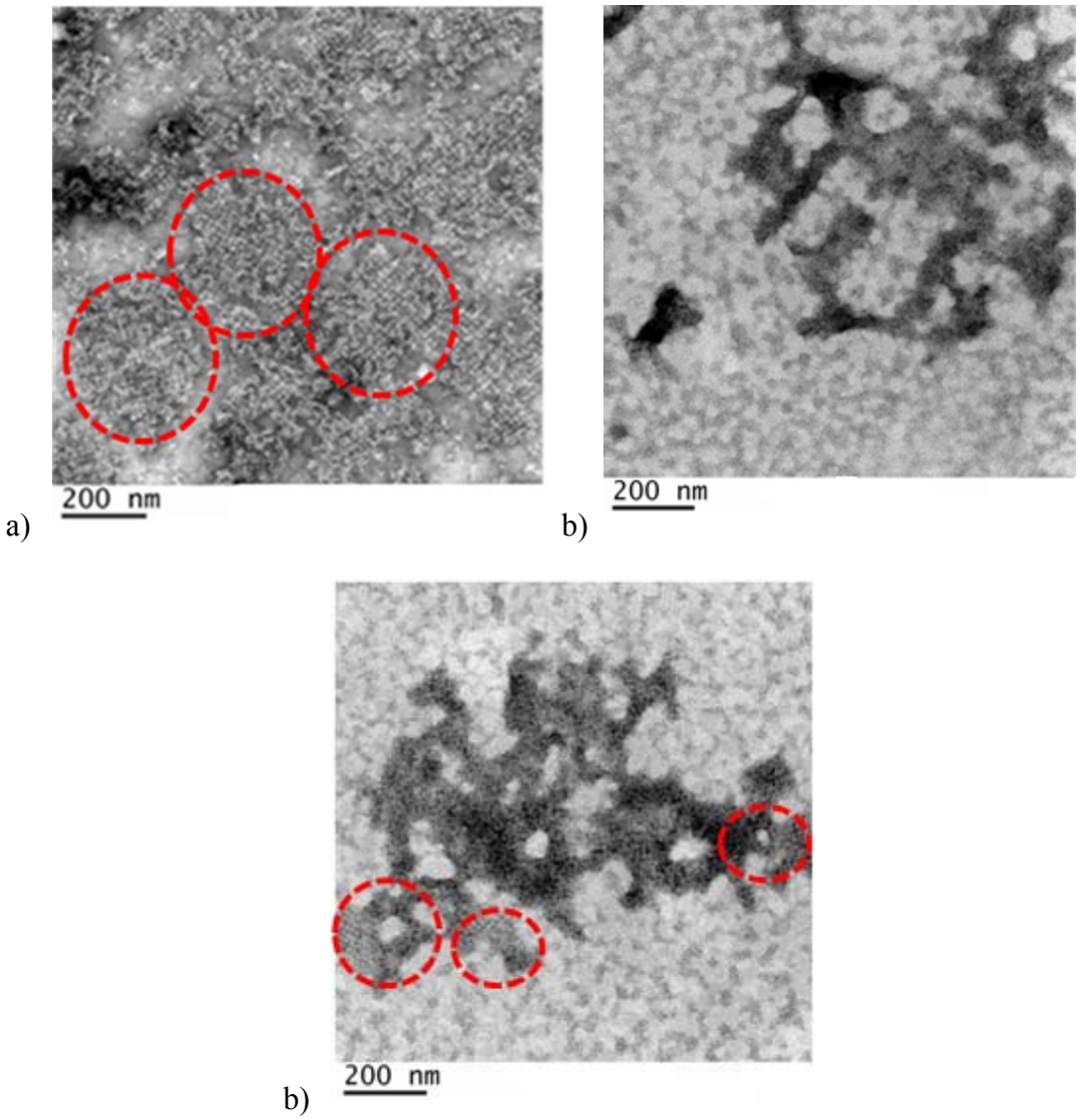

a) b) b)

Figure 6.20. EM-micrographs of SbpA protein recrystallized onto lipid monolayers: (a) DPPC; (b) DPPC/DOPS (1:1); (c) DPPC/DMPG (1:1). Red circles show areas with recrystallized S-protein. Note: uranyl acetate makes protein look white.

A condensed DPPC monolayer is a suitable substrate for SbpA protein crystallization as several patches (red empty circles) with crystalline structure can be observed (a).

In section 6.3.3, we have seen that SbpA protein does not adsorb on DPPC vesicles, while in this case, SbpA protein is able to form a protein layer due to the fact that the lipid monolayer is in a condensed state. Thus, closer interaction between the lipids and proteins occurs. The interaction is primarily electrostatic (probably dipolar) and the contact between the lipid monolayer and the adsorbed protein occurs through the "primary" binding sites on the protein surface [23].

Regular structures which do not correspond to the known protein crystalline structure are present in (b). Only small areas could be associated to a protein crystal. This experiment shows that a condensed monolayer made of DPPC/DOPS (1:1) mixture is not a good surface for S-layer crystallization but for S-layer protein adsorption.

This fact is not unexpected since, in section 6.3.5, DOPS was responsible for S-protein adsorption when mixed with DOPC. Some S-layer areas (red empty circles) on the DPPC/DMPG (1:1) mixture (c) are present.

It has to be said that DMPG vesicles are a good surface for SbpA protein recrystallization as shown in section 6.3.4. This process is not only driven by dipolar interactions (DPPC molecules) but also through charge interactions (DMPG). In this last section, we have shown that lipid monolayers can be suitable surface for SbpA recrystallization.

However, many parameters have to be improved, such as the appropriate lipid ratio mixture, temperature conditions (the π-A isotherms) and solvent conditions (ionic strength, pH, etc); many questions remain still unanswered.

6.4 Conclusions

The interaction of SbpA protein with saturated, unsaturated, charged and uncharged lipids has been investigated.

It has been found that zwitterionic DOPC bilayers, negatively charged DMPG vesicles, and DOPC/DMPG bilayers adsorbed on mica, together with DPPC and DPPC/DMPG monolayers have high affinity for SbpA protein, leading to the formation of crystalline protein layers.

Further investigations indicated a weak interaction between SbpA proteins and DOPC and DOPC/DOPS bilayers supported on silicon. Due to the nature of this interaction, no protein crystal could be formed. Finally, two lipid systems, DMPC vesicles adsorbed on polyelectrolytes multilayers and DPPC vesicles supported on silicon, did not have any affinity for SbpA proteins.

In this work we have shown the importance of the surface chemistry and roughness of the substrates used for lipid deposition. This can be stated by the fact that mica is a better support for the protein/lipid system.

Also the thermodynamic state of the lipid layer plays a role for protein recrystallization. The clearest case was the observed regular S-layer structures on condensed DPPC monolayers at 25ºC, while no S-protein adsorption took place on DPPC vesicles.

Although we have found experimental conditions leading to the building of a macromolecular system composed of phospholipids and S-proteins, still very little is known about the recrystallization of different S-proteins on supported flat lipid layers and vesicles. More basic research has to be carried out to understand and control the formation of stable S-layers on lipid supports by improving experimental conditions (lipid ratio mixture, temperature, solvent conditions etc.).

Finally, this is an important issue to develop in the near future potential applications of S-layer (fusion) proteins, which will provide many different functionalities to the natural lipidic systems.

References

[1] M.M. Parmar, K. Edwards and T.D. Madden (1999). *Biochimica et Biophysica Acta* 1421: 77-90.

[2] A.R. Curran, R.H. Templer and P.J. Booth (1999). *Biochemistry* 38: 9328-9336.

[3] H. Möhwald (1990). *Annual Review of Physical Chemistry* 41: 441-476.

[4] H.M. McConnell (1991). *Annual Review of Physical Chemistry* 42: 171-195.

[5] C.M. Knobler (1992). *Annual Review of Physical Chemistry* 43: 207-236.

[6] G. Brezesinski and H. Möhwald (2003). *Advanced Colloid and Interface Science* 100-102: 563-584.

[7] J.L. Toca-Herrera, H.J. Müller, R. Krustev, T. Pfohl and H. Möhwald (1999). *Colloids and Surfaces A* 152: 357-365.

[8] J.L. Toca-Herrera, R. Krustev, H.J. Müller and H. Möhwald (2000). *Colloid and Polymer Science* 278: 771-776.

[9] P. Nollert, H. Kiefer and F. Jähnig (1995) *Biophysical Journal* 69: 1447-1455.

[10] E. Sackmann (1996) *Science* 271: 43-48.

[11] M. Gerstein and H. Hegyi (1998). *FEMS Microbiology Reviews* 22: 277-304.

[12] C. Ellis and A. Smith (2004). *Nature Reviews Drug Discovery* 3: 237-278.

[13] R.P. Richter, J.L. Kee Him, B. Tessier, C. Tessier and A. R. Brisson (2005). *Biophysical Journal* 89: 3372-3385.

[14] S. Heyse, H. Vogel, M. Sanger and H. Sigrist (1995). *Protein Science* 4: 2532-2544.

[15] F. Giess, M.G. Friedrich, J. Heberle, R.L. Naumann and W. Knoll (2004). *Biophysical Journal* 87: 3213-3220.

[16] J.N. Herron, W. Muller, M. Paudler, H. Riegler, H. Ringsdorf and P.A. Suci (1992). *Langmuir* 8: 1413-1416.

[17] I.V. Turko, I.S. Yurkevich and V.L. Chashchin (1992). *Thin Solid Films 210/211*: 710.

[18] S.-P. Heyn, M. Egger and H.E. Gaub (1990). *Journal of Physical Chemistry* 94: 5073-5078.

[19] U.B. Sleytr and M. Sara (1997). *Trends Biotechnology* 15: 20-26.

[20] U.B. Sleytr and T.J. Beveridge (1999). *Trends Microbiology* 15: 253-259.

[21] M. Sara, D. Pum, B. Schuster and U.B. Sleytr (2005). *Journal of Nanoscience and Nanotechnology* 5: 1939-1953.

[22] D. Pum, M. Weinhandl, C. Hodl and U.B. Sleytr (1993). *Journal of Bacteriology* 175: 2762-2766.

[23] B. Wetzer, A. Pfandler, E. Györvary, D. Pum, M. Lösche and U.B. Sleytr (1998). *Langmuir* 14: 6899-6906.

[24] B. Schuster, P.C. Gufler, D. Pum and U.B. Sleytr (2003). *Langmuir* 19: 3393-3397.

[25] B. Schuster, D. Pum, O. Braha, H. Bayley and U.B. Sleytr (1998). *Biochimica et. Biophysica Acta* 1370: 280-288.

[26] B. Schuster, D. Pum, and U.B. Sleytr (1998). *Biochimica et. Biophysica Acta* 1369: 51-60.

[27] S. Küpcü, M. Sara and U.B. Sleytr (1995). *Biochimica et. Biophysica Acta* 1235: 263-269.

[28] C. Mader, S. Küpcü, U.B. Sleytr and M. Sara (2000). *Biochimica et. Biophysica Acta*, 1463: 142-150.

[29] M. Bogdanov, M. Umeda and W. Dowhan (1999). *Journal of Biological Chemistry* 274: 12339-12345.

[30] M. Bogdanov, J. Sun, H. R. Kaback and W. Dowhan (1996). *Journal of Biological Chemistry* 271: 11615-11618.

[31] E. Crooke (2001). *Biochimie* 83: 19-23.

[32] U.B. Sleytr, M. Sara, S. Küpcü and P. Messner (1986). *Archives of Microbiology* 146: 19-24.

[33] D.J. Shaw, *Colloid and Surface Chemistry*, Chapter 7, 4th edition Butterworth-Heinemann, Oxford, 1999.

[34] J.R. Harris, *Methods in Molecular Biology* 117, Chapter II, Ed. N. Hajibahen, Humana Press INC, New York, 1999.

[35] M.C .Wiener, G.I. King and S.H. White (1991). *Biophysical Journal* 60: 568-576.

[36] M. Delcea, R. Krastev, T. Gutberlet, D. Pum, U.B. Sleytr and J.L. Toca-Herrera (2007). *Journal of Nanoscience and Nanotechnology* 7: 4260-4266.

[37] R.P. Richter and A.R. Brisson (2004). *Langmuir* 20: 4609-4613.

[38] A. Martin-Molina, S. Moreno-Flores, E. Perez, D. Pum, U.B. Sleytr and J.L. Toca-Herrera (2006). *Biophysical Journal* 90: 1821-1829.

[39] C. Delajon, T. Gutberlet, R. Steitz, H. Möhwald and R. Krastev (2005). *Langmuir* 21: 8509-8514.

[40] G. Sauerbrey (1959). *Zeitschrift für Physik* 155: 206-222.

[41] M. Delcea, R. Krastev, T. Gutberlet, D. Pum, U.B. Sleytr and J.L. Toca-Herrera (2008). *Soft Matter* 4: 1414-1421.

[42] A. Eleta, S. Moreno-Flores, D. Pum, U.B. Sleytr and J.L. Toca-Herrera, Biomimetics in Biophysics, Ed. J. L. Toca-Herrera, Research Signpost, Kerala, *in press*.

[43] R.P. Richter, A. Mukhopadhyay and A. Brisson (2003). *Biophysical Journal* 85: 3035-3047.

[44] I. Pera, R. Stark, M. Kappl, H.-J. Butt and F. Benfenati (2004). *Biophysical Journal* 87: 2446-2455.

[45] S. Moreno-Flores, A. Kasry, H.-J. Butt, C. Vavilala, M. Schmittel, D. Pum, U.B. Sleytr and J.L. Toca-Herrera (2008). *Angewandte Chemie International Edition* 47: 4785-4788.

[46] R.D. Hunt, M.L. Mitchell and R.A. Dluhy (1989). *Journal of Molecular Structure* 214: 93-109.

Chapter 7

Conclusions and future work

The most relevant conclusions and perspectives opened by this work can be summarized as follows:

The affinity of S-protein to polyelectrolytes has been elucidated by combining polyelectrolyte multilayer (PEM) deposition and S-layer technology through a sandwich-like supramolecular structure.

SbpA protein recrystallization took place only on anionic PSS and only cationic PAH shows affinity to the exposed crystalline S-layer surface. A compression of 20 nN unfolds the S-layer proteins, constituting the limit of the mechanical stability of recrystallized S-layers on PSS.

The inhomogeneity of the sandwich-like supramolecular structure induced formation of recrystallized S-layer patches after a second adsorption of SbpA monomers, with a mechanical stability of 9 nN. These results suggest that S-layer surface should be chemically modified in order to attract negative polyelectrolytes.

S-protein recrystallized on PSS-terminated polyelectrolyte multilayers loses its crystalline regularity at 55ºC. This critical denaturation temperature (Tcd) is about 10°C higher than denaturation in solution. The crystalline structure of the S-layer cannot be recovered either by decreasing the temperature or with recrystallization buffer. The mechanical properties of the S-proteins are also changed by temperature: aggregates of denatured proteins unfold at lower loads than the proteins that constitute the 2D crystal.

The combination of atomic force microscopy, quartz microbalance with dissipation monitoring and neutron reflectometry is able to deliver information about the water volume fraction around the S-protein layer.

The recrystallization of S-proteins builds very loosely packed layers on polyelectrolyte multilayers incorporating around 68% water.

The surface properties of SbpA protein recrystallized on hydrophilic silicon wafers, PEI and PSS-terminated polyelectrolyte multilayers have been investigated as a function of pH, by combining atomic force microscopy, contact angle measurements and quartz crystal microbalance with dissipation monitoring.

AFM micrographs do not show significant influence of pH in the range 4-8 on the global structure of the protein layer recrystallized on silicon wafers, on silicon coated with PEI and on PSS-terminated polyelectrolyte multilayers.

SbpA protein confers hydrophobicity to the substrates and the system silicon/PEI/SbpA looses more mass than the system silicon/SbpA and silicon/PSS/SbpA after treatment at pH 4.

The interaction of SbpA protein with saturated, unsaturated, charged and uncharged lipids has been investigated. SbpA protein has high affinity for DOPC bilayers, DMPG vesicles, DOPC/DMPG bilayers supported on mica, and for DPPC and DPPC/DMPG monolayers and builds crystalline structure.

SbpA protein interacts weakly with DOPC and DOPC/DOPS bilayers supported on silicon and has no affinity for DMPC vesicles adsorbed on PEM and DPPC vesicles supported on silicon.

The importance of the surface chemistry and roughness of the substrates used for lipid deposition and the thermodynamic state of the lipid layer were shown.

Future work involves i) the optimization of the PEM/S-layer macromolecular building process, ii) the building of biomimetic surfaces adsorbing fusion proteins with different biological functionalities, iii) the use of polyelectrolytes with different electrical and hydrophobic properties as antibacterial surface layer agents, iv) the variation in thickness of the hybrid PEM/S-layer system and the influence of the support on the water film stability on recrystallized S-layers, v) the formation of stable S-layers on lipid supports by improving experimental conditions (lipid ratio mixture, temperature, solvent conditions etc.).